CAPITAL UNIVERSITY OF SCIENCE AND TECHNOLOGY, ISLAMABAD

Whole Genome Sequencing of Fungi Involved in Plastic Degradation from Dumping Sites

by

Zoya Khan

A thesis submitted in partial fulfillment for the degree of Master of Science

in the

Faculty of Health and Life Sciences
Department of Bioinformatics and Biosciences

2026

CERTIFICATE OF APPROVAL

Whole Genome Sequencing of Fungi Involved in Plastic Degradation from Dumping Sites

by

Zoya Khan

(MBS243013)

THESIS EXAMINING COMMITTEE

S. No.	Examiner	Name	Organization
(a)	External Examiner	Dr. Maria Shabbir	NUST, Islamabad
(b)	Internal Examiner	Dr. Sohail Ahmad Jan	CUST, Islamabad

Dr. Sahar Fazal
Thesis Supervisor
August, 2026

Dr. Syeda Marriam Bakhtiar
Head
Dept. of Bioinfo. & Biosciences
August, 2026

Dr. Sahar Fazal
Dean
Faculty of Health & Life Sciences
August, 2026

Author's Declaration

I, **Zoya Khan** hereby state that my MS thesis titled "**Whole Genome Sequencing of Fungi Involved in Plastic Degradation from Dumping Sites**" is my own work and has not been submitted previously by me for taking any degree from Capital University of Science and Technology, Islamabad or anywhere else in the country/abroad.

At any time if my statement is found to be incorrect even after my graduation, the University has the right to withdraw my MS Degree.

(Zoya Khan)
Registration No: MBS243013

Plagiarism Undertaking

I solemnly declare that research work presented in this thesis titled "**Whole Genome Sequencing of Fungi Involved in Plastic Degradation from Dumping Sites**" is solely my research work with no significant contribution from any other person. Small contribution/help wherever taken has been duly acknowledged and that complete thesis has been written by me.

I understand the zero tolerance policy of the HEC and Capital University of Science and Technology towards plagiarism. Therefore, I as an author of the above titled thesis declare that no portion of my thesis has been plagiarized and any material used as reference is properly referred/cited.

I undertake that if I am found guilty of any formal plagiarism in the above titled thesis even after award of MS Degree, the University reserves the right to withdraw/revoke my MS degree and that HEC and the University have the right to publish my name on the HEC/University website on which names of students are placed who submitted plagiarized work.

(Zoya Khan)

Registration No: MBS243013

Acknowledgement

All praise and gratitude are due to Almighty Allah, the Most Beneficent and the Most Merciful, whose blessings and guidance enabled me to complete this research work successfully.

I would like to express my sincere gratitude to my respected supervisor, Dr. Sahar Fazal, for their continuous guidance, valuable suggestions, and unwavering support throughout the course of this study. Their encouragement and insightful feedback greatly contributed to the completion of this thesis.

I would like to thank Dr. Marriam Bakhtiar, Head, Department of Biosciences and Bioinformatics, CUST, for providing me with knowledge, resources, and a conducive learning environment. I would also like to thank all the faculty members for their support and guidance, especially Dr. Sohail Ahmed Jan for his continuous support and insights as Lab In-Charge. I extend my appreciation to my friends who supported me during this journey, whether through academic discussions or moral encouragement.

My deepest thanks go to my family, especially my mother,my husband, M. Jamil, and my kids, for their continuous support throughout this journey. Their constant support and motivation have been the foundation of my success. Finally, I acknowledge all those who directly or indirectly contributed to the completion of this research work.

(Zoya Khan)

Abstract

Plastic pollution signifies one of the most persistent environmental challenges of the twenty-first century, driven by the inadequacy of existing waste management infrastructures, particularly in low- and middle-income countries such as Pakistan. Fungi represent a largely untapped biological resource for plastic biodegradation. The present study employed a two-phase approach to identify, characterise, and genomically profile plastic-degrading fungi isolated from a municipal solid waste site in H-11, Islamabad. In Phase 1, thirteen morphologically distinct fungal isolates were recovered from plastic-contaminated soil samples on potato dextrose agar (PDA) and sub-cultured to yield ten representative strains, designated S1–S10. Halo zone formation assays on plastic-supplemented media revealed extracellular enzymatic activity across all isolates, with zone diameters ranging from 10 mm (S2) to 70 mm (S6 and S8), indicating substantial variation in secreted polymer-active enzyme productivity. Molecular identification by BLAST homology analysis against the NCBI GenBank database identified the ten isolates as: *Rhizopus delemar* (S1; 98.71%), *Aspergillus niger* (S2; 100%), *Aspergillus fumigatus* (S3; 100%), *Penicillium chrysogenum* (S4; 100%), *Rhizopus arrhizus* (S5; 99.1%), *Fusarium fujikuroi* (S6; 100%), *Schizophyllum commune* (S7; 100%), *Aspergillus nidulans* (S8; 99.81%), *Fusarium proliferatum* (S9; 100%), and *Fusarium oxysporum* (S10; 100%). An *in vitro* PE biodegradation assay confirmed that *R. arrhizus* reduced the mass of a 0.04 g polyethylene strip by 50% (to 0.02 g) following 15 days of incubation at 25°C on a soil plat, providing the primary justification for advancing this isolate to whole-genome analysis. In Phase 2, the *R. arrhizus* isolate was subjected to comprehensive computational genome analysis. Assembly quality assessment using QUAST confirmed a high-quality genome of 50,257,580 bp (∼50.26 Mb) which was distributed across 41 contigs, with an N50 of 1,791,908 bp, a largest contig of 3.24 Mb, placing the assembly in the high-quality tier for fungal genomes. The GC content of 35.58% is consistent with published values for Rhizopus arrhizus. Structural gene annotation using AUGUSTUS predicted 16,813 protein-coding genes distributed across all 41 contigs, with a gene density of 334.6 genes per Mb and 69.6% of the total assembly classified as genic sequence.

Functional annotation of 662 non-redundant protein sequences using InterProScan (v5) across eight integrated databases yielded the most abundant InterPro domains included the IGFBP N-terminal cysteine-rich domain (IPR017891; 23.3% of proteins), Functional annotation using eggNOG-Mapper v2 analysed 41,844 predicted protein sequences, achieving 90.8% annotation coverage. COG functional category analysis assigned 85.1% of sequences to 38,373 COG categories, with the largest characterised functional class being Cellular Processes and Signalling (28.2%), dominated by Signal Transduction Mechanisms (COG-T; 8.2%), reflecting a rich environmental sensing repertoire. KEGG pathway mapping assigned 16,574 sequences to KO identifiers, with Metabolic pathways (ko01100; n = 3,384) and Biosynthesis of secondary metabolites (ko01110; n = 1,389) as the most represented pathways. Carbohydrate-Active Enzyme (CAZy) annotation identified 528 predicted CAZymes across nine families. Cellulolytic families directly relevant to plastic degradation included GH5 (endoglucanase; n = 20), GH9 (endoglucanase; n = 20), and GH3 (beta-glucosidase; n = 35), all of which have reported activity against oxidised polyethylene substrates in related fungal species. Cell wall biosynthesis and remodelling families (GT2 chitin/cellulose synthases; GH18 chitinases; GH47, GT39, GT15 mannosylation enzymes) were well represented, confirming the organism's capacity for dynamic surface adaptation during polymer colonisation. These findings position *R. arrhizus* as a high-priority candidate for the development of biological plastic waste treatment.

Keywords: plastic biodegradation; *Rhizopus arrhizus*; polyethylene degradation; fungal isolation; CAZymes; municipal solid waste; Pakistan ‘

Contents

List of Figures

List of Tables

Abbreviations

bp	Base Pair
HDPE	High-Density Polyethylene
LDPE	Low-Density Polyethylene
MSM	Minimal Salt Medium
NGS	Next Generation Sequencing
OTUs	Operational Taxonomic Units
PCR	Polymerase Chain Reaction
PE	Polyethylene
PET	Polyethylene Terephthalate
PS	Polystyrene
PUR / PU	Polyurethane
PVC	Polyvinyl Chloride
rDNA	Ribosomal DNA
WGS	Whole Genome Sequencing

Chapter 1

Introduction

Plastic has become a cornerstone of modern life, thanks to its adaptability, strength, low weight, and affordability. Ever since large-scale production took off in the mid-1900s, plastics have found their way into packaging, farming, healthcare, electronics, and construction [1]. The very traits that make them so useful resistance to chemical and physical breakdown also mean they linger in the environment for a very long time [2],[3]. As a result, plastic pollution has turned into one of the most urgent environmental issues worldwide, with serious consequences for ecosystems, wildlife, and human health [4, 5]. At their core, plastics are polymers made up of long chains of repeating units known as monomers. They can be split into two broad groups: natural and synthetic. Natural polymers like cellulose, starch, chitin, proteins, and natural rubber are biodegradable [6]. Microorganisms can easily break them down using enzymes, and they fit neatly into natural cycles without building up in the environment. Synthetic polymers, on the other hand, are human-made, mostly from petroleum [1]. This group includes common plastics such as polyethylene (PE), polypropylene (PP), polyethylene terephthalate (PET), polyvinyl chloride (PVC), polystyrene (PS), and polyurethane (PU) [7]. These materials are tough for microbes to attack because they are water-repellent, have high molecular weights, are crystalline in structure, and contain stable chemical bonds like carbon–carbon and ester linkages [6, 8].

Plastics can also be grouped by how they respond to heat. Thermoplastics like PE, PP, and PET can be melted and reshaped multiple times, making them easier to recycle. Thermosetting plastics, including epoxy resins and certain polyurethanes, undergo permanent chemical changes when heated, forming rigid, cross-linked networks that cannot be melted again [7]. This makes getting rid of or recycling them especially tricky. The total volume of production and consumption has led to huge amounts of plastic waste piling up in landfills, oceans, and other natural spaces [1].

The harm plastic waste causes to the environment are complex. Plastics can stick around in ecosystems for hundreds of years, slowly breaking into smaller pieces called microplastics and nanoplastics through sunlight, heat, and physical wear [2],[3]. These tiny particles are easily swallowed by animals on land and in water, leading to physical harm and chemical toxicity [9], [10]. They are like magnets for dangerous pollutants, such as heavy metals and stubborn organic pollutants, making the problem even worse [11]. In addition, plastic waste clogs drainage systems, lowers soil quality, and destroys habitats [12]. Traditional waste management methods like burying or burning plastic are not sustainable, as they can contaminate soil and groundwater and release toxic gases and greenhouse emissions [13].

Faced with these challenges, the idea of breaking down plastics biologically has drawn increasing interest as an eco-friendly and sustainable solution [14]. Biodegradation means using microorganisms and their enzymes to turn complex plastics into simpler compounds [8]. The process usually starts with microbes settling on the plastic's surface, and then releasing extracellular enzymes that chop the polymer chains into smaller pieces like oligomers and monomers [15],[8]. These smaller molecules are then taken into the microbial cells and metabolized, eventually becoming carbon dioxide, water, and biomass [8].

Many microorganisms, including bacteria and fungi have been found to break down plastics [16]. Bacterial species like Pseudomonas aeruginosa, Bacillus subtilis, and Ideonella sakaiensis are known to degrade certain plastics, especially PET and polyurethane [17]. But fungi have attracted special attention because of their

powerful enzyme systems and ability to thrive in a wide range of conditions [18]. Fungi can release various extracellular enzymes that break down tough organic materials, including stubborn polymers [18].

Several fungal species have been identified as promising plastic degraders. For example, *Aspergillus niger* and *Aspergillus flavus* have been reported to break down polyethylene and polystyrene [19]. *Penicillium chrysogenum* and other Penicillium species are known to degrade synthetic polymers through enzyme activity [20]. *Rhizopus arrhizus* has shown strong potential to break down plastics in a relatively short time under lab conditions [21]. White-rot fungi such as *Phanerochaete chrysosporium* and *Trametes versicolor* are especially effective because they produce ligninolytic enzymes like laccases and peroxidases that can oxidize complex polymer structures [18]. Other fungi, including *Fusarium solani*, *Cladosporium cladosporioides, Alternaria alternata*, and Mucor species, have also been reported to degrade plastics [22].

The enzymatic mechanisms behind plastic breakdown vary depending on the polymer's chemical structure. Hydrolytic enzymes like PETase, cutinase, lipase, and esterase play a key role in breaking down polymers with ester bonds [23],[24]. They catalyze the hydrolysis of those bonds, breaking the polymer chains into smaller pieces. For example, PETase breaks down PET into mono (2-hydroxyethyl) terephthalate (MHET), which is then further broken down by MHETase into terephthalic acid and ethylene glycol [25]. Oxidative enzymes known as laccases, manganese peroxidases, and lignin peroxidases are involved in degrading more strong plastics like polyethylene and polystyrene [16]. These enzymes produce reactive oxygen species that kick off the oxidation and splitting of polymer chains.

Fungi have several advantages over bacteria when it comes to plastic degradation. Their thread-like growth allows them to dig into solid surfaces and form wide networks on plastic, improving contact between enzymes and the material [18]. Fungi can also survive in extreme conditions, including low nutrients and varying pH levels, making them well-suited for real-world environmental use [26]. Their ability to produce large amounts of extracellular enzymes further boosts their efficiency in breaking down complex polymers [18].

Recent progress in molecular biology and genomics has transformed the study of plastic-degrading microbes. Whole genome sequencing (WGS) has become a powerful tool for finding genes and metabolic pathways involved in plastic breakdown. By analyzing a microorganism's complete genome, researchers can identify genes that code for key enzymes, transport proteins, and regulatory elements tied to the degradation process. This information offers valuable insights into the molecular workings of plastic biodegradation.

In fungi, WGS makes it possible to find gene clusters responsible for producing extracellular enzymes like laccases, peroxidases, and hydrolases. It also helps researchers study the regulatory networks that control gene expression in response to environmental signals. Bioinformatics tools are used to annotate genomic sequences, predict protein functions, and reconstruct metabolic pathways. Functional genomics approaches like transcriptomics and proteomics further deepen our understanding by showing how genes and proteins are expressed during degradation.

Combining genomic data with lab experiments allows researchers to identify efficient plastic-degrading strains and optimize conditions for breakdown. It also opens the door to genetic engineering and synthetic biology aimed at boosting degradation efficiency [27]. For example, genes coding for plastic degrading enzymes can be cloned and expressed in suitable host organisms to create engineered strains with improved abilities.

In addition, studying microbial consortia where multiple species work together has shown promise for enhancing plastic degradation [28]. Different microorganisms may bring different enzyme activities to the table, leading to more complete breakdown of complex polymers. Understanding how these consortia interact is an important area of ongoing research.

In this context, isolating and characterizing fungal strains from plastic-polluted environments, followed by genomic and bioinformatic analysis, offers a comprehensive way to tackle plastic pollution. By identifying the key enzymes, genes, and

metabolic pathways involved in degradation, it becomes possible to develop sustainable and eco-friendly strategies for managing plastic waste. Such approaches not only help protect the environment but also support the development of globular economy models, where plastic waste is converted into valuable resources [29].

Overall, bringing together microbial biotechnology, enzymology, and genomic analysis provides a promising path forward for dealing with the global plastic pollution crisis. Exploring fungal diversity and applying whole genome sequencing technologies are expected to play a crucial role in advancing this field and creating innovative solutions for a cleaner, more sustainable world.

1.1 Statement of the Problem

The increasing buildup of plastic waste in dumping sites has become a main environmental problem due to the non-degradable nature of synthetic polymers and the inefficiency of traditional disposal methods. However, the genetic determinants, regulatory mechanisms, and evolutionary adaptations that enable indigenous fungi to efficiently degrade synthetic plastics remain largely unexplored. Without a comprehensive genomic blueprint, the development of robust enzyme-based biocatalysts or fungal consortia for industrial-scale plastic bioremediation remains hindered.

1.2 Study Gap

Therefore, this study addresses these gaps by conducting a comprehensive whole genome analysis of fungi isolated from plastic dumping sites. Dumping sites act as natural laboratories where fungi have adapted to utilize plastics as carbon sources, potentially harboring strains with enhanced degradative capabilities.

Whole genome sequencing provides complete genetic blueprints, allowing the identification of all genes potentially involved in plastic degradation, including those that cannot be detected through conventional activity assays.

In addition, genomic analysis reveals regulatory elements, metabolic pathways, and evolutionary adaptations that are not evident from degradation experiments alone. Comparative genomics with known plastic-degrading fungi further helps in identifying both conserved and novel genetic features associated with degradative potential.

Moreover, the deposition of newly identified genomes in GenBank creates valuable resources for the broader scientific community, thereby accelerating research progress in this field.

1.3 Aim and Objectives

1.3.1 Aim

To identify plastic-degrading genes and metabolic pathways in fungi isolated from municipal dumping sites using whole genome sequencing, along with structural and functional annotation.

1.3.2 Objectives

i. To perform whole genome sequencing and de novo assembly of plastic - degrading fungi isolated from municipal dumping sites, followed by structural and functional annotation of the assembled genome.

ii. To determine the key genetic determinants/genes involved in plastic depolymerization.

iii. To predict metabolic pathways associated with plastic degradation and carbon metabolism.

1.4 Scope of Study

This study is confined to the isolation, phenotypic screening, and molecular identification of fungal strains recovered from a single municipal solid waste site (H-11, Islamabad), followed by in vitro assessment of polyethylene-degrading activity and whole-genome sequencing of one selected isolate, *Rhizopus arrhizus*. The scope covers culture-based isolation on plastic-supplemented and minimal media, halo zone screening, 18S rRNA-based species identification, a laboratory-scale PE weight-loss biodegradation assay, and genome assembly with structural and functional annotation (AUGUSTUS, InterProScan, eggNOG-Mapper, KEGG, and CAZyme analysis) to identify candidate genes and enzyme families associated with plastic degradation. The study does not extend to field-scale or pilot bioremediation trials, biochemical characterisation or heterologous expression of the identified enzymes, transcriptomic validation of gene expression under PE-induced conditions, or comparative genomic analysis against other plastic-degrading fungal genomes; these fall outside the present work and are proposed as directions for future research.

Chapter 2

Literature Review

2.1 What is Plastic?

The word "plastic" refers to a broad range of synthetic or semi-synthetic organic materials that can be molded or shaped into films, objects or fibers [1]. The name comes from the property of plasticity the ability to be deformed and shaped while in a semi-liquid state. A polymer is a molecule made up of repeated units of a particular chemical base segment, and while all plastics are organic polymers, not every polymer qualifies as plastic, since many need additives to become useful materials [6]. The term itself has ancient Greek roots, combining poly (many) and meros (parts or units).

2.2 Etymology and Historical Development

People have used polymeric materials for centuries, relying on natural organic polymers like waxes and shellacs. Natural rubber, tapped from rubber trees, was already widely used by the early 1800s [6]. The development of modern plastics began with modifications to these natural polymers. In 1839, Charles Goodyear invented vulcanization, a process of heating rubber with sulphur that

created sulphur bonds linking separate isoprene polymers, greatly improving the material's strength, elasticity, and chemical resistance.

The first man-made plastic, celluloid, was introduced in 1863 by John Wesley Hyatt, who discovered that camphor could plasticize cellulose treated with nitric acid [1]. However, Bakelite was the first truly synthetic plastic created by Leo Hendrik Baekeland in 1909 [1]. This phenolic plastic was completely synthetic, not based on any natural molecule, and was also the first "thermoset" plastic, meaning it couldn't be remelted once cured [7]. The years after World War I and II saw an explosion of new plastics, including polystyrene (PS), polyvinyl chloride (PVC), nylon, acrylic, neoprene, and polyethylene, dramatically changing the material landscape of modern society [1].

2.3 Worldwide Use and Production

Plastics have become the defining material of our era because of their versatility, durability, convenience, and low cost. They are used in nearly every part of modern life, including packaging, construction, cars, medical devices, electronics, textiles, and farming [1]. Plastics have caused a unlimited ecological problems that have attracted a lot of attention worldwide. Plastic products are useful as they bring ease to our lives. However, they can remain in natural environment for hundreds of years or longer, as a persistent pollutant [4]. In 1950, the global production of plastics (excluding fiber) was 1.3 million tons, and by 2018, it extended to an alarming level of 359 million tons (excluding fiber), resulting in extensive environmental contamination [2]. According to an estimation, only 10% of plastic waste is recycled, 14% is incinerated, and the rest is dumped into landfills, which ultimately enters the natural environment [30]. In fact, plastics and microplastics (MPs, size 5 mm) have been commonly known to be found in freshwater, the atmosphere, and soil environments across the world [9, 10]. Plastics in general is referred to as a class of high molecular weight polymers. The formation of "white pollution" has become the major cause of serious environmental pollution and ecological damage around the world [12].

The scale of global plastic production is staggering. Annual production has grown more than 250-fold from less than 2 million metric tons (Mt) in 1950 to 475 Mt in 2022, with projections reaching 1,200 Mt by 2060 [1]. More recent data shows that global plastic production has increased 430.9 million metric tons in 2024, growing at an average annual rate of 4.8 percent since 2009 [1]. The global plastics market was valued at about USD 524.48 billion in 2024, with projections to hit USD 754.23 billion by 2032 [1]. Asia-Pacific leads the world in plastic production, which is more than half of both production and consumption, with China alone making up 34.5% of global production [1]. Packaging remains the single biggest use, representing more than 35% of demand worldwide [1].

2.4 Classification of Plastics

Plastics can be broadly grouped on basis of their origin and whether they break down naturally. Understanding these categories is essential for assessing their environmental impact and potential for biodegradation.

2.4.1 Classification by Origin

2.4.1.1 Synthetic Polymers

Conventional plastics are synthetic polymers generally derived from fossil fuels like natural gas, crude oil, , and coal [1]. More than 98% of plastics come from fossil carbon. These materials are generally non-biodegradable and remain in the environment for hundreds to thousands of years, breaking into smaller fragments rather than fully decomposing [2, 3].

TABLE 2.1: Particular features of major commercial thermoplastic polymers [4]

Polymer	**Abbreviation**	**Density (23/4°C)**	**Crystallinity (%)**	**Lifespan (year)**
Polyethylene	PE	0.91–0.925	50	10–600

Table 2.1 continued from previous page

Polymer	**Abbreviation**	**Density (23/4°C)**	**Crystallinity (%)**	**Lifespan (year)**
Polypropylene	PP	0.94–0.97	50	10–600
Polystyrene	PS	0.902–0.909	0	50–80
Polyethylene glycol terephthalate	PET	1.03–1.09	0–50	450

2.4.1.2 Natural Plastics

Natural plastics come from biological sources and have been used for centuries. These include tar, shellac, tortoise shell, horns, amber, and latex from tree sap [1]. Semi-synthetic plastics are made by chemically modifying natural polymers. Historical examples include vulcanized rubber (natural rubber treated with sulphur) and celluloid (cellulose treated with nitric acid and camphor) [1]. Rayon, introduced in 1911, is another cellulose-based semi-synthetic fiber [1].

2.4.2 Classification by Degradability

Most conventional plastics are non-biodegradable, meaning they don't break down through natural processes within a short timeframe. Instead, they degrade over very long periods (hundreds to thousands of years) through physical processes like sunlight or wave action, eventually fragmenting into smaller particles while the polymer structure stays mostly intact [2, 3].

2.4.2.1 Bioplastics

Bioplastics are made fully or partly from biological raw materials, including plant starch, vegetable oils, or algae. They are designed to reduce reliance on fossil fuels. However, not all bioplastics are biodegradable their environmental benefit depends on their chemical structure and how they are disposed of. According to CAS classification, biopolymers fall into three categories; natural polymers, included in Class

A are directly obtained from biomass, such as starch, cellulose, proteins, and amino acids. These are 100% bio-based and biodegradable. Class B Polymers biosynthesized by microorganisms or plants, or made from monomers produced through biosynthesis. Examples include polyhydroxyalkanoates (PHA) and polylactic acid (PLA). These are biodegradable and nearly 100% bio-based. Traditional oil-based polymers of Class C made from alternative bio-derived monomers, such as bio-PET and bio-polyethylene. These are structurally matching to oil-based plastics and are mostly non-biodegradable, presenting the same disposal challenges [6]. Bioplastics currently make up less than 2% of global plastic production, though they are growing at double rates, especially in packaging and disposable items [1].

Biodegradable plastics are specifically aimed to decompose in water or soil through natural processes driven by microorganisms. Bacteria and fungi break the chemical bonds in the plastic, with decomposition rates depending on both biological factors (microbial activity) and physical factors (temperature, moisture, oxygen levels) [8]. Warmer, wetter conditions with lots of microbial activity speed up biodegradation.

2.4.2.2 Microplastics

Plastic fragments smaller than 5 mm in length are microplastics, often invisible to the naked eye [2]. They form when larger plastics break down over time through physical, chemical, and biological processes [2, 3]. Microplastics can also be manufactured intentionally for use in products like cosmetic and microbeads [9]. These fragments spread easily through water and soil and have been found in the most remote places on Earth, from the atmosphere to the deep ocean [10].

2.4.2.3 Complications Caused by Plastics

Plastics pose significant threats to wildlife and the environment. These impacts include environmental degradation, harm to natural ecosystems, destruction of marine life, and serious risks to human health [4, 5]. Globally, nearly 5 trillion plastic items are used only once, and a large percentage of this waste ends up in

the oceans, disrupting both living (biotic) and non-living (abiotic) components of ecosystems [12].

Many animals die after ingesting plastic or becoming entangled in it [9]. Marine environments are especially affected, with approximately 8 trillion plastic pieces entering oceans each year [2]. Due to their non-biodegradable nature, plastics persist in the environment for long periods [3]. These pollutants also enter the human food chain through fish consumption [10]. As a result, hundreds of marine species die annually. Researchers warn that if current trends continue, the amount of plastic in oceans could eventually surpass the number of fish [4].

In addition to environmental damage, plastics also pose health risks. Certain plastic components can mimic human hormones, leading to various health issues, including cancer. The International Agency for Research on Cancer (IARC) has classified vinyl chloride as a human carcinogen. Styrene has also been associated with cancer, particularly breast cancer. Bisphenol A (BPA) has been linked to premature births, impaired growth, and stillbirths [31]. It can also disrupt female hormones, including progesterone.

2.5 The Global Plastic Burden

The combination of widespread plastic production and poor waste management has created a global environmental crisis [4]. The total plastic waste generated worldwide between 1950 and 2020 is estimated at 8,000 million metric tons (8 gigatonnes). Half of all plastic ever made has been produced since 2010, and half of all waste plastic has been generated since 2011 [2].

Plastic waste now significantly pollutes every corner of the planet from the top of Mount Everest to the bottom of the Mariana Trench [3]. The problem is especially severe in marine environments, where plastic debris dominates ocean pollution and harms marine life through entanglement and ingestion [9]. The buildup of plastic waste on land, including dumpsites and landfills, creates lasting pollution that can persist for centuries [12].

2.5.1 The Recycling Crisis

Despite decades of awareness about plastic pollution, recycling rates remain very low. Less than 10% of plastic waste is recycled into reusable products globally. This recycling rate is far lower than those for paper, glass, steel, and aluminium. The rest of the plastic waste is landfilled, incinerated, or released directly into the environment [30].

The reasons for low recycling rates include; the complexity of plastic formulations with over 16,000 chemical additives, contamination of plastic waste streams, economic challenges in sorting and processing mixed plastics and lack of collection infrastructure in many regions [29].

The Organisation for Economic Co-operation and Development (OECD) estimates that only 9% of plastic waste is currently recycled world-wide, far below the level needed to meet policy mandates and corporate sustainability commitments [29]. This has created a structural shortage where demand for post-consumer recycled plastics is growing three folds faster than supply.

2.5.2 Human Health Impacts

Plastics pose serious and often overlooked dangers to human health at every stage of their lifecycle from extracting raw materials to production, use, and disposal. The annual health-related economic losses linked to plastics exceed US$1.5 trillion [31].

Plastic chemicals are a major health concern. More than 16,000 chemicals can be found in plastics, including monomers, catalysts, processing aids, and additives such as plasticizers, flame retardants, and stabilizers [29]. Common plastic additives like PBDEs (flame retardants), BPA, and DEHP (phthalates) are linked to significant health risks. National biomonitoring surveys have detected multiple plastic chemicals including bisphenols, phthalates, brominated flame retardants, and per- and polyfluoroalkyl substances (PFAS) in the bodies of nearly all people tested, including newborn infants and pregnant women [31].

Microplastic and nanoplastic particles (MNPs) are progressively being reported in human biological samples, including blood, breastmilk, kidney, colon, liver, placenta, spleen, lung, brain, and heart in populations around the world [10, 31].

Health effects associated with plastic exposure include higher risks of stillbirth, premature birth, asthma, leukemia in communities near production facilities, and potential heart-related effects from nanoplastic exposure [31].

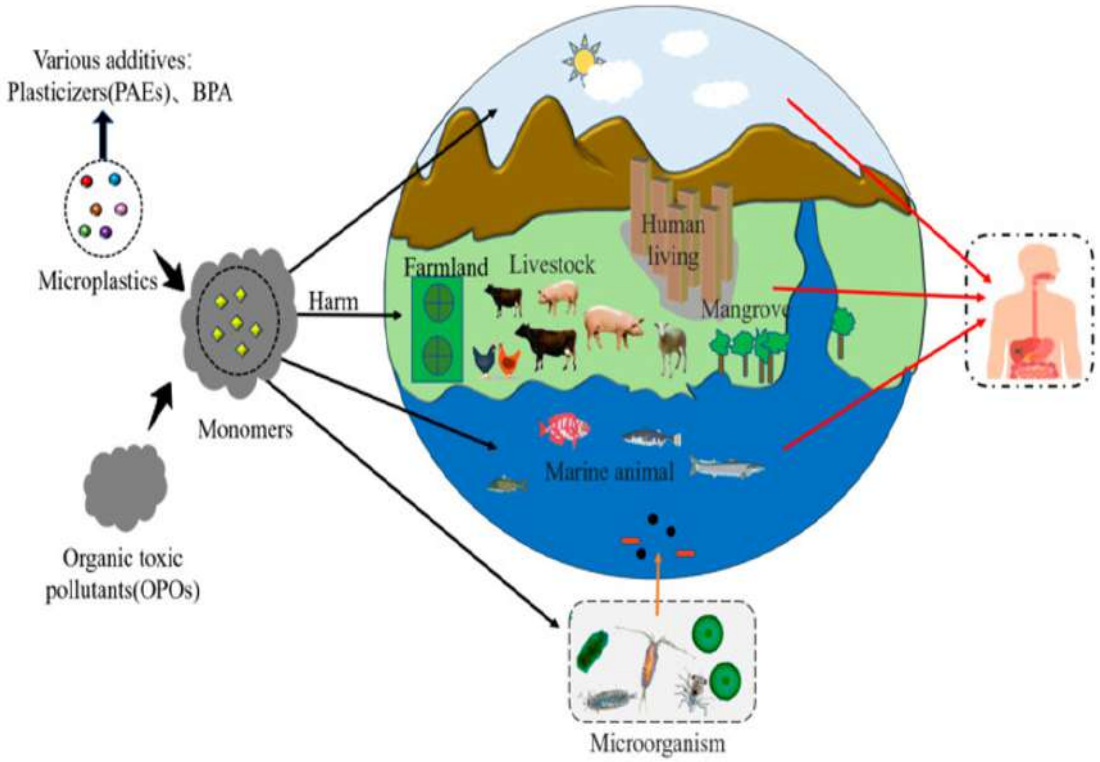

FIGURE 2.1: Additives, dyes, and organic pollutants in plastics can have adverse effects on both humans and nature. Human exposure to monomers and POPs can cause disrupt ing the natural gut microbiota balance through inhalation, ingestion, and skin contact

2.5.3 Climate Change Connection

The plastic industry's dependence on fossil fuels contributes significantly to climate change. Plastic production uses an estimated 8-10% of global oil supply, a figure expected to double by 2040. The energy-intensive manufacturing process, combined with emissions from feedstock extraction and waste incineration, results in about 2 billion tons of CO_2 emissions each year [29].

2.5.3.1 Microbial Degradation of Plastics

In the search for effective methods to reduce microplastic pollution, researchers have discovered that microplastics can persist in the environment yet still be degraded by microorganisms [8]. Microbes are highly adaptable and capable of surviving in diverse environments, where they can breakdown down a wide range of substances, including microplastics [16].

Microorganisms are increasingly being utilized for plastic degradation as part of bioremediation strategies. This process offers an environmentally friendly approach, as it helps in reducing pollution without causing harmful side effects, thereby contributing to the restoration of natural ecosystems [14]. However, only a limited number of effective microbial species have been isolated so far [16]. Moreover, the connection between microorganisms and microplastics is not yet fully understood due to insufficient data [8].

Therefore, it is essential to analyze and review existing research to identify microorganisms that can efficiently degrade microplastics, as well as to enhance understanding of microbial metabolic activities involved in plastic utilization. This review aims to systematically categorize and evaluate recent studies on microbially mediated microplastic degradation, along with explaining the characteristics and mechanisms involved in this process [8].

2.5.3.2 Plastic Degradation through Biofilm Contribution

Microplastics interact with inorganic molecules, organic matter, and microorganisms present in water. Due to this interaction, various types and sizes of microbes, including bacteria, algae, protists, fungi, , and viruses, attach to the surface layer of plastics. The colonization of these microorganisms leads to the formation of biofilms, which are complex ecosystems composed of microbial communities along with organic and inorganic materials [15]. Microplastic surfaces serve as a substrate for biofilm development, possessing both rough and smooth outer layers with varying densities [8]. These biofilms have capability to alter the morphology

and functionality of microplastics in several ways by secreting degrading enzymes and releasing metabolic by-products [8, 15].

2.5.3.3 Mechanism of Plastics Or MP's Biodegradation

Microorganisms break down microplastics (MPs) through depolymerization by releasing extracellular enzymes and free radicals that catalytically split the plastics into smaller components. This microbial degradation process involves converting large polymer chains into shorter fragments such as dimers, oligomers, and ultimately monomers. Once reduced to sufficiently small sizes, these monomers can pass through semipermeable membranes and be taken up by microbial cells to support growth. Inside the cells, the monomers undergo mineralization producing H_2O and CO_2 under aerobic conditions, or CO_2, H_2O, and CH_4 under anaerobic conditions while also contributing to biomass formation and energy production [8].

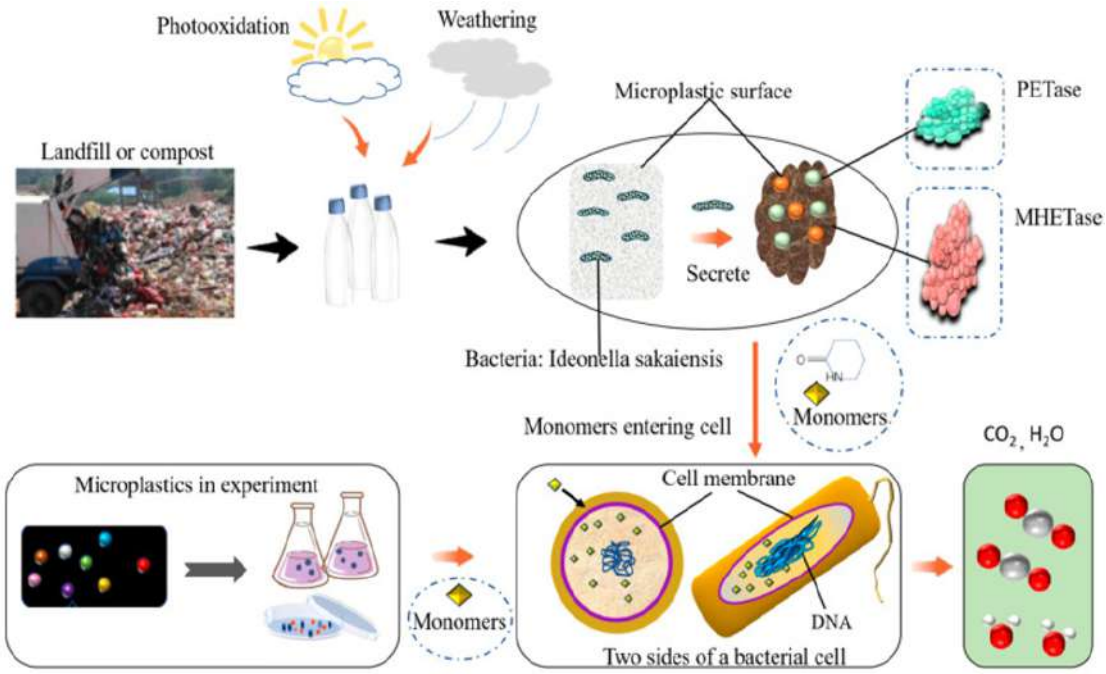

FIGURE 2.2: Microplastic degradation pathways involve the breakdown of larger plastic materials into smaller fragments, forming microplastics. These particles can enter cells after decomposition, where they may be assimilated into biomass for energy production or further mineralized into simpler inorganic compounds [8]

First step in plastic degradation is microbial colonization on plastic surfaces through adhesion or direct exposure and forms the basis for enzymatic breakdown. The second stage includes hydrolysis, where enzymes interact with the polymer matrix, followed by catalytic cleavage and fragmentation. The enzymes involved are mainly hydrolases, which catalyze the breakdown of organic materials. Both intracellular and extracellular enzymes from microorganisms play essential roles in this process. Extracellular enzymes, such as depolymerases and hydrolases, initiate hydrolytic cleavage of polymer chains, producing smaller units like oligomers and monomers. These smaller molecules can then be taken up by microbial cells and further metabolized by intracellular enzymes.

In contrast to oxidative degradation of larger plastic fragments, enzymatic degradation is often estimated by weight loss and the formation of new functional groups. A major indicator of microplastic (MP) biodegradation is the reduction in plastic weight, measured by comparing the initial mass with the mass after microbial exposure. Additionally, the byproducts of microbial degradation and metabolism are generally environmentally beneficial.

Polymer characteristics, particularly morphology and crystallinity, significantly influence biodegradability and degradation rate. Enzymes primarily target the amorphous regions of polymers, where molecules are less densely packed and more liable to breakdown. Consequently, microbial enzymes are crucial for environmental remediation and ecological balance, as they drive biodegradation and biotransformation processes. Biocatalytic approaches become more competitive, sustainable, safe, and environmentally friendly due to efficiency and functionality of enzymes.

2.5.3.4 Microbial Involvement

Various microorganisms, including fungi, bacteria, and biofilms, have been reported to degrade different types of microplastics such as polyethylene, polypropylene, polyvinyl chloride, polyethylene terephthalate, polyhydroxybutyrate, and

polybutylene succinate. Several physicochemical and environmental factors influence the microbial degradation of plastics. Although microplastics are generally more resistant to microbial attack compared to other biodegradable materials, their structural properties can still be altered through microbial activity.

2.6 Microorganisms and Their Enzymes in Plastics Or MPs Degradation

2.6.1 Microbial Degradation of Commonly Used Plastics Or MPs

Evidence of plastic biodegradation can primarily be determined through three key indicators: (1) structural changes in plastics or microplastics, (2) reduction in their physical mass, and (3) the production of degradation metabolites. Together, these factors provide the most reliable confirmation of plastics and microplastics biodegradation [30].

2.6.1.1 Microbial Degradation of the Commonly Used Recalcitrant Plastics Or MPs

Non-hydrolyzable plastics consist mainly of carbon–carbon (C–C) backbone chain, including materials such as polypropylene (PP), polyvinyl chloride (PVC), polyethylene (PE), and polystyrene (PS). Although these plastics are widely used, their biodegradability is very limited. Microorganisms typically convert such non-hydrolyzable microplastics (MPs) into smaller organic molecules through redox reactions carried out by bacteria or fungi before they can be utilized [32]. In contrast, hydrolyzable plastics like polyamide (PA) and polyethylene terephthalate (PET) are comparatively easier to degrade. Increasing evidence shows that certain microorganisms possess the capability to break down plastic materials. The most widely produced thermoplastic is PET, with an annual global production of

nearly 70 million tons, primarily used in textile fibers and packaging, with smaller applications in films and engineering [25]. However, very few bacteria and fungi are known to partially degrade PET. Most PET-degrading bacteria belong to the Gram-positive phylum Actinobacteria [24], including genera such as Thermobifida and Thermomonospora [33]. Several key enzymes involved in PET metabolism have been identified, including, MHETase, TPA dioxygenase, PETaseand PCA dioxygenase [17].

A notable discovery is *Ideonella sakaiensis* 201-F, a bacterium capable of using PET as its primary carbon and energy source, causing visible structural changes in PET films. This organism is unique because it can utilize plastic as its sole nutrient source. It produces two specialized enzymes that efficiently hydrolyze PET into environmentally harmless monomers. Specifically, it secretes PET hydrolase (PETase), which plays a crucial role in PET degradation [17].

Similar to other microorganisms, this strain releases enzymes that actively breaks down MPs and mineralize them within cells [6]. The degradation process involves two main steps, relying on the enzymes PETase and MHETase, although the precise binding mechanism of PETase remains unclear. Additionally, *Pseudomonas nitroreducens* S8 and *Pseudomonas monteilii* S17 can colonize PET surfaces by forming biofilms with stable populations, enabling them to use PET as a carbon source. When used together, these strains exhibit a synergistic effect, enhancing PET surface breakdown by improving accessibility for hydrolase enzymes [34].

Polystyrene (PS) is a hydrophobic, high–molecular-weight synthetic polymer that is highly resistant to microbial attack, making its biodegradation extremely slow [35]. However, studies have shown that PS degradation can occur in the gut of mealworms. The gut microbiome contains operational taxonomic units (OTUs) such as Citrobacter sp. and Kosakonia sp., which are associated with plastics like PE and PS, indicating their potential for degrading chemically diverse polymers. Further research is needed to utilize mealworm gut microbiota for PS biodegradation [36]. Similarly, polyethylene (PE), another non-hydrolyzable plastic, is also difficult to degrade due to its stable hydrocarbon structure, corrosion resistance,

and insulating properties, which makes it one of the most widely produced synthetic polymers [37].

PE's carbon–carbon backbone and strong covalent bonds contribute to its high resistance to degradation. Microbial consortia are considered a promising approach for PE degradation due to their synergistic interactions [38]. Several bacterial species, including *Pseudomonas*, *Bacillus*, *Mycobacterium*, and *Nocardia*, have been reported to degrade PE [39]. Studies show that bacterial consortia can form thick biofilms on weathered PE surfaces, altering their physical and structural properties. For example, a mesophilic consortium isolated from landfill sediments demonstrated that *Bacillus* sp. and *Paenibacillus* sp. reduced MP particle size and dry weight by 22.8% and 14.7% after 60 days [16].

Among PE types, high-density polyethylene (HDPE) and low-density polyethylene (LDPE) are the most commonly used. HDPE has a highly crystalline, nonpolar structure with a higher softening point (125–135 °C), while LDPE softens at 90–100 °C. HDPE is more resistant to oxidation, acids, alkalis, and salts, whereas LDPE shows relatively lower solvent resistance. Due to its structural properties, HDPE is more resistant to microbial degradation than LDPE [39, 40]. Comparative studies indicate that fungi are generally more effective than bacteria in degrading PE. Fungal treatment of LDPE films results in greater weight loss compared to bacterial treatment [21]. Both individual strains and microbial consortia can effectively degrade LDPE, often producing surface features like ridges and grooves that indicate degradation [41]. Marine bacteria have also been shown to utilize LDPE as a carbon source, with measurable weight loss and structural damage observed over incubation periods. Analytical techniques such as FTIR and SEM confirm chemical changes and surface deterioration, including cracks and fragmentation, in treated LDPE films [39].

Among fungal degraders, *Penicillium oxalicum* NS4 and *Penicillium chrysogenum* NS10 have demonstrated the ability to degrade HDPE and LDPE, causing visible structural changes in plastic films [20]. The genus *Aspergillus* is particularly notable for its strong plastic-degrading potential, including species such as *A.*

clavatus, *A. fumigatus*, and *A. niger*, which can degrade PE and PP [42]. Isolates like Aspergillus niger (ITCC No. 6052) from plastic-contaminated sites have shown the ability to break down HDPE [43]. Studying the enzyme systems of such fungi is essential for understanding their role in biodegradation. Other fungi, including *Rhizopus oryzae* and various *Penicillium* species, also contribute to LDPE and HDPE degradation [19]. The extent of degradation, often measured by weight loss, depends on factors such as polymer form, with films, foils, and strips showing the most significant reductions.

TABLE 2.2: Fungal strains involved in plastic degradation

Fungal Strains	**Environmental Source**	**Microplastic Type**	**Ref.**
Penicillium raperi, Aspergillus flavus	Soil, activated sludge, farm sludge, and worms	*Polyethylene terephthalate* (PET), Polyethylene (PE), Polystyrene (PS) High-DensityPolyethylene (HDPE)	[44]
Aspergillus tubingensis (VRKPT1)	Coastal (marine) area	High-Density Polyethylene (HDPE)	[45]
Penicillium simplicissimum (YK)	Soil and leaves of coastal area	Polyethylene (PE, UV-treated for 500 h)	[46]
Penicillium pinophilum (ATCC 11797)	Strain center (woody plant origin)	Low-Density Polyethylene (LDPE)	[47]
Aspergillus flavus PEDX3	Gut of Galleria mellonella	High-Density Polyethylene (HDPE) and Polyethylene (PE)	[48]

2.6.2 Microbial Degradation of Toxic Components in Commonly Used Plastics Or MPs

Since the 1950s, with the large scale production of plastics, the manufacturing of diverse polymers containing various additives and fillers has increased significantly. Among these, bisphenol A (BPA) and phthalic acid esters (PAEs) are notable for their harmful effects. BPA is toxic to many marine organisms and vertebrates and is considered possibly carcinogenic due to its structural similarity to diethylstilbestrol (DES). As plastic particles break down into smaller fragments, their toxicity tends to increase upon exposure [49].

PAEs and BPA, are also involved in biodegradation processes. Most research on the biodegradation of PAEs focuses on bacterial species such as *Pseudomonas, Arthrobacter, Rhodococcus, Bacillus, Mycobacterium, Delfia*, and *Gordonia* [50]. Microbial degradation of PAEs primarily occurs through hydrolysis of ester bonds, forming monoesters that further break down into phthalic acid (PA) and alcohols. These products are subsequently converted into short-chain acids that enter the Krebs cycle [44]. Enzymes such as oxygenases and hydrolases play a essential role in this process. Among them, esterases exhibit particularly high efficiency in degrading phthalates, functioning optimally at pH levels between 7 and 10 and temperatures ranging from 30 to 70 °C [51].

Studies have shown that pretreatment conditions, including temperature and hydrolase activity, significantly enhance degradation efficiency, often reflected by weight reduction. For example, *Bacillus* sp. GZB, a facultative anaerobic bacterium isolated from an estuarine electronic waste dismantling site, has demonstrated the ability to accelerate BPA biodegradation in water–sediment environments. The introduction of this strain was strongly associated with improved degradation performance. Furthermore, BPA biodegradation can be enhanced through the addition of electron donors, co-substrates, or supplements such as yeast extract, NaCl, humic acid, and glucose [45]. These strategies, including bioaugmentation and biostimulation, have been shown to significantly improve BPA degradation in water sediment microcosms [46].

2.6.3 Microbial Degradation of Commonly Used Biodegradable Plastics Or MPs

Emerging materials known as biodegradable plastics are generally more susceptible to degradation compared to conventional high-molecular-weight polymers. Biodegradable plastics (BPs) such as polycaprolactone (PCL), polybutylene succinate - co adipate (PBSA), polybutylene succinate (PBS), and polylactic acid (PLA) are designed to reduce environmental pollution and address the challenges caused by synthetic plastics. Several biodegradable polymers used in composting

systems, including PCL, polyhydroxybutyrate (PHB), PLA, and PBS, can undergo significant degradation. A key factor in their breakdown is their chemical structure, particularly the presence of ester bonds, which are highly vulnerable to enzymatic attack by microbial systems [52].

Thermophilic actinomycetes capable of degrading PHB, PCL, and polyethersulfone (PES) have been isolated from different environments, including compost sites in Taiwan [47]. In compost conditions at around 50 °C, two thermophilic bacterial strains showed strong synergistic effects in degrading PCL wastes, significantly enhancing polymer disintegration and increasing degradation efficiency [48]. Since PCL is a thermoplastic crystalline polyester, it can be hydrolyzed into low-molecular-weight compounds by lipase enzymes and subsequently utilized by microorganisms.

For example, *Aspergillus* sp. strain ST-01, isolated from soil, was able to completely degrade PCL within six days at 50 °C under thermotolerant conditions. This strain secretes enzymes such as catalase and protease that contribute to polymer breakdown. In addition, marine microorganisms, including *Pseudomonas*, *Alcanivorax*, and *Tenacibaculum* species isolated from deep-sea sediments, have also demonstrated effective degradation of PCL [53].

TABLE 2.3: Enzymes and their degradation factors corresponding to degrading bacteria

Source	**Enzyme**	**Major Mechanism of Degradation**	**Plastics/ Microplastics**	**Optimum Conditions**	**Ref**
Ideonella sakaiensis 201-F	PETase	Hydrolysis	PET	Temperature 70–75 °C	[25]
Ideonella sakaiensis 201-F	MHETase	Hydrolysis	PET	Temperature 70–75 °C	[25]
Amycolaptosis sp.	——	Hydrolysis	PLA	Temperature 50 °C	[47]
Aspergillus oryzae	——	Hydrolysis	PBS	Temperature 50 °C	[52]
Penicillium funiculosum	——	Hydrolysis	PHB	Temperature 50 °C	[52]

Table 2.3 continued from previous page

Source	Enzyme	Major Mechanism of Degradation	Plastics/ Microplastics	Optimum Conditions	Ref
Thermomonospora and *curvata (cutinase homolog from leaf-branch compost)*	LC-cutinase	Hydrolysis	PET	Temperature 50 °C	[54]
Thermophilic, alkaliphilic, halophilic, and *psychrophilic bacteria*	Bacteriophilic enzyme	Hydrolysis	Various plastic	Salt, low, or high pH, temperatures	[26]
Pseudomonas, Arthrobacter	PME hydrolases	Hydrolysis and oxidation	PVC, PE, PP, PS (PAEs)	Temperature 30–70 °C	[50]
Bacillus sp. *GZB*	A spore-laccase	The expression of different functional genes	PC (BPA)	Adding electron donors and co-substrates	[55]
Aspergillus sp. *strain ST-01*	Catalase, Protease	Colonization	PCL	Temperature 50 °C	[53]

2.7 Enzymes Involved in the Biodegradation of Plastics Or Microplastics

2.7.1 Enzymes Responsible for the Hydrolysis of Plastics Or Microplastics

A broad range of enzymes, including cutinases, lipases, esterases, laccases, proteases,speroxidases, and ureases derived from both bacterial and fungal sources, have been reported to degrade plastics such as PE, PET, and PP [16]. In fungi, cellulase systems can depolymerize cellulose by allowing free enzymes to directly attack solid polymeric substrates, ultimately converting oligomeric products (for

example, the hydrolysis of cellobiose into glucose) [56]. Fungal enzymes, particularly depolymerases, possess strong capabilities to break down various polymers and are generally effective against materials like PET and PE. The growth and penetration of fungal hyphae play an important role in initial colonization and subsequent depolymerization, as they enhance adhesion to hydrophobic surfaces and improve enzyme–substrate interactions.

Actinomycetes, *Rhodococcus ruber*, and fungi produce lacases such as *Aspergillus flavus* and *Pleurotus ostreatus* have shown notable activity in degrading PE, likely through oxidation of the polyethylene hydrocarbon backbone [16]. In addition, several fungal species involved in the biodegradation of low-density polyethylene (LDPE) include *Fusarium solani, Aspergillus fumigatus, Alternaria solani, Spicaria spp., Phoma sp, Geomyces pannorum,* and *Penicillium* spp. [22].

The main PE-degrading microorganisms are bacteria and fungi, with fungi such as Fusarium oxysporum and Aspergillus fumigatus playing key roles. Cultures of *F. oxysporum* have demonstrated strong tolerance to high PE concentrations, inducing oxidation and visible morphological changes in PE films, while *A. fumigatus* forms biofilms that assist in LDPE degradation, achieving effective breakdown in laboratory conditions [57, 58].

In contrast, hydrolyzable plastics such as PET are degraded either by specialized microorganisms like *Ideonella sakaiensis* 201-F or by bacterial enzymes including hydrolases and keratinases. Enzymatic systems such as PETase and MHETase act cooperatively in PET degradation. Earlier studies mainly focused on esterases, lipases, keratinases, and related hydrolases for PET breakdown. Once a PET-specific hydrolase is identified, it is termed PETase [29]. Recent research has shown that PET-degrading bacteria secrete enzymes in a stepwise manner, where the combined action of two enzymes significantly enhances degradation efficiency by up to six times (Figure 3). In *I. sakaiensis*, PET is hydrolyzed into its monomers, ethylene glycol (EG) and terephthalic acid (TPA), through enzymatic depolymerization [27]. During this process, PETase and MHETase work synergistically: PETase breaks PET into intermediates such as BHET and MHET, and MHETase further converts MHET into TPA and EG [56]. This coordinated

enzymatic action has attracted considerable interest for its potential in reducing plastic waste. PETase destabilizes PET by cleaving ester bonds, while MHETase completes the conversion of intermediates into final monomers [25].

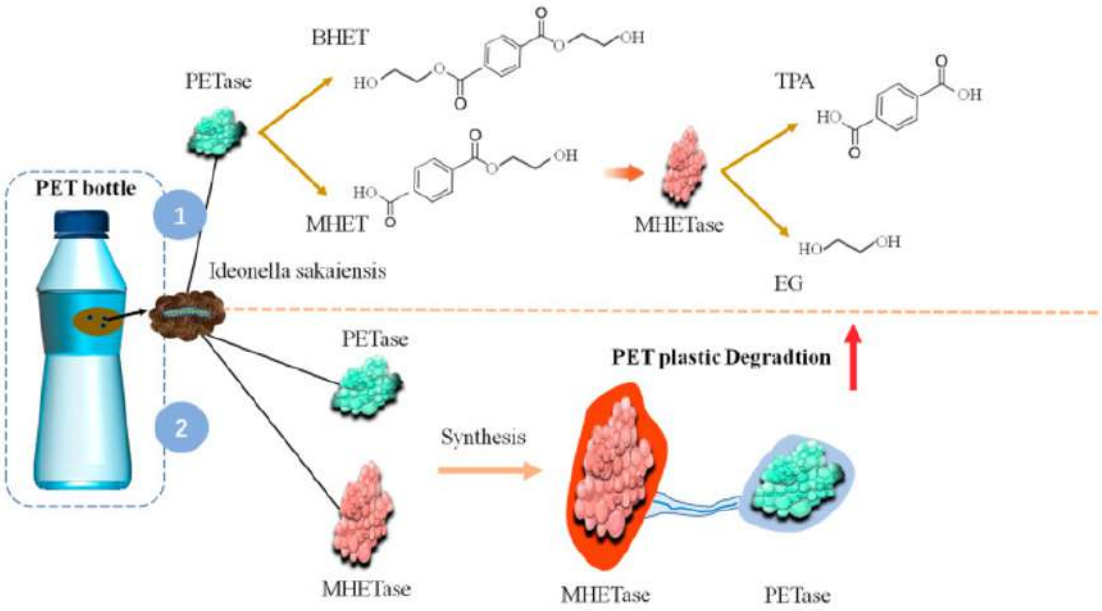

FIGURE 2.3: The enzymes responsible for PET degradation are secreted by Ideonella sakaiensis. This bacterial strain produces two key enzymes, PETase and MHETase, which work together to break down PET plastic. Furthermore, the combination of engineered PETase with MHETase has been shown to significantly enhance the overall degradation efficiency [25].

2.7.2 Biodegradation Associated Enzymes Produced by Microorganisms in the Extreme Environments

Extreme environmental microorganisms, including psychrophiles and halophiles, have shown significant potential for plastic degradation. In addition, thermophilic, halophilic, alkaliphilic, and psychrophilic bacteria found in various extreme habitats are considered capable of breaking down synthetic polymers (Table 1). These specialized environments require targeted screening to identify more efficient plastic degrading microorganisms [26]. In reality, plastic-contaminated sites often present harsh conditions such as very high or low temperatures, acidic or alkaline pH, high salinity, or elevated pressure.

Because of the unique properties of thermophilic and halophilic enzymes, they often have enhanced stability and longer functional lifespans, allowing them to be stored at room temperature with minimal loss of activity [59].

Therefore, thermophilic and extremophilic microbiomes represent a valuable and largely untapped source of plastic-degrading enzymes and microorganisms. For instance, the most thermostable leaf-branching compost cutinase (LCC) has demonstrated maximum PET depolymerization efficiency at around 65 °C [30]. At higher temperatures, many thermophilic organisms exhibit strong polymer-degrading abilities similar to high-temperature degradation systems, as they produce enzymes with increased activity that improve substrate solubility and accessibility [26].

It has also been stated for the first time that *Chelatococcus* sp. E1, isolated from compostis potentially involved in degrading polyethylene (PE). After incubation of pretreated PE sample at 60 °C, this thermophilic strain produced an evident shift in molecular weight distribution toward lower values, thereby enhancing the biodegradability of both LDPE and HDPE [39]. Overall, the development of extremozymes and the exploration of extremophilic microorganisms in harsh environments may provide an important solution to one of society's major environmental challenges.

2.8 Ways to Improve Biodegradation of Plastics Or MPs

Pretreatment of plastic waste involves its collection or recycling, including the removal of microplastics from sewage, to reduce the toxicity of additives, limit the adsorption of persistent organic pollutants (POPs), and facilitate the breakdown of polymer chains [60].

To enhance microbial attachment and subsequent degradation, the hydrophilicity of polymers must be increased through biological or chemical oxidation processes. Various pretreatment strategies have been shown to significantly improve

biodegradation efficiency. Combined approaches such as recycling and biological processing can effectively reduce plastic-related toxicity and enhance degradation outcomes (Figure 2.4).

For improved polymer degradation, the specific characteristics of different plastics are considered. Biodegradable plastics are generally more responsive to pretreatment than conventional plastics due to their favorable physicochemical properties, including greater flexibility, lower molecular weight, and the presence of reactive functional groups.

A range of physical and chemical methods are used to pretreat plastics to modify their structural and surface properties. These treatments may reduce molecular weight, break chemical bonds, create surface cracks, and introduce additional functional groups, all of which promote subsequent microbial degradation [42].

Evaluating the effects of different pretreatment methods on the biodegradation of plastics and microplastics is essential for maximizing degradation efficiency. Techniques such as high-temperature treatment, photo-oxidative catalysis, and enzymatic catalysis by microorganisms have been shown to enhance the biodegradability of plastic polymers and improve overall degradation rates (Figure 2.4).

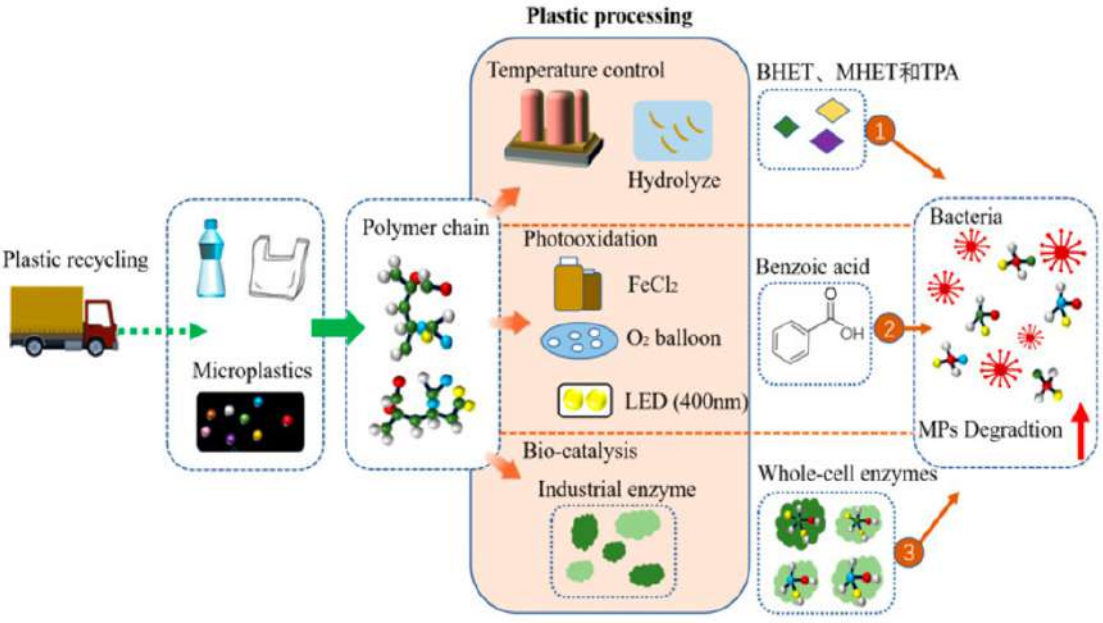

FIGURE 2.4: Pretreatment through physical and chemical methods can greatly make plastics susceptible to degradation.

Pretreatment of polyethylene (PE), such as pyrolysis, enhances its susceptibility to microbial metabolism [61]. Similarly, temperature-based pretreatment for polyethylene terephthalate (PET) improves the performance of PET-hydrolyzing enzymes, thereby increasing degradation efficiency. Temperature treatment is considered one of the most effective methods for PET pretreatment. The activity of enzymes, particularly PETase, is strongly influenced by environmental temperature and the structural properties of PET. Reduced molecular flexibility at certain temperatures can limit enzymatic action; however, at optimal temperatures, enzyme activity increases, leading to more efficient catalysis. Studies also indicate that plastics subjected to thermal treatment exhibit enhanced biodegradability, as enzymes more effectively cleave long polymer chains after structural weakening [8].

For example, thermally pretreated high-density polyethylene (HDPE) showed efficient biodegradation by Klebsiella pneumoniae CH001, with a notable reduction in tensile strength following treatment [42] (Figure 4).

The incorporation of biodegradable additives, photo-initiators, or copolymerization techniques can further enhance PE degradation and promote weight reduction [62]. Photocatalysis has emerged as an environmentally friendly approach in recent years [63]. Research demonstrates that simple iron salts can efficiently catalyze oxidative bond cleavage under 400 nm LED irradiation in the presence of oxygen or air, with ferrous chloride acting as an efficient photocatalyst [64]. Likewise, aromatic hydrocarbons such as cyclohexylbenzene and isopropylbenzene can undergo catalytic oxidation, resulting in C–C bond cleavage and conversion into compounds like benzoic acid under suitable conditions [65]. Experimental findings confirm that for effective degradation light, $FeCl_3$, and oxygen are essential (Figure 4), and this method has also proven useful in degrading high–molecular-weight polystyrene (PS) [64].

Enzymatic surface adjustment of polymer fibers, involving modifications to functional groups on plastic surfaces, can improve properties such as wettability, dyeing efficiency, durability, and resistance to pilling. This process ultimately increases polymer hydrophilicity, as demonstrated by enzymes like lipase from *Candida*

antarctica and keratinase from *Aspergillus oryzae* [39]. For plastics with carbon–carbon backbones, biodegradation using whole-cell enzyme systems is considered particularly effective [66]. A multidisciplinary strategy involving monomer-level biocatalysis of PET through whole-cell systems enables the formation of a biological recycling cycle. Whole cell catalysis enhances enzyme–substrate interactions by reducing hydrophobicity and improving binding to highly crystalline PET, involving two main stages: adsorption and hydrolysis [27].

An example of this approach is the anaerobic thermophilic bacterium *Clostridium thermocellum*, which integrates enzyme production and PET hydrolysis within a single system (Figure 4). Experimental results show that PET films can lose nearly 60% of their weight after 14 days of incubation at 60 °C using this organism [67]. Therefore, whole-cell catalysis represents a promising strategy for pretreatment and biodegradation enhancement. Overall, the use of diverse pretreatment techniques including thermal methods, photo-treatment, enzymatic modification, and additive incorporation has significantly improved the biodegradation of plastics and microplastics [68].

Chapter 3

Materials and Methods

3.1 Material and Methods

3.1.1 List of Equipment

Autoclave, Incubator, electric Stirrer, Vortex, Microscope, Shaker, Measuring Balance, Laminar Flow, Grinder, PCR Thermocycler, Thermometer, Nucleotide Sequencer and Shaker.

3.1.2 List of Apparatus

Falcon Tubes (50 ml), Sample Storage Bags (7 inch * 8 inch), Beakers, Spatula, Petri plates (100mm * 15mm), Spirit Lamp, Conical Flask (250ml, 500ml, and 1000ml), measuring cylinders, Test tubes (20 ml), Eppendorf Tubes (2ml), Micropipettes (200 μl, 1000 μl), Micropipette tips, Dropper, Gloves, Mortar, Pestle, Parafilm tape, Paper tape, Spreader and Inoculation Loop.

3.1.3 List of Chemicals

Potato Dextrose Agar, Ethanol, Distilled Water, Lactophenol Blue Dye, Polyethylene Powder, Polyethylene strips, Czepak Agar, Pectin Substrate.

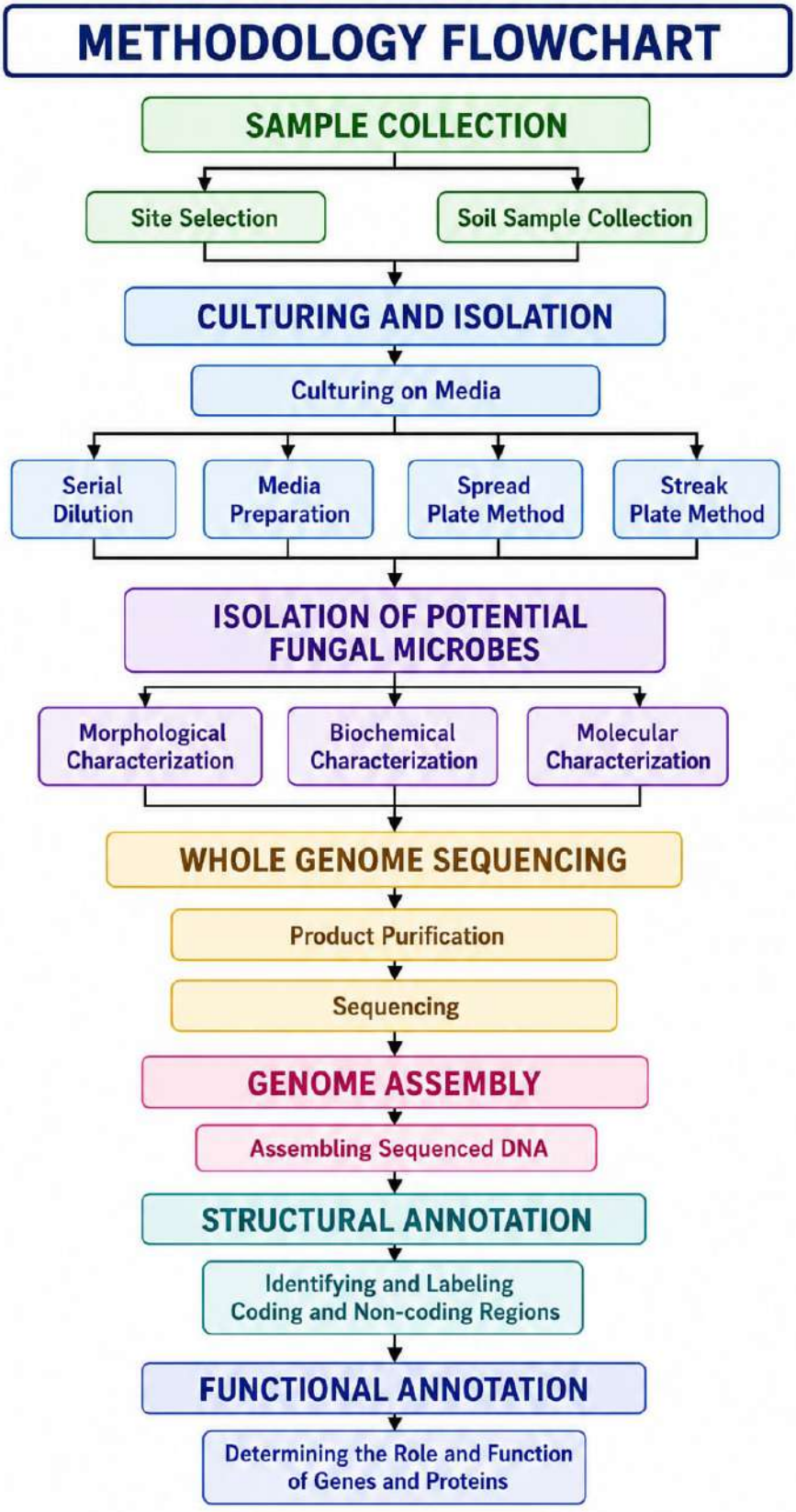

FIGURE 3.1: Flow Chart Shows Major Steps of Methodology

3.2 Sample Collection

3.2.1 Site Selection

The H-11 municipal solid waste site located in the H-11 sector; situated in the northern part of Islamabad, near the Margalla Hills was selected for sampling. The garbage site covered a large area and received waste from various sources, including households, markets, and industries.

The site also received a large volume of plastic waste, which could serve as a potential source for the isolation of plastic-degrading fungal strains (Waheed et al., 2010).

3.2.2 Selection Criteria

The site was easily accessible by road and located in close proximity to various residential and commercial areas. This site was selected as the site for the collection of soil samples for isolation of potential fungal strains responsible for degradation of plastic (Figure 3.2). The site was chosen because of its reputation as a major landfill and garbage disposal area.

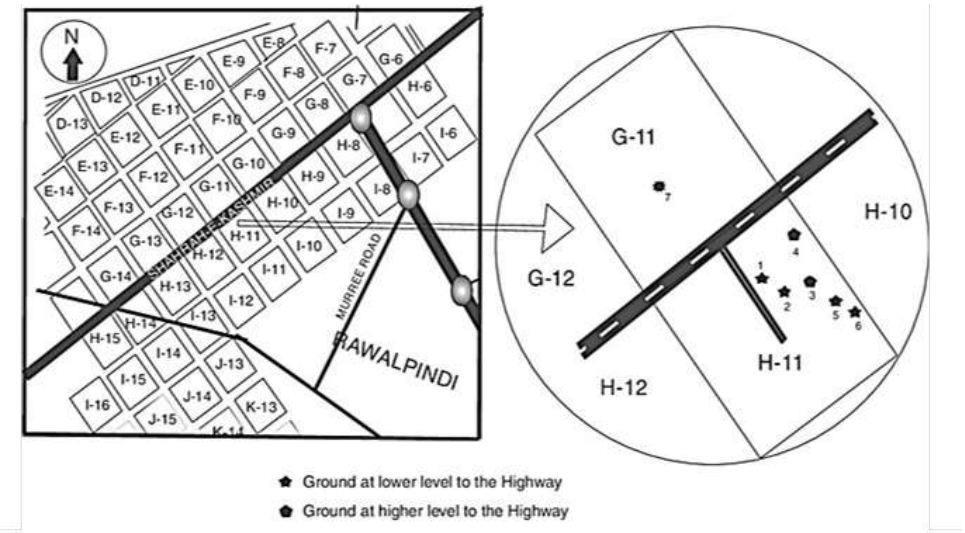

(a)

(b)

FIGURE 3.2: Pictures of theH-11 Municipal Solid Waste garbage sites

3.2.3 Soil Samples Collection

The soil sample collection from the H-11 garbage site in Islamabad was conducted using proper safety measures and protocols to ensure the samples' quality and minimize potential risks to personnel. The collection was performed at a depth of 5cm for each of the five designated sampling locations, labeled as S1 to S5 (Figure 3.3, 3.4).

At each sampling location, the top layer of the soil was removed using the sterilized shovel to expose the undisturbed soil. A sterile sampling tube was then inserted into the soil to a depth of 5cm, and the soil was carefully extracted and placed

into a sterile sample container. The sampling tube was thoroughly cleaned with 70% ethanol after each use to prevent any potential cross-contamination.

The samples were labeled as per the designated sampling locations and shifted to the laboratory under sterile conditions and stored at 4°C in refrigerator till further analysis. Proper labeling were carried out to ensure proper identification of each sample. All waste materials, including used gloves, masks, and other contaminated materials, were collected and disposed of appropriately, following the safety protocols.

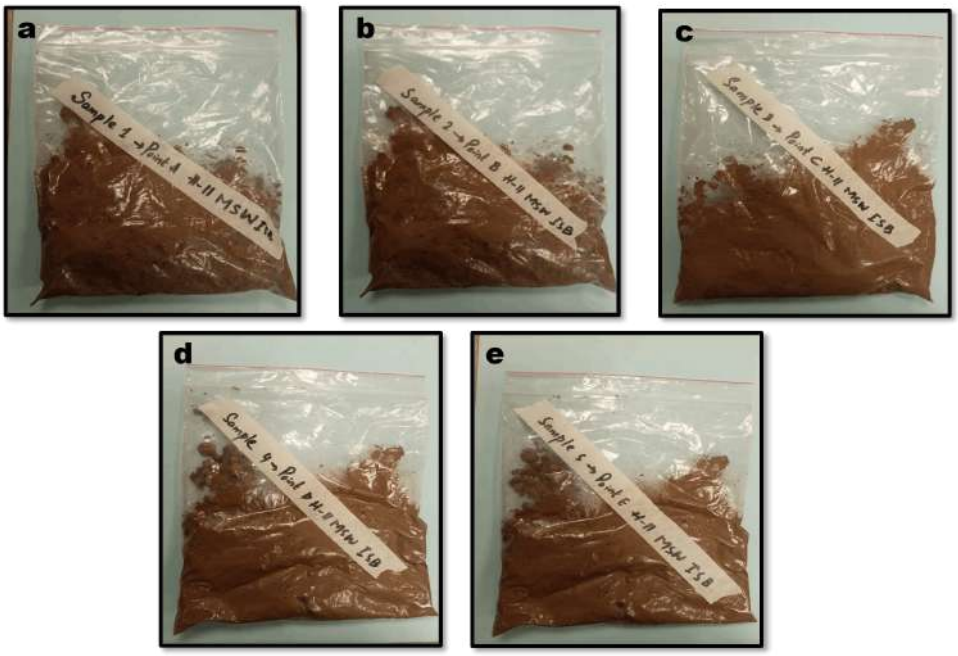

FIGURE 3.3: Pictures of 5 samples collected from the H-11 Garbage site Islamabad; a (Sample 1), b (Sample 2), c (Sample 3), d (Sample 4), e (Sample 5).

3.2.4 Culturing on Media

3.2.4.1 Serial Dilution of Collected Soil Samples

The 5 soil samples (Sample 1 to Sample 5) serial dilution (10^1 to 10^7) were prepared. From each Sample, 1 gram of soil was weighed and placed into a sterile tube containing 9 ml of sterile water. The tube was thoroughly mixed to ensure

that the soil was evenly distributed in the water. From this 7 dilutions were prepared with the appropriate dilution factors, ranging from 101 to 107. Each tube was filled with 9 ml of sterile water (Figure 3.5).

Tubes were labeled as S1D1, S1D2, S1D3, S1D4, S1D5, S1D6, and S1D7, respectively.

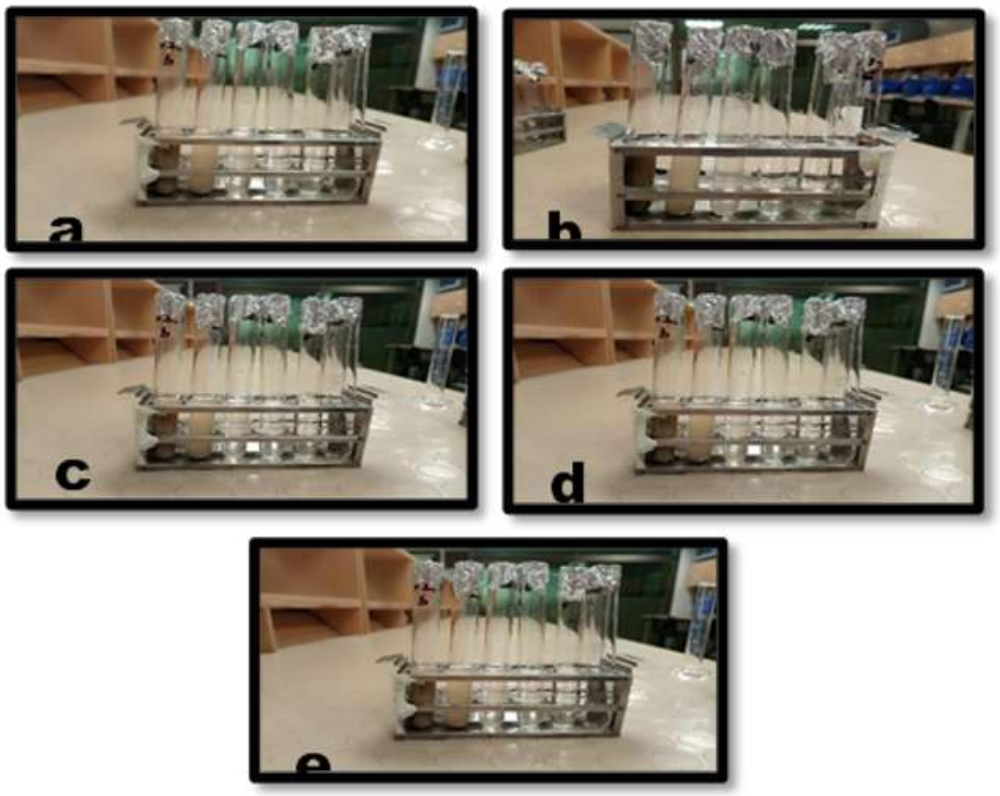

FIGURE 3.4: Pictures of the Serial Dilutions of the above samples collected from H-11 Garbage site Islamabad; a (Sample 1), b (Sample 2), c (Sample 3), d (Sample 4), e (Sample 5).

3.3 Isolation of Plastic Degrading Fungi

3.3.1 Media Preparation

The following method was used to prepare Potato Dextrose Agar (PDA) from scratch using raw potatoes, dextrose sugar, and agar (Table 3.1). The required volume prepared was 525 ml.

TABLE 3.1: Composition of Potato Dextrose Agar Media, required to prepare for 525ml

Ingredients	**Quantity**
Potatoes	250 g
Dextrose sugar	10 g
Agar	10 g
Distilled water	525 ml

First, 250 g of raw potatoes were washed, and cut into small pieces. The potato pieces were added to 250 ml of distilled water in a saucepan and boiled for 30 minutes until the potatoes were soft and the water had turned cloudy. The potato mixture was then filtered through cheesecloth into a sterile flask. The volume of the resulting potato extract was adjusted to 525 ml with additional distilled water.

Next, 10.5 g of agar powder was added to the potato extract and stirred until completely dissolved. Then, 10.5 g of dextrose sugar was added and stirred until it was fully dissolved. 10 grams of Polyethylene Powder was also added during media preparation.

The polyethylene powder was used to evaluate the degradation capability of fungi and to observe the formation of halo zones or zones of activity. Polyethylene powder was added to the Potato Dextrose Agar (PDA) media during preparation, in which the fungi were cultured. The powder serves as the sole carbon source for the fungi to grow, which then break down the polyethylene through their metabolic activity. As the fungi degrade the polyethylene, they create clear zones of activity around their colonies on the PDA plates, which are referred to as halo zones. The size of the halo zone reflects the fungal degradation capability, with larger halo zones indicating greater degradation.

The flask containing the PDA mixture was sterilized by autoclaving at 121°C and 15 psi for 15 minutes. After sterilization, the flask was removed from the autoclave and allowed to cool to 45-50°C.

Prior to pouring the PDA, the glass petri plates were autoclaved to ensure sterility. Once the PDA mixture had cooled to 45-50°C, it was dispensed into each sterile petri dish using a sterile pipette. Approximately 15 ml of the PDA mixture was dispensed into each petri dish.

The plates were then allowed to cool and solidify in a sterile environment a laminar flow hood. Once the plates had solidified, they were labeled with appropriate information, including the sample number (S1, S2, S3, S4, or S5) and the dilution number (D1 to D7).

For sample 1, the first PDA plate was labeled as S1D1 and the subsequent plates were labeled sequentially as S1D2, S1D3, S1D4, S1D5, S1D6, and S1D7. The same labeling scheme was applied to the plates for samples 2, 3, 4, and 5.

3.3.2 Spread Plate Method

The spread plate method was used to spread the serially diluted soil samples on 35 petri plates that were previously prepared with Potato Dextrose Agar (PDA) and labeled according to their dilution level (e.g., S1D1, S1D2, S1D3, etc.).

0.1 ml of the diluted soil sample from each dilution was poured on the surface of the corresponding labeled petri plate.

A sterile spreader was used to evenly spread the soil sample on the surface of the PDA. The spreader was held at an angle and gently moved back and forth over the surface of the agar to ensure an even distribution of the sample.

This step was repeated for all of the petri plates corresponding to each dilution level of each sample (i.e., S1D1 to S1D7 for sample 1, S2D1 to S2D7 for sample 2, and so on).After spreading the soil samples, the petri plates were sealed using parafilm to prevent moisture loss and contamination. The plates were then incubated at an appropriate temperature for the growth of microorganisms, such as 25°C for isolation of potential fungi strains.

3.3.3 Sub Culturing Technique

The tease mount technique was used for sub culturing the fungal growth on multiple plates and total 13 different colonies observed on the above plates to other plates for isolation.

A sterile bent needle was used to gently tease apart the fungal colony and transfer a small portion of it to a new sterile plate containing fresh PDA.

The bent needle allowed for greater precision and control during sub culturing in a sterile environment using proper aseptic techniques to prevent contamination. Multiple subcultures were performed using these techniques to ensure the isolation of pure cultures.

3.3.4 Growth of Isolated Fungal Strains on Minimal Salt Media

Ten different fungal strains were tested for their growth on Minimal Salt Media (MSM). The MSM was prepared from scratch by adding specific nutrients and salts in distilled water to make it suitable for fungal growth under sterilized environment.

The composition of MSM included $NaNO_3$, KH_2PO_4, $MgSO_4 \cdot 7\,H_2O$, $FeSO_4 \cdot 7\,H_2O$, and glucose. The pH of the media was adjusted to 6.5 before autoclaving.

TABLE 3.2: Composition of Minimal Salt Media, required to prepare for 1000ml

Sr. No.	**Nutrient/ Salt**	**Quantity (g/L)**
1	$NaNO_3$	2.0
2	KH_2PO_4	0.5
3	$MgSO_4.7H_2O$	0.5
4	$FeSO_4.7H_2O$	0.01
5	Glucose	10.0

3.4 Isolation of Potential Fungal Strains

3.4.1 Morphological Characterization using Lactophenol Blue Dye

The lactophenol blue dye was used for the preparation of slides to observe the morphology of 10 different isolated fungi. The tease mount method was utilized to spread the inoculant on a slide. The inoculant was obtained from the subcultured fungal growth on PDA plates.

To prepare the slide, a clean glass slide was taken and labeled with the sample identification. A small amount of lactophenol blue dye was added to the center of the slide, and a sterile bent type needle was used to carefully transfer the fungal colony from the MSM plate to the center of the slide. The fungal growth was teased apart using the bent type needle to make it thin and evenly spread.

The slide was then gently heated over a flame until the lactophenol blue dye was evaporated, and the slide was left to air-dry. Once the inoculant was spread on the slide, a coverslip was carefully placed over the specimen using sterile forceps to prevent any air bubbles from forming. The slide was then gently pressed to ensure even distribution of the inoculant and to remove any excess liquid.

The prepared slide was then observed under a compound microscope to study the morphology of the fungus. The use of lactophenol blue dye helped in highlighting the important structures of the fungus and aided in the identification of various morphological features of the fungus. This technique allowed for the visualization of important structures, such as the hyphae, spores, and reproductive structures of the fungi.

This technique allowed for the visualization of important structures, such as the hyphae, spores, and reproductive structures of the fungi.

3.5 Biochemical Characterization

3.5.1 Biochemical Characterization using Czepak Agar Test

Czapek agar was used for the biochemical identification of fungi. To prepare the Czapek plates, the ingredients were obtained in sterile conditions (Table 3.3).

TABLE 3.3: Composition of Czepak Agar Media, required to prepare for 1000ml

Ingredients	**Quantity**
Sodium nitrate	3.0 g
Potassium chloride	0.5 g
Magnesium sulfate heptahydrate	0.5 g
Dipotassium phosphate	1.0 g
Ferrous sulfate heptahydrate	0.01 g
Glucose	30 g
Agar	20 g
Distilled water	1000 mL

The ingredients were mixed in the distilled water and the pH was adjusted to 7.3. Autoclaving was done at 121°C for 15 minutes to sterilize the mixture. After sterilization, the mixture was poured into sterile Petri dishes and allowed to cool and solidify.

To inoculate the isolated fungal strains S1 to S10, a sterile inoculation loop was used to transfer a small amount of the fungal growth onto the Czapek agar plates. The plates were then incubated at the appropriate temperature and time for the respective fungal strains. The biochemical characteristics of the fungi were observed by monitoring their growth patterns and colony morphology on the Czapek agar plates.

3.5.2 Pectin Powder Test

Pectin powder can be used as a substrate for the biochemical characterization of isolated fungal strains. Pectin is a complex polysaccharide that can be broken

down by certain enzymes produced by fungi. When pectin is broken down, it produces various compounds, including galacturonic acid, which can be measured as a way to determine the activity of the fungal enzyme.

To use pectin powder for biochemical characterization, a small amount can be added to a liquid culture medium, such as potato dextrose broth, and inoculated with the fungal strain. The culture was incubated for a specific period of time to allow for the fungal enzyme to break down the pectin.

3.6 Molecular Characterization of Isolated Fungal Strains using 18s RNA

3.6.1 DNA Extraction Method

The fungal DNA extraction method was performed using the following procedure. A well-crushed sample weighing between 50 to 200mg was prepared. To this sample, 500μL of CTAB buffer was added, followed by the addition of 2-3μL of Merceptoethanol, Proteinase K, and 40μL of 10% SDS. The mixture was then incubated at 95°C overnight to facilitate cell lysis and release of DNA.

Then 500μL of Chloroform: Isoamyl alcohol was added to the sample tube. The tube was then subjected to centrifugation at 13000 rpm for 10 minutes. The upper aqueous layer containing the DNA was carefully transferred to a new tube after centrifugation, leaving behind the organic phase.

To the transferred aqueous layer, 500μL of ice-chilled isopropanol was added, and the mixture was incubated for 20 minutes at room temperature. Following the incubation, the tube was subjected to centrifugation at 13000 rpm for 15 minutes. This resulted in the formation of a DNA pellet at the bottom of the tube, while the supernatant was discarded.

The DNA pellet was washed by adding 500μL of 70% ethanol to the tube. Subsequently, the tube was centrifuged at 8000 rpm for 5 minutes. The supernatant was discarded, and the pellet was allowed to air dry.

To resuspend the DNA pellet, 40μL of Low TE buffer was added to the tube. To facilitate the dissolution of the DNA in the buffer the tube was then incubated at 60°C for 30 minutes .

It is important to note that the purified extracted fungal DNA sample was stored at -20°C for further analysis and experimentation. The reagents and their respective volumes used in the DNA extraction process are available in Appendix 1.

3.6.1.1 Primers

The primers used for PCR amplification were ITS1 (forward) and ITS4 (reverse). The primer sequences, melting temperatures (Tm), and expected product size are listed in Table 3.4.

TABLE 3.4: Primer details

Primers	**Sequence**	**Tm**	**Product Size**
Forward	5'-TCCGTAGGTGAACCTGCGG-3' (19mer)	61.7°C	530 bp
Reverse	5'-TCCTCCGCTTATTGATATGC-3' (20mer)	56.4°C	530 bp

Please note that the above tables provide an overview of the PCR reaction mixture components, amplification program, and primer details used in the PCR method for amplifying DNA fragments with the ITS1 and ITS4 primers.

3.6.1.2 Gel Electrophoresis

The purified PCR products were subjected to electrophoresis using a 1.5% agarose gel. To prepare the gel, 0.45g of agarose was added to 30ml of 1x TBE buffer. The

solution was then heated in a microwave for 1 minute and allowed to cool down slightly. After cooling, 5μl of ethidium bromide was added to the gel solution.

For loading the PCR purified samples onto the gel, 5μl of each sample was mixed with 2μl of loading dye. The mixture was then carefully loaded into the wells of the agarose gel. To facilitate the visualization and estimation of DNA fragment sizes, a ladder was included in one of the wells.

3.6.1.3 18s RNA Sequencing

The gel was then subjected to electrophoresis at an appropriate voltage for a suitable duration. This process enabled the DNA fragments to move through the gel matrix according to their size. After electrophoresis, the gel was examined under UV light to visualize and confirm the presence of DNA bands. The ethidium bromide incorporated in the gel fluoresced upon interaction with the DNA, enabling the visualization of the DNA bands.

Overall, the electrophoresis process enabled the separation and visualization of the PCR products on a 1.5% agarose gel. The addition of loading dye and the use of a ladder aided in sample loading and size estimation, respectively. The resulting gel image provided valuable information about the size and integrity of the amplified DNA fragments.

3.7 Plastic Degradation Using *R. arrhizus*

The biodegradation of a polyethylene strip, with a mass of 0.04 g, was analyzed in vitro using a fungal culture of Rhizopus arrhizus. The strip was incubated at 25°C for 15 days on a soil plate. During the incubation period, the strip's weight was reduced to 0.02 g.

In vitro analysis of the biodegradation process was conducted, and it was observed that the polyethylene strip's weight was passively reduced to 0.02 g by the fungal culture of Rhizopus arrhizus. The strip had been incubated at 25°C for 15 days

on a soil plate, providing an ideal environment for the degradation process to occur. Throughout the incubation period, the strip underwent degradation, and the reduction in weight was evident.

The passive reduction of the strip's weight to 0.02 g indicated the effectiveness of the fungal culture in breaking down the polyethylene material. The fungal culture of Rhizopus arrhizus demonstrated its capability to actively degrade the polyethylene strip under the given conditions.

3.8 Whole Genome Sequencing

3.8.1 Sequencing

The commercial service of Macrogen Korea was utilized for whole genome sequencing including DNA extraction.

3.9 Whole Genome Annotation

Whole genome annotation refers to identifying genomic elements such as genes, coding regions, and their biological functions within a genome sequence. In fungal genomics, annotation is divided into two major components: structural annotation and functional annotation.

3.9.1 Galaxy Platform

Galaxy Project is a web-based bioinformatics platform that enables the analysis of high-throughput sequencing data through an easy graphical interface. It allows researchers to process raw sequencing data into meaningful biological information without requiring advanced programming skills. Galaxy is widely used in genomics and molecular biology for building reproducible and transparent analysis workflows.

The platform integrates multiple bioinformatics tools within a single system, enabling data upload, preprocessing, genome analysis, and visualization in one environment. It ensures reproducibility by recording every step of the workflow. In fungal genome studies, Galaxy is particularly useful for converting raw sequencing reads into assembled genomes and annotated gene datasets for downstream biological interpretation.

The Galaxy workflow integrates several bioinformatics tools for fungal genome analysis, including FastQC and MultiQC, fastp/Trimmomatic, QUAST, BUSCO, Augustus, BLAST+, InterProScan, and eggNOG-mapper are used, while fungal identification is supported through comparison with the UNITE database.

3.9.2 Tools and Databases

A variety of computational tools and biological databases were used for accurate annotation of fungal genomes. These tools are categorized based on their roles in sequence similarity, domain identification, orthology assignment, and pathway mapping

3.9.2.1 QUAST

QUAST (Quality Assessment Tool for Genome Assemblies) is a powerful tool used to evaluate and compare genome assemblies. It generates detailed statistical summaries, including metrics such as total assembly size, number of contigs, N50 and L50 values, GC content, genome fraction, and detection of misassemblies. QUAST can also compare assemblies against a reference genome, if available, to identify structural errors, gaps, and inconsistencies.

This allows researchers to assess the continuity, completeness, and correctness of assembled genomes. By providing both numerical results and visual plots, QUAST helps in selecting the best assembly among multiple versions and ensures high-quality genome reconstruction.

3.9.2.2 BUSCO

BUSCO (Benchmarking Universal Single-Copy Orthologs) is a bioinformatics tool used to sevaluate the completeness and quality of genome assemblies and gene annotations. It evaluates genomes based on the presence of conserved single-copy orthologous genes that are expected to exist in a given lineage, such as fungi or eukaryotes. BUSCO classifies results into categories like complete (single-copy or duplicated), fragmented, and missing genes, providing a clear measure of genome completeness. This analysis helps researchers determine whether important genes are present or absent in the assembly, making it a reliable method for validating genome quality and annotation accuracy.

3.9.2.3 Augustus

Augustus is a gene prediction software designed for eukaryotic genomes, including fungi. It identifies protein-coding genes by analyzing genomic sequences and predicting exon-intron structures using statistical models. Augustus is widely used in genome annotation pipelines to generate accurate gene models in newly assembled genomes.

3.9.2.4 InterProScan

InterProScan integrates multiple protein signature databases such as Pfam, SMART, and PROSITE to identify conserved domains, motifs, and protein families. In fungal genome annotation, it provides detailed functional classification of proteins and helps predict enzyme activity, structural roles, and biological processes.

3.9.2.5 EggNOG-mapper

EggNOG-mapper assigns functional annotations based on orthologous groups from evolutionary databases. It provides Gene Ontology (GO) terms, KEGG pathways,

and functional descriptions for fungal genes. It is widely used for predicting functions of unknown or hypothetical fungal proteins.

3.9.2.6 KEGG Pathway Analysis

KEGG is used to map fungal genes into metabolic and biochemical pathways. It helps in understanding the organism's metabolism, energy production, and biosynthetic capabilities, which are important for interpreting fungal biological functions.

3.9.2.7 tRNAscan-SE and Barrnap

These tools identify non-coding RNA genes in fungal genomes. tRNAscan-SE detects transfer RNA genes, while Barrnap identifies ribosomal RNA regions, contributing to complete genome functional annotation.

3.9.3 Whole Genome Analysis

3.9.3.1 Data Acquisition and Preprocessing

Raw sequencing data of the fungal genome generated from Illumina platforms were obtained in FASTQ format and imported into Galaxy for initial processing. Quality assessment of the reads was performed using FastQC to evaluate parameters such as per-base quality scores, GC content, and sequence duplication levels.

Low-quality reads and technical artifacts were removed using Trimmomatic, where reads with a Phred quality score below Q20 were filtered out, and adapter sequences were trimmed. Additionally, a minimum read length of 50 bp was applied to retain only high-quality reads.

This preprocessing step ensured that clean and reliable data were used for downstream genome assembly and analysis.

3.9.3.2 De Novo Genome Assembly

High-quality filtered reads were subjected to de novo genome assembly to reconstruct the fungal genome without the use of a reference sequence. The assembly was performed using SPAdes, which employs a de Bruijn graph-based algorithm optimized for assembling short-read sequencing data. Multiple k-mer sizes (typically ranging from 21 to 127 bp) were utilized to improve assembly accuracy and resolve repetitive regions commonly found in fungal genomes.

Prior to assembly, error correction of reads was carried out within SPAdes to enhance sequence accuracy. The assembler effectively handled variations in sequencing depth and genome complexity, producing contiguous sequences (contigs) representing the draft fungal genome. The resulting assembly was further processed for downstream structural and functional annotation.

3.9.3.3 Assembly Evaluation and Quality Assessment

The quality and reliability of the assembled fungal genome were evaluated using QUAST (Quality Assessment Tool for Genome Assemblies). QUAST generated comprehensive statistical metrics, including total genome length, number of contigs, N50 and L50 values, GC content, and detection of misassemblies. These parameters provided insights into the continuity and structural accuracy of the assembled genome.

To further assess genome completeness, BUSCO (Benchmarking Universal Single-Copy Orthologs) analysis was performed using a fungi-specific lineage dataset. BUSCO evaluates the presence of conserved single-copy orthologous genes expected in fungal genomes and categorizes them as complete (single-copy or duplicated), fragmented, or missing.

This assessment ensured that the assembled genome contained the majority of expected conserved genes, indicating a high-quality and near-complete genome assembly.

3.9.3.4 Structural Annotation

The structural annotation of the fungal genome was carried out using the Galaxy platform through a workflow specifically designed for eukaryotic organisms. The process began with a high-quality assembled genome, which was preprocessed by filtering contigs and removing sequences shorter than 500 bp to eliminate low-confidence regions and potential assembly artifacts. Gene prediction was performed using AUGUSTUS and GeneMark-ES, both of which are optimized for fungal genomes and capable of accurately identifying complex gene structures, including exons, introns, coding regions, and splice sites. These tools utilize de novo prediction methods along with self-training algorithms, and they analyze important sequence features such as codon usage bias, GC content variation, and conserved exon–intron boundaries to improve prediction accuracy in intron-rich fungal genomes.

In addition to protein-coding genes, non-coding RNA elements were identified using specialized tools within Galaxy. tRNAscan-SE was used to detect transfer RNA genes, while Barrnap was applied for the identification of ribosomal RNA regions. Repetitive and transposable elements, which are abundant in fungal genomes, were detected and masked using RepeatMasker to prevent false gene predictions. Furthermore, predicted protein sequences were validated through similarity searches using BLAST against databases such as NCBI NR and UniProt, while conserved protein domains were identified using HMMER with the Pfam database. The final outputs included standardized GFF3 annotation files, FASTA files of predicted sequences, and detailed reports summarizing annotation quality and statistics, providing a reliable basis for downstream functional analysis.

3.9.3.5 Functional Annotation

The functional annotation of the fungal genome was performed in the Galaxy platform using a combination of homology-based searches and domain-based analysis to assign biological functions to predicted genes. The workflow started with a high-quality assembled genome and its corresponding structural annotation file

(GFF3). Predicted protein sequences were analyzed using BLAST+ against curated databases such as UniProt and NCBI NR to identify homologous sequences and infer potential gene functions based on sequence similarity. This step provided the initial functional classification of genes and helped in identifying conserved and species-specific fungal proteins.

Further functional characterization was carried out using InterProScan within Galaxy, which integrates multiple protein signature databases such as Pfam, SMART, and PROSITE to identify conserved domains, motifs, and protein families. This allowed detailed annotation of protein functions, including enzymatic activities and structural roles. In addition, EggNOG-mapper was used to assign orthologous groups, Gene Ontology (GO) terms, and pathway-level functions, providing insight into the biological processes, molecular functions, and cellular components associated with fungal genes. KEGG pathway mapping was also performed to reconstruct metabolic pathways and understand the biochemical capabilities of the fungal organism.

To enhance annotation accuracy, hypothetical proteins were further analyzed based on conserved domain predictions and sequence similarity patterns to assign putative functions wherever possible. Non-coding RNA elements such as tRNAs and rRNAs, previously identified during structural annotation, were integrated into the functional dataset to provide a complete genomic overview. This comprehensive functional annotation pipeline in Galaxy enabled the systematic interpretation of fungal gene functions and metabolic potential, forming a strong basis for comparative genomics and downstream biological analysis.

Chapter 4

Results

4.1 Phase 1: Identification of Plastic Degrading Fungus

4.1.1 Colony Morphology of 13 PDA Isolated Fungal Strains

The Colony Morphology of the 13 Different PDA Isolated Fungal strains was observed by examining the growth on Petri dishes. The morphology of the colonies was observed by noting the size, shape, color, texture, and elevation of the colonies. The color of the colonies was also observed from both the front and the back sides of the Petri dishes, and any color changes were noted. The observations were recorded in a systematic and standardized manner (Table 4.1).

TABLE 4.1: Growth Analysis of 13 Different Fungal Isolates on PDA Media and Colony Morphology

Fungal Isolates	**Colony Appearance**	**Size of colony (mm)**	**Color / Reverse Color**	**Surface & Margin**	**Elevation**	**Form**
S1-C (a)		80x80	Greyish Black / Orange brown	Smooth & Entire	Raised Spreading edge	Circular Filamentous

Table 4.1 continued from previous page

Fungal Isolates	Colony Appearance	Size of colony (mm)	Color / Reverse Color	Surface & Margin	Elevation	Form
S1-B1 (b)		80x80	Orange Center, White margin / Black center, Pale white margin	Wrinkled & Lobate	Wrinkled umbonate	Irregular
S3-33 (c)		45x20	Pale green Center, White margin / Dark orange center, Pale orange margins	Smooth & Entire	Raised spreading edge	Circular filamentous
S3-31 (d)		80x80	Dark green color / Black center, Yellowish green margins	Dry powdery & Curled Margins	Flat	Rhizoid
S1-33 (e)		70x80	Sea green / Brown spots, Orangish white margin	Dry powdery & Curled Margins	Flat	Irregular
S4-2 (f)		40x35	Greyish white with black dots / Reddish orange center, Pale orange margins	Smooth & Entire Margins	Raised spreading edge	Circular filamentous
S4-1 (g)		80x80	White with black dots / Brown Center, Yellow margins	Smooth & Entire Margins	Raised spreading edge	Circular filamentous

Table 4.1 continued from previous page

Fungal Isolates	Colony Appearance	Size of colony (mm)	Color / Reverse Color	Surface & Margin	Elevation	Form
S1-B3 (h)		70x80	Bright green / Bright orange	Dry powdery & Lobate	Umbonate	Rhizoid
S1-31 (i)		10x20	Turquoise / White center, with yellow margins	Dry powdery & Undulate	Flat	Irregular
S1-1A (j)		70x70	Milky white / Orangish yellow	Smooth & Entire margin	Raised Spreading edge	Circular filamentous
S5-32 (k)		70x70	Milky white with black dots / Black center with pale white margin	Smooth & Entire margin	Raised Spreading edge	Circular filamentous
S1-B2 (l)		60x60	Black and white / Reddish orange	Smooth & Entire margin	Raised Spreading edge	Circular filamentous
S1-C1 (m)		80x80	White center with black edges / Black center with orangish yellow margin	Smooth & Entire margin	Raised Spreading edge	Circular filamentous

The analysis of colony morphology of the 13 different fungal strains isolated from the samples collected from the H-11 garbage site in Islamabad revealed interesting findings. The colony color of most strains was mostly white with black dotted appearance, while the surface was smooth, and the form was circular and filamentous

(Figure 4.1). The margins were mostly entire, but some were lobate and undulate, while the elevation of most was flat, some were raised and spreading edges. The colors of few strains were orange, grey, green, turquoise, and milky white, with a reverse color of red, green, orange, and yellow in some. Most of the strains had black and pale white colors. The study suggest that these fungi have morphology of *Fusarium* species, *Penicillium* and *Aspergillus* species.

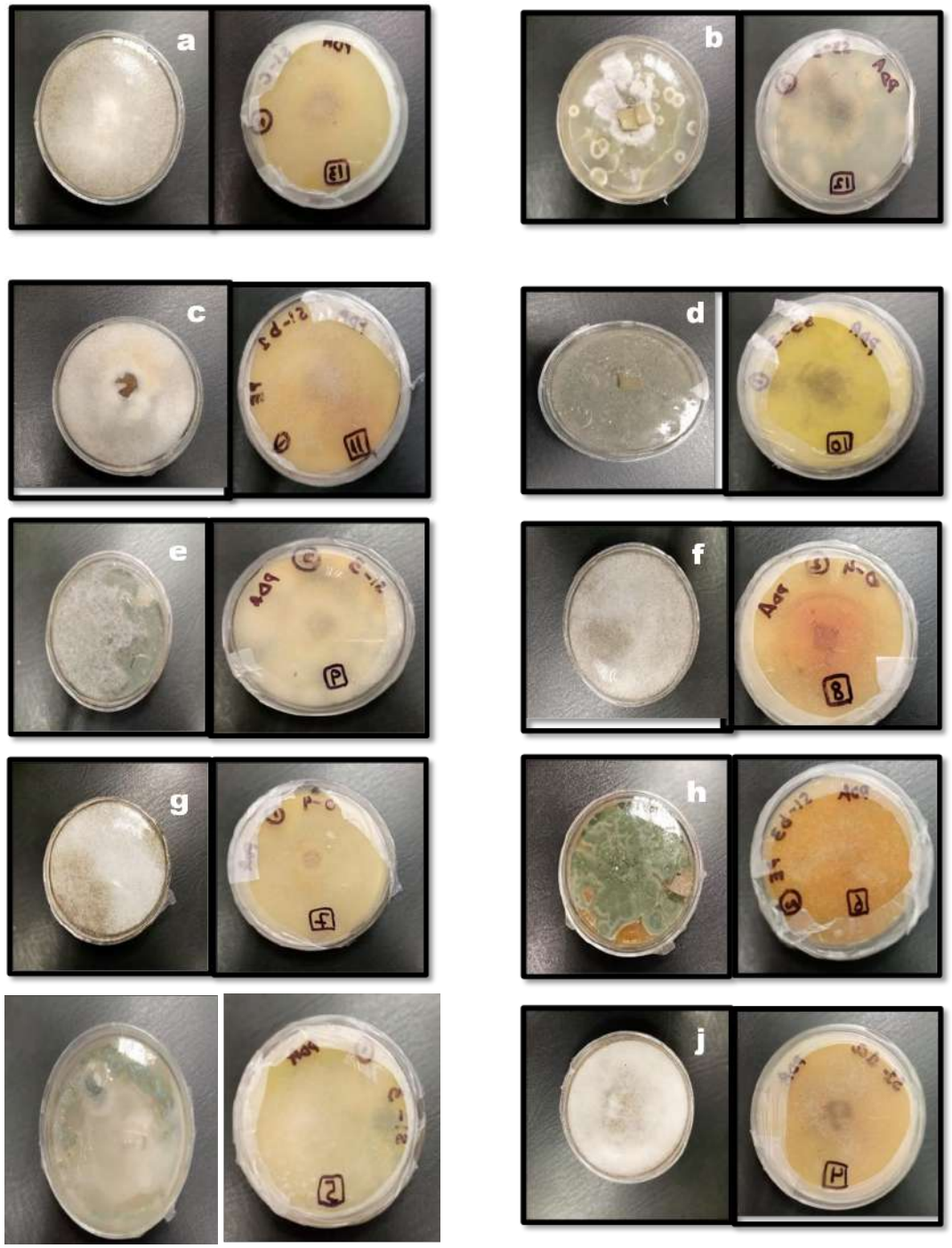

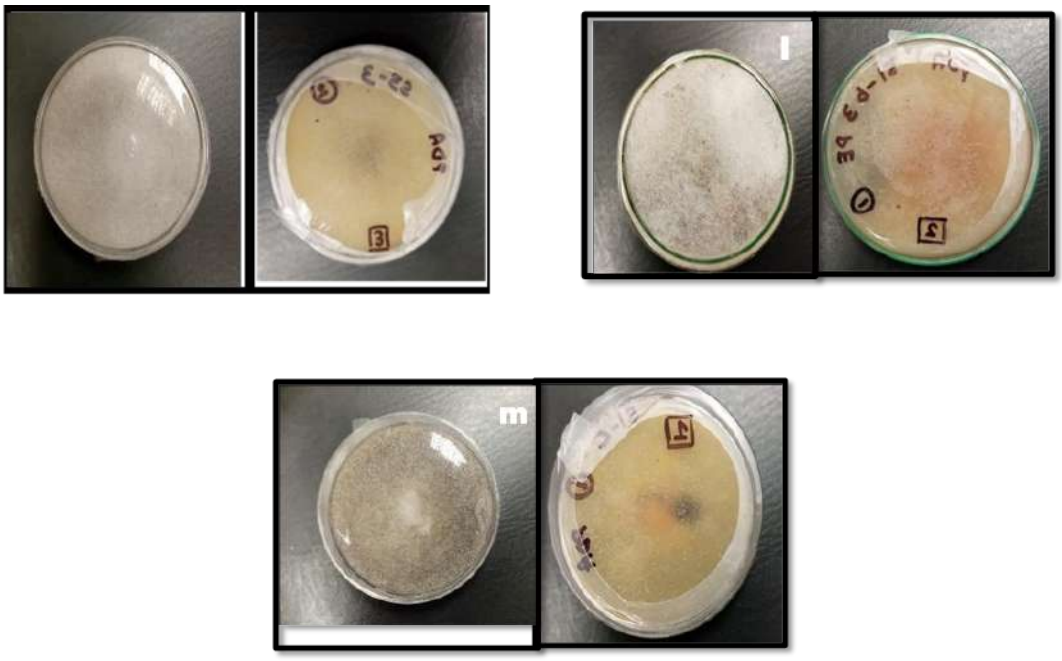

FIGURE 4.1: Pictures of the cultured plates of all 13 strains of fungus; Front and Back morphology and color change also presented; from a to m; possessing Biodegradation capability for plastic.

4.1.2 Growth of 10 Fungal Strains isolated and Sub Cultured

The growth of 10 fungal strains that were isolated and sub cultured was observed by examining the colonies on the PDA plates (Table 4.2 and Figure 4.2). The colonies were observed for their size, texture, and color change from front and back. The size was measured in millimeters, and the texture was determined by observing the surface of the colony for features like smoothness, wrinkling, or roughness. The color change from front and back was observed by holding the plate up to a light source and observing the difference in color between the front and back of the colony. This provided these fungi have morphology of *Fusarium* species, *Penicillium*, *Aspergillus* species. The observations were recorded in a table and used to identify the strains based on their colony morphology.

The results of the fungal isolates obtained from the different samples (S1, S2, S3, S4, S5, S6, S7, S8, S9, and S10) revealed a diverse range of colony appearances and characteristics. In sample S1, the colony appeared white at the center with

black margins, while the reverse color showed a reddish-orange center with yellow margins. Sample S2 exhibited a black colony with pale white margins and a smooth surface. Sample S3 displayed a dark green color with a powdery dry and lobate surface, and the reverse color showed a red center with orange margins.

Sample S4 had a green center with white margins, and the reverse color was red with pale white margins. Samples S5 and S6 exhibited greyish white colonies with black centers and pale-yellow margins. Sample S7 showed a milky white colony with a reddish-brown center and orange margins. Sample S8 had a pale green center with white margins, and the reverse color was dark green with pale yellow margins.

Sample S9 displayed a greyish black center with white margins, and the reverse color was brownish yellow. Lastly, sample S10 had a white center with pale yellow margins, and the reverse color was black with pale white margins. Overall, the colonies exhibited a smooth surface, mostly circular filamentous form, raised spreading edges, and various color combinations.

Further identification of the fungal species would require additional characterization techniques such as DNA sequencing or biochemical tests.

TABLE 4.2: Growth Analysis of 10 Different Fungal Isolates on PDA Media and Colony Morphology

Fungal Isolates	**Colony Appearance**	**Size (mm)**	**Color**	**Reverse Color**	**Surface & Margin**	**Elevation**	**Form**
S1		80x80	White center with black margins	Reddish orange center, with yellow margins	Smooth & Entire Margin	Raised Spreading edge	Circular filamentous
S2		80x80	Black	Black center, pale white margins	Smooth & Entire Margin	Raised Spreading edge	Circular filamentous

Table 4.2 continued from previous page

Fungal Isolates	Colony Appearance	Size (mm)	Color	Reverse Color	Surface & Margin	Elevation	Form
S3		45x50	Dark green	Red center, with orange margins	Powdery dry & Lobate	Flat	Irregular
S4		25x30	Green center with white margins	Red center with pale white margins	Smooth & filiform	Convex	Circular filamentous
S5		80x80	Greyish white	Black center with pale yellow margins	Smooth & Entire Margin	Raised Spreading edge	Circular filamentous
S6		80x80	Milky white with grey margins	Black center with pale yellow margins	Smooth & Entire Margin	Raised Spreading edge	Circular filamentous
S7		35x40	Milky white with	reddish brown center with orange margins	Smooth & Entire Margin	Raised Spreading edge	Circular filamentous
S8		25x15	Pale green Center with white margins	Dark green Center with pale yellow margins	Smooth & filiform	Convex	Circular filamentous
S9		45x50	Greyish black center with white margins	Brownish yellow	Smooth & Entire Margin	Raised Spreading edge	Circular filamentous

Table 4.2 continued from previous page

Fungal Isolates	Colony Appearance	Size (mm)	Color	Reverse Color	Surface & Margin	Elevation	Form
S10		30x45	White center with pale yellow margins	Black center with pale white margins	Smooth & Entire Margin	Raised Spreading edge	Circular filamentous

In conclusion, the analysis of colony morphology of 10 different fungal strains isolated from the samples collected revealed that most of the strains had circular and filamentous forms with smooth surfaces. The majority of the strains had entire margins while some had lobate and undulate margins.

The elevation of most of them was flat with some raised and spreading edges. The colony colors varied from orange, grey, green, turquoise, to milky white, while their reverse color varied from red, green, orange, yellow, to black and pale white.

The predominant color observed was white with black dotted appearance. All 10 strains were cultured in Potato Dextrose Agar (PDA) and showed similar colony morphology.

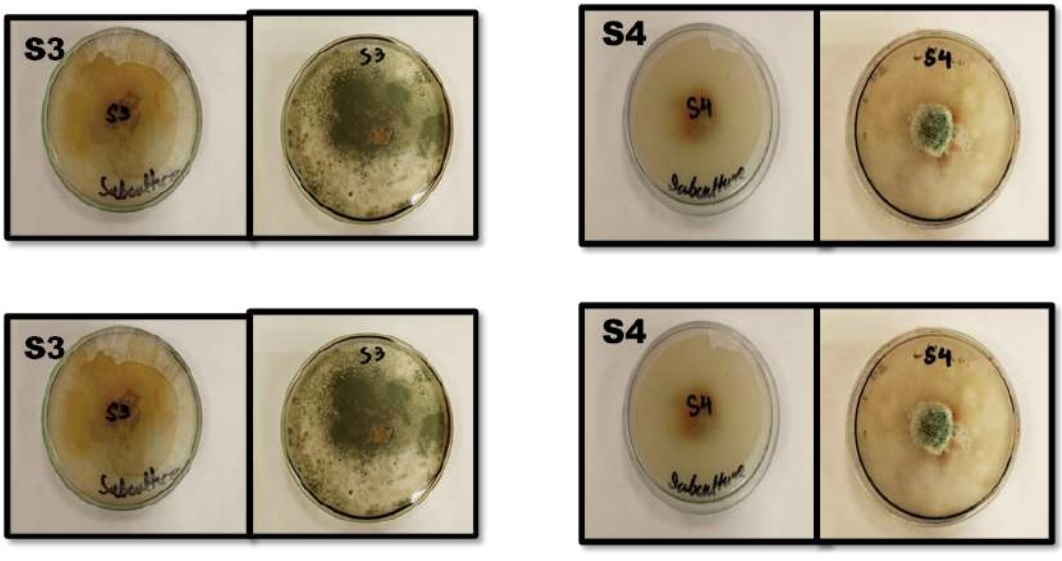

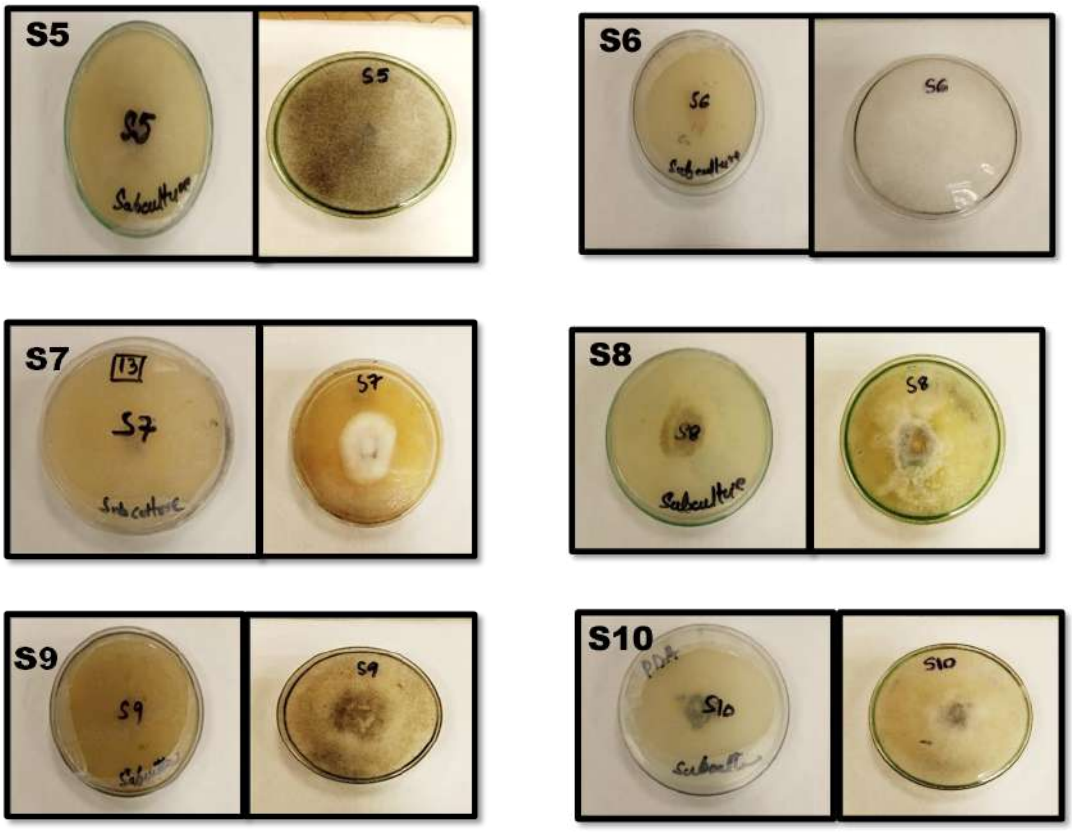

FIGURE 4.2: The cultured plates of all 10 isolated strains of fungi possess biodegradation capability for plastic; From S1 to S10, Front and back morphology is presented

4.1.3 Formation of Halo Zones Or Zone of Activity of 10 Isolated Fungal Strains

The formation of halo zones, also known as zones of activity, was observed for 10 isolated fungal strains. To do so, each strain was streaked on PDA plates and incubated at the optimal temperature and time for growth. After incubation, a layer of agarose with the substrate for the enzyme of interest was added on top of the fungal growth.

The plates were then incubated again to allow for diffusion of the enzyme into the agarose layer, resulting in the formation of a clear halo zone around the fungal colony. The size of the halo zone was measured and recorded for each strain. This method was used to determine the presence and activity of various enzymes produced by the isolated fungal strains.

The results of the fungal isolates (S1, S2, S3, S4, S5, S6, S7, S8, S9, and S10) showed the appearance of halo zones or zones of activity around the colonies, indicating their ability to produce substances that cause color changes in the surrounding medium (Table 4.3).

Sample S1 exhibited a halo zone with a size of 15mm x 15mm, resulting in a color change from yellow PDA to a reddish-orange center with yellow margins. Sample S2 had a halo zone with a size of 10mm x 10mm, leading to a color change from yellow PDA to a black center with pale white margins.

Sample S3 displayed a halo zone with a size of 30mm x 30mm, causing a color change from yellow PDA to a red center with orange margins.

Sample S4 showed a halo zone with a size of 40mm x 35mm, resulting in a color change from yellow PDA to a red center with pale white margins.

Sample S5 exhibited halo zones with sizes of 40mm x 40mm and 25mm x 25mm, leading to a color change from yellow PDA to a black center with pale yellow margins.

Sample S6 had a large halo zone with a size of 70mm x 70mm, causing a color change from yellow PDA to a black center with pale yellow margins.

Sample S7 displayed a halo zone with a size of 20mm x 10mm, resulting in a color change from yellow PDA to a reddish-brown center with orange margins.

Sample S8 showed a large halo zone with a size of 70mm x 70mm, causing a color change from yellow PDA to a dark green center with pale yellow margins.

Sample S9 exhibited halo zones with sizes of 20mm x 20mm and 20mm x 10mm, leading to a color change from yellow PDA to a brownish-yellow shade.

Lastly, sample S10 displayed halo zones with sizes of 20mm x 20mm and 10mm x 10mm, resulting in a color change from yellow PDA to a black center with pale white margins. These results indicate the potential enzymatic activities of the fungal isolates in degrading the polyethylene plastic material present in the medium.

TABLE 4.3: Formation of Halo zones or Zone of Activity & Analysis on 10 PDA plates, showcasing the degradation of plastic

Fungal Isolates	**Appearance of Halo Zone/Zone of Activity**	**Size (mm)**	**Reverse Color Change**
S1		15mm x 15mm	From Yellow PDA color to Reddish orange center, with yellow margins
S2		10mm x 10mm	From Yellow PDA color to Black center, pale white margins
S3		30mm x 30mm	From Yellow PDA color to Red center, with orange margins
S4		40mm x 35mm	From Yellow PDA color to Red center with pale white margins
S5		40mm x 40mm 25mm x 25mm	From Yellow PDA color to Black center with pale yellow margins
S6		70mm x 70 mm	From Yellow PDA color to Black center with pale yellow margins
S7		20mm x 10mm	From Yellow PDA color to reddish brown center with orange margins
S8		70mm x 70mm	From Yellow PDA color to Dark green Center with pale yellow margins

Table 4.3 continued from previous page

Fungal Isolates	Appearance of Halo Zone/Zone of Activity	Size (mm)	Reverse Color Change
S9		20mm x 20mm 20mm x 10mm	From Yellow PDA color to Brownish yellow
S10		20mm x 20mm 10mm x 10mm	From Yellow PDA color to Black center with pale white margins

The size of halozones was observed as an indicator of fungal metabolic activity and their potential to produce useful bioactive compounds.. The ability of the fungal strain to produce and secrete active compounds was indicated by the size of the halozones, and it was used for screening and selection of potential fungal strains for biotechnological applications.

4.1.4 Growth of 10 Isolated Fungal Strains on Minimal Salt Media

Minimal Salt Medium (MSM) is a selective culture medium that contains only essential inorganic salts, such as nitrogen, phosphorus, and other minerals, but does not include any organic carbon source. Because of the absence of carbon, microorganisms inoculated in this medium are forced to utilize an externally provided substrate, such as plastics, hydrocarbons, or other pollutants, as their sole source of carbon and energy. This creates a selective environment in which only those microorganisms capable of degrading and metabolizing the added compound are able to grow. Therefore, MSM is widely used to isolate and identify microorganisms with biodegradation potential and to assess their ability to break down specific substances. It is especially important in environmental microbiology and bioremediation studies, where it helps in screening microbes that can degrade harmful pollutants and contribute to environmental cleanup.

The results showed positive growth for all the strains on MSM. This indicates that the MSM provides the necessary nutrients and environment for the growth of these fungal strains. The growth pattern and rate varied among different strains, which could be attributed to their unique characteristics and growth requirements (Table 4.4, Figure 4.3).

TABLE 4.4: Growth of 10 Isolated Fungal Strains on Minimal Salt Media

Fungal Isolates	**Colony Appearance**	**Growth Results**
S1		Positive
S2		Positive
S3		Positive
S4		Positive
S5		Positive

Table 4.4 continued from previous page

Fungal Isolates	Colony Appearance	Growth Results
S6		Positive
S7		Positive
S8		Positive
S9		Positive
S10		Positive

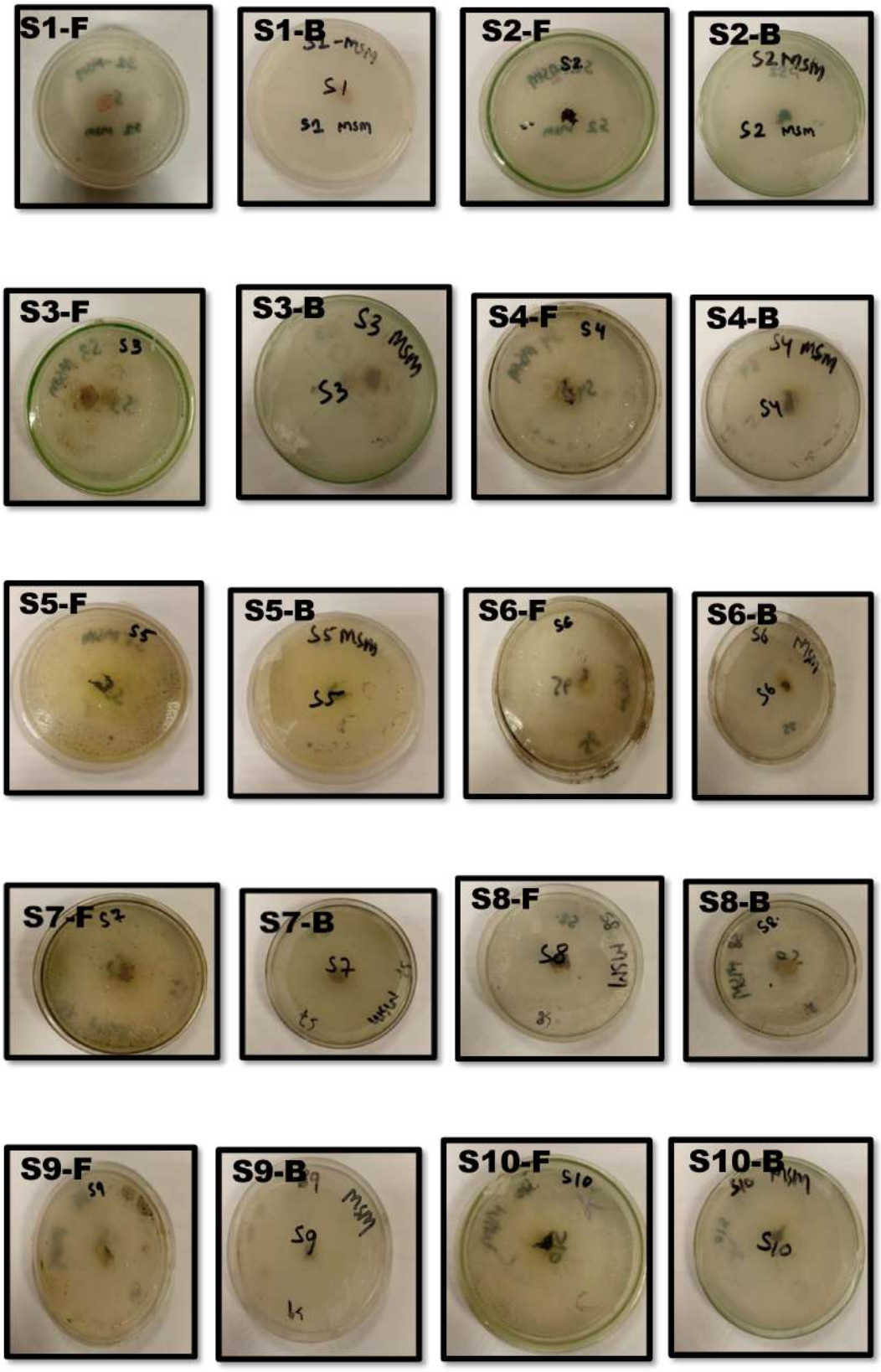

FIGURE 4.3: Results for the growth of 10 isolated strains on MSM (Minimal Salt Media), all Shows their capability to grow in stringent environment. S stands for Strain, F stands for Front, B stands for Back.

4.1.5 Morphological Characterization of the Isolated Fungal Strains

4.1.5.1 Lactophenol

Lactophenol cotton blue (LPCB) staining is a widely used technique in mycology for the morphological identification of fungal isolates, particularly for visualizing filamentous structures and hyphae.

The stain consists of three main components: phenol, which kills the fungal cells and prevents further growth or decomposition, acting as a disinfectant; lactic acid, which preserves the fungal structures by preventing them from shrinking or distorting during the staining process; and cotton blue, a dye that selectively stains the chitin present in fungal cell walls, giving the hyphae, spores, and other reproductive structures a distinct blue color against a lighter background.

This staining method is performed because it allows for clear, detailed visualization of fungal morphological features such as hyphal arrangement, septation, conidiophores, and spore formation, which are essential for the presumptive identification and classification of fungal species based on their characteristic microscopic structures.

The morphological characterization of the 10 isolated fungal strains was done by observing their colony morphology, hyphal characteristics, and spore formation. Based on colony morphology, the strains were classified as filamentous or yeast-like.

Filamentous strains exhibited characteristics such as radial growth, aerial mycelium, and pigmentation, while yeast-like strains exhibited smooth, creamy, and opaque colonies.

Hyphal characteristics were observed using lactophenol cotton blue staining, which revealed the presence of septate or aseptate hyphae (Figure 4.4). Spore formation was observed using tease mount slides, which showed different types of spores, such as conidia, sporangiospores, and chlamydospores (Table 4.5).

TABLE 4.5: Microscopic Analysis of Isolated 10 Fungal Strains with their Basic Structural Observation

Fungal Isolates	**Microscopic Image**	**Hyphae**	**Septate Hyphae**	**Fruiting body**	**Spores**
S1		Present	Absent	Absent	Present
S2	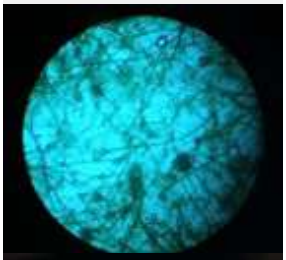	Present	Absent	Present	Present
S3	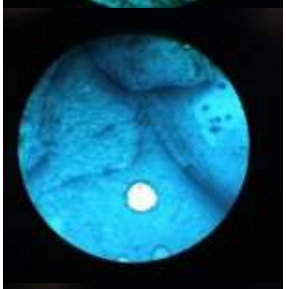	Present	Present	Absent	Present
S4	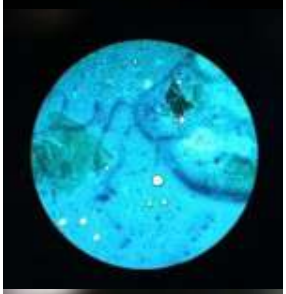	Present	Present	Absent	Present
S5		Present	Absent	Present	Present
S6	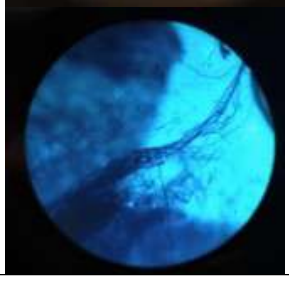	Present	Present	Absent	Absent

Table 4.5 continued from previous page

Fungal Isolates	Microscopic Image	Hyphae	Septate Hyphae	Fruiting body	Spores
S7	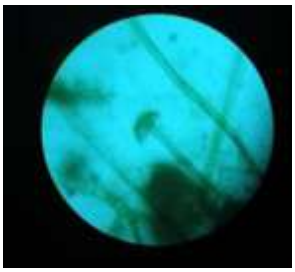	Present	Present	Present	Absent
S8	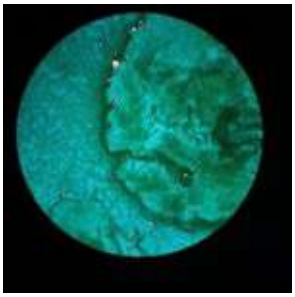	Absent	Absent	Absent	Present
S9		Present	Present	Present	Absent
S10	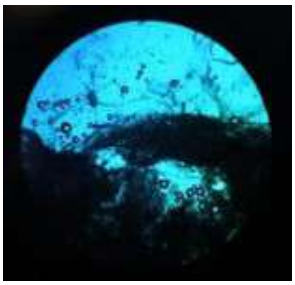	Present	Present	Present	Present

In conclusion, the microscopic examination of 10 different fungal strains using lactophenol blue stain revealed a diverse range of hyphal structures, which were mostly septate. Additionally, most of the strains were found to acquire fruiting bodies, indicating their reproductive capabilities. The use of lactophenol blue stain enabled a clear visualization of the various structures and components of the fungal cells, including the nuclei and cell walls.

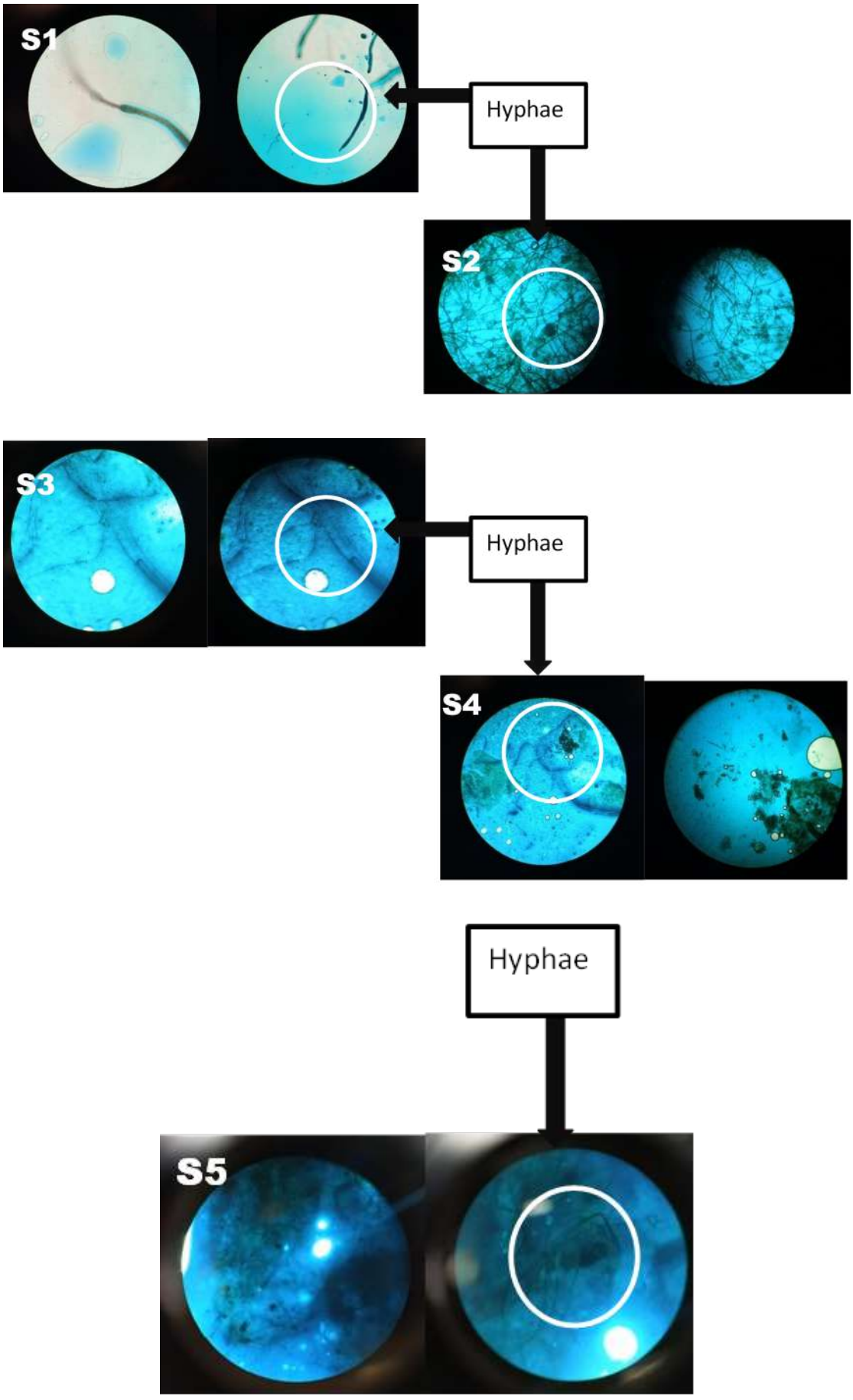
S1
Hyphae
S2
S3
Hyphae
S4
Hyphae
S5

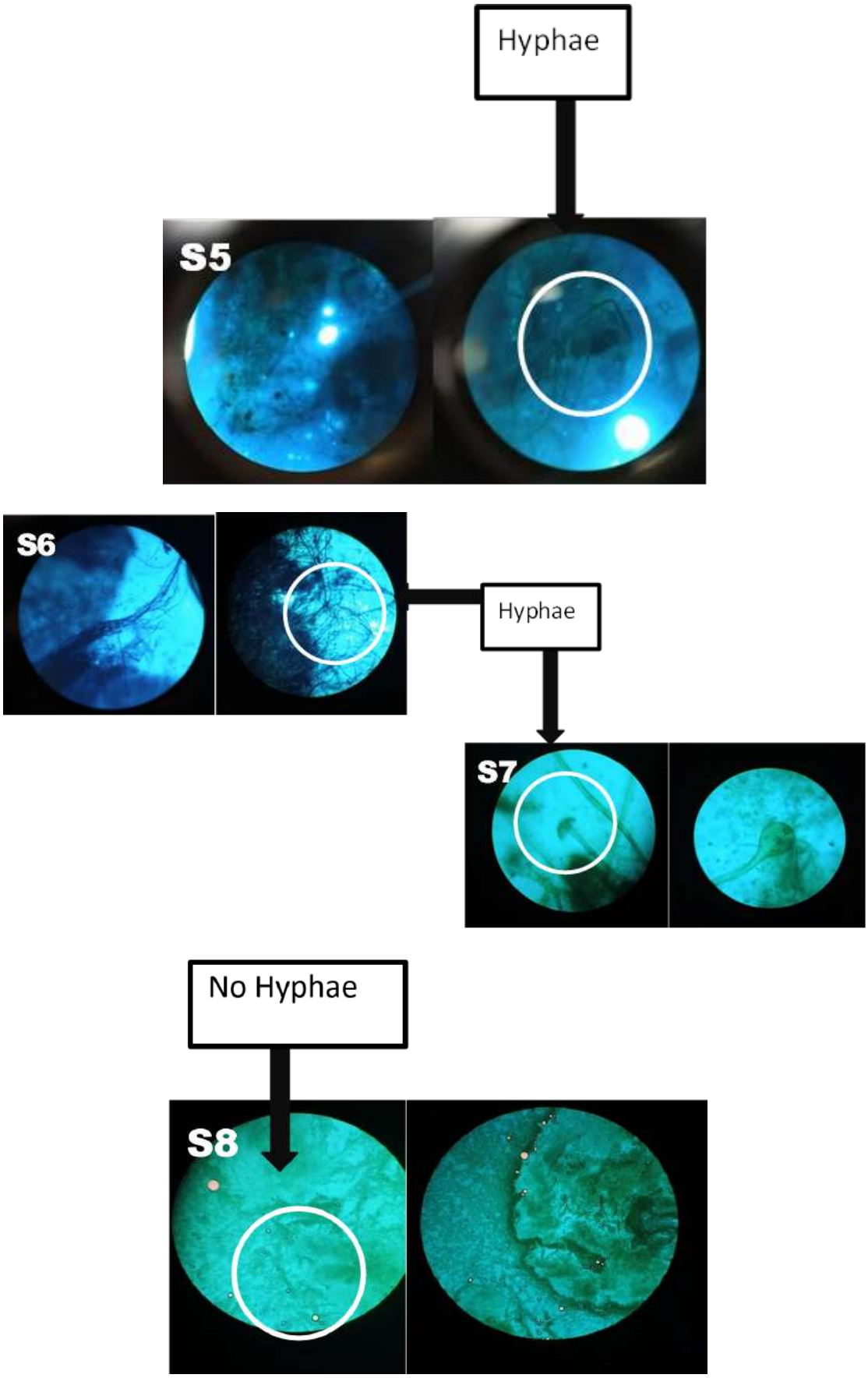
Hyphae
S5
S6
Hyphae
S7
No Hyphae
S8

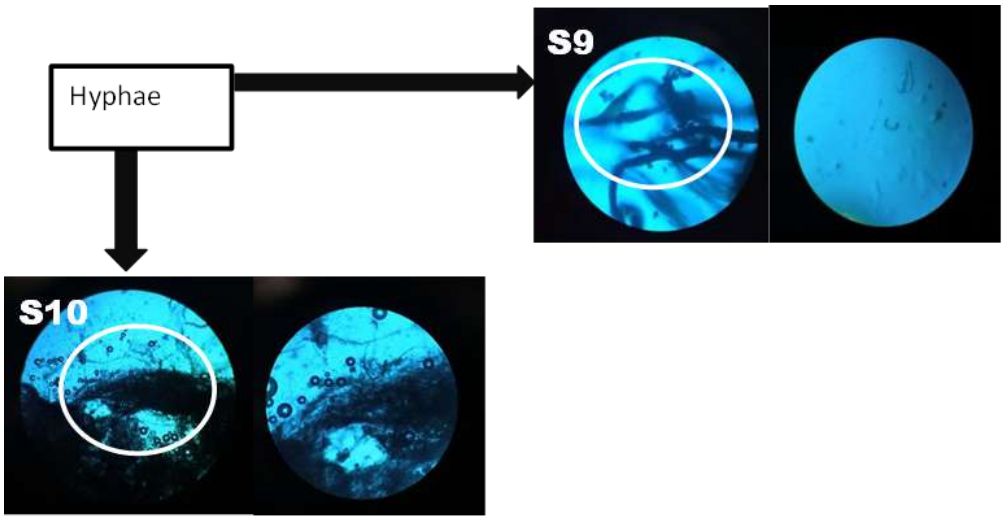

FIGURE 4.4: Microscopic images of the isolated fungal strains and hyphal observation of S1 to S10.

4.1.6 Biochemical Characterization

4.1.6.1 Growth analysis of Isolated 10 Fungal Strains on Czepak Agar

Czaepak is a chemically defined, nutritionally minimal culture medium primarily used for the cultivation and morphological characterization of fungi, especially Aspergillus and Penicillium species. Its basic principle relies on providing sucrose as the sole carbon source, sodium nitrate as the sole nitrogen source, along with essential minerals like potassium phosphate, magnesium sulfate, potassium chloride, and ferrous sulfate, which together support fungal growth while restricting that of most bacteria and non-fungal organisms. This selective and minimal composition is performed because it standardizes growth conditions, allowing for consistent observation of colony characteristics such as color, texture, growth rate, and sporulation pattern, which are key diagnostic features used in fungal taxonomy and species-level identification.

The growth analysis of 10 isolated fungal strains on Czepak Agar was performed. All strains showed good growth on the medium after incubation at 28°C for 5 days. The appearance of the colonies was examined, and the following characteristics were observed: Colony color varied from white to brownish or greenish; Colony texture ranged from cottony to powdery or leathery; Colony margin varied

from smooth to undulate or irregular. The diameter of the colonies ranged from 25mm to 90mm. The fungal strains were identified based on the morphological characteristics of the colonies (Table 4.6).

TABLE 4.6: Table shows Growth, Colony Morphology, Color Change of 10 different fungal strains on Czepak Agar

Fungal Isolates	**Colony Appearance**	**Size (mm)**	**Color**
S1		40x30	White center with pale yellow margins
S2		80x80	Orangish white
S3		0x0	No growth observed
S4		80x80	Orange center white margins
S5		30x25	Pale yellow
S6		30x20	Brown center white margins

Table 4.6 continued from previous page

Fungal Isolates	Colony Appearance	Size (mm)	Color
S7		35x40	Milky white
S8		0x0	No growth observed
S9		55x70	Greyish black center with white margins
S10		0x0	No growth observed

Seven out of 10 different strains shown growth on Czepak agar; (S1, S2, S4, S5, S6, S7, S9), whereas, S3, S8, S10, strains had no growth appearance of Czepak agar. The colony morphology analysis of the seven different fungal strains has shown that they mostly have a milky white appearance, with smooth surfaces and circular, filamentous forms.

The margins of most strains were found to be entire, although some were lobate, raised, or had spreading edges. The reverse color of the colonies was mostly black or pale white. The results also showed that all 10 strains were cultured on czepak agar, and seven of them showed growth on this medium, which is commonly used for biochemical analysis of fungi.

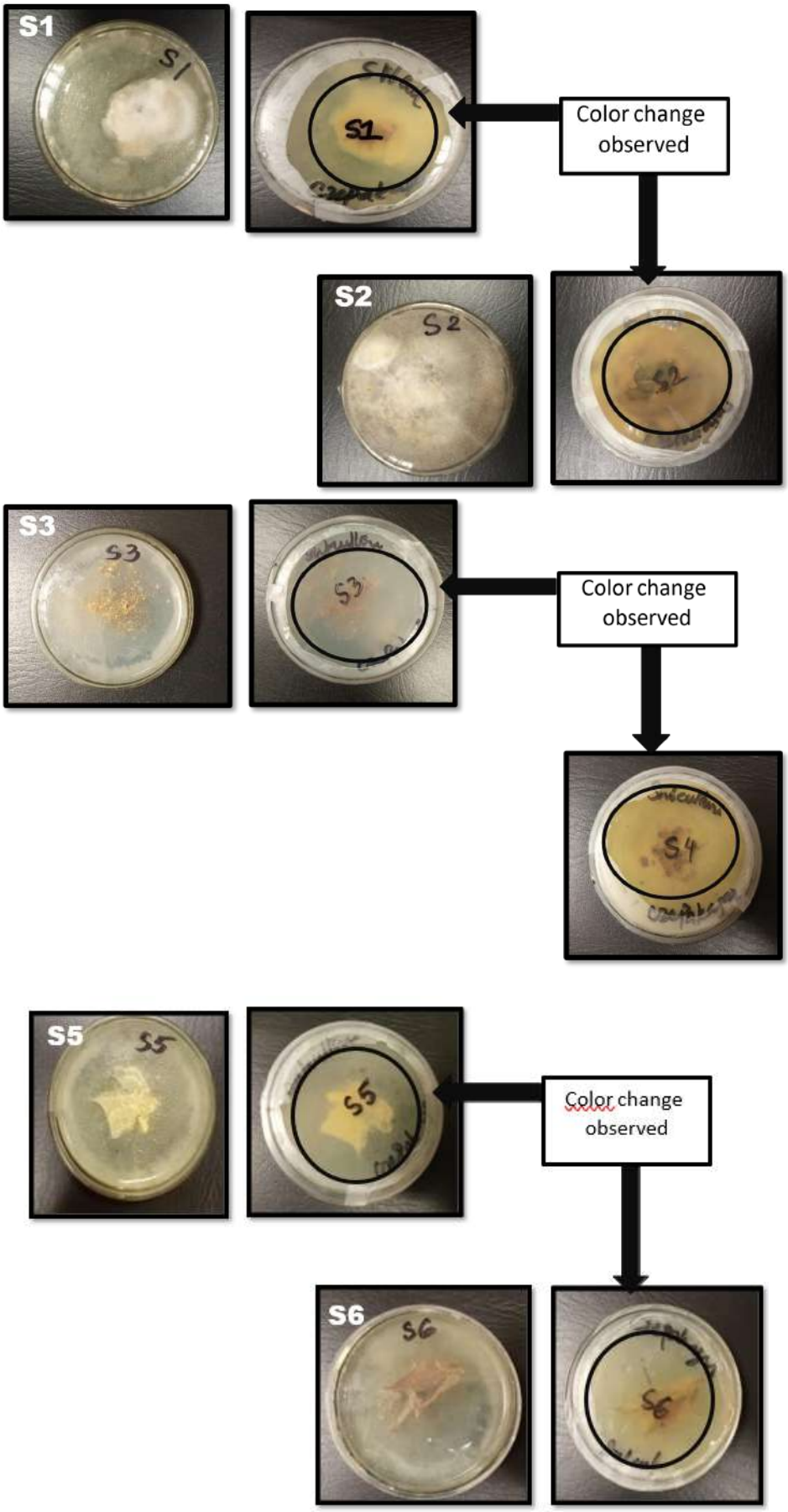
S1
S1
S1
Color change observed
S2
S2
S2
S3
S3
S3
Color change observed
S4
S5
S5
S5
Color change observed
S6
S6
S6

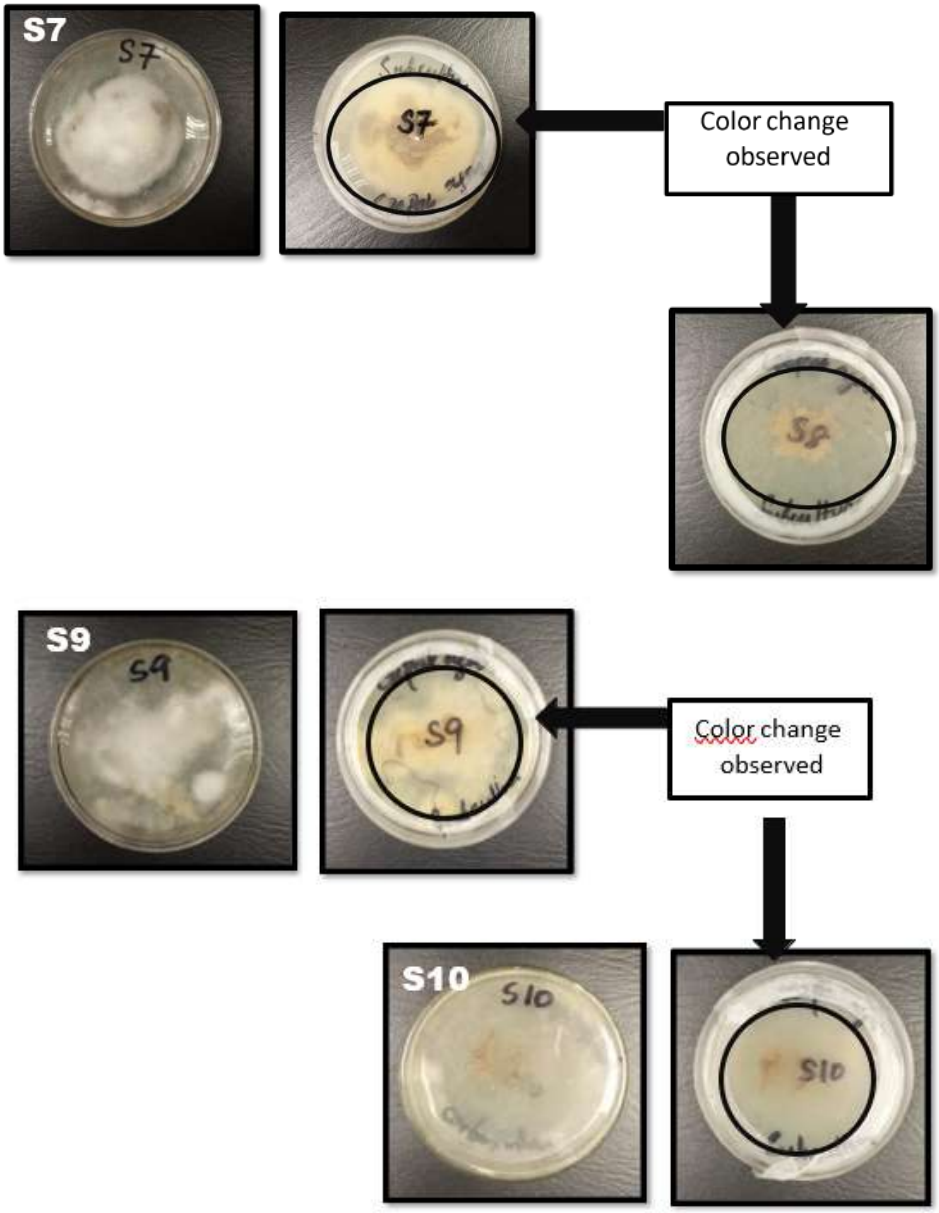

FIGURE 4.5: Images for the growth and color change observed on czepak agar; from S1 to S10 (S stands for Strain); S1, S2, S4, S5, S6,S7,S9 Shows positive results and growth on Czepak agar plates, whereas, S3, S8, S10 show negative results (No growth observed).

4.1.7 Growth of 10 Isolated Fungal Strains on Pectin Media

Pectin media, on the other hand, is used to assess the pectinolytic activity of microorganisms, meaning their ability to produce pectinase enzymes that break

down pectin, a structural polysaccharide found in plant cell walls. The basic principle involves incorporating pectin as the primary substrate in the medium; if the test organism produces pectinase, it will hydrolyze the pectin into simpler compounds, which can be visualized through clearing zones around the colony after staining with an indicator (commonly iodine or ruthenium red) or through changes in medium consistency. This test is performed because it helps determine the enzymatic capability of an isolate to degrade plant material, which is useful in identifying certain fungal or bacterial species, especially those involved in plant pathogenesis, decomposition, or industrial applications such as fruit juice clarification and textile processing.

The process of fungi growth analysis on pectin plates involved observing the colony appearance, color change, and measuring the colony size. Several fungal isolates were examined. The colonies were grown on pectin plates, and their growth characteristics were noted (Figure 4.6). The colony appearance was described for each isolate. The S1 displayed a pale white center with pale brown margins, while S2 had a cream white color. The color change of the colonies was also observed. S4 exhibited a reddish pigmented growth, while S5 had a pale-yellow center with brown margins. Additionally, the size of each colony was measured using millimeters. S1 had a size of 80x70 mm, S2 was 40x50 mm, and S3 measured 70x60 mm. The colony sizes varied among the different isolates, providing valuable information about their growth patterns and characteristics (Table 4.7)

Table 4.7: Growth of 10 isolated fungal strains on Pectin media

Fungal Isolates	**Colony Appearance**	**Size (mm)**	**Color**
S1		80x70	Pale white center with pale brown margins
S2		40x50	Cream white

Table 4.7 continued from previous page

Fungal Isolates	Colony Appearance	Size (mm)	Color
S3		70x60	Pale green
S4		80x80	Reddish pigmented growth
S5		70x50	Pale yellow center with brown margins
S6		30x20	White center with brown margins
S7		35x40	Reddish orange
S8		30x70	White center with black margins
S9		55x70	Greyish black center with white margins

Table 4.7 continued from previous page

Fungal Isolates	Colony Appearance	Size (mm)	Color
S10		20x10	White center with pale margins

The fungal isolates were observed and their colony appearances were recorded. S1 exhibited a size of 80x70 mm with a pale white center and pale brown margins, while S2 had a cream white appearance. S3 had a size of 70x60 mm and a pale green color, whereas S4 displayed a reddish pigmented growth with a size of 80x80 mm.

S5 had a pale yellow center with brown margins and a size of 70x50 mm, while S6 showed a white center with brown margins and a size of 30x20 mm. S7 appeared reddish orange and had a size of 35x40 mm, while S8 displayed a white center with black margins and a size of 30x70 mm.

S9 had a greyish black center with white margins and a size of 55x70 mm, and finally, S10 exhibited a white center with pale margins and a size of 20x10 mm (Table 4.7).

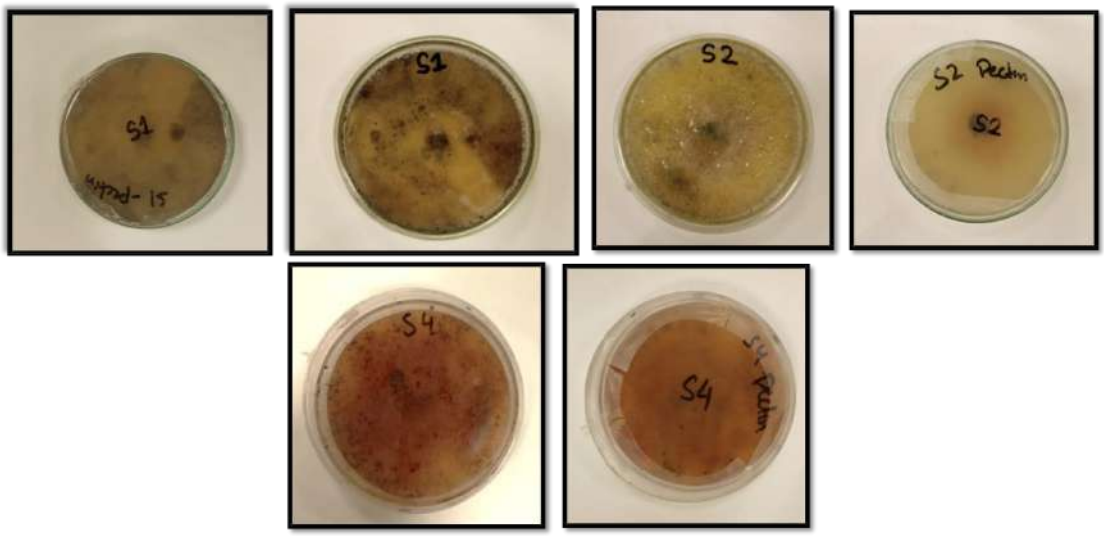

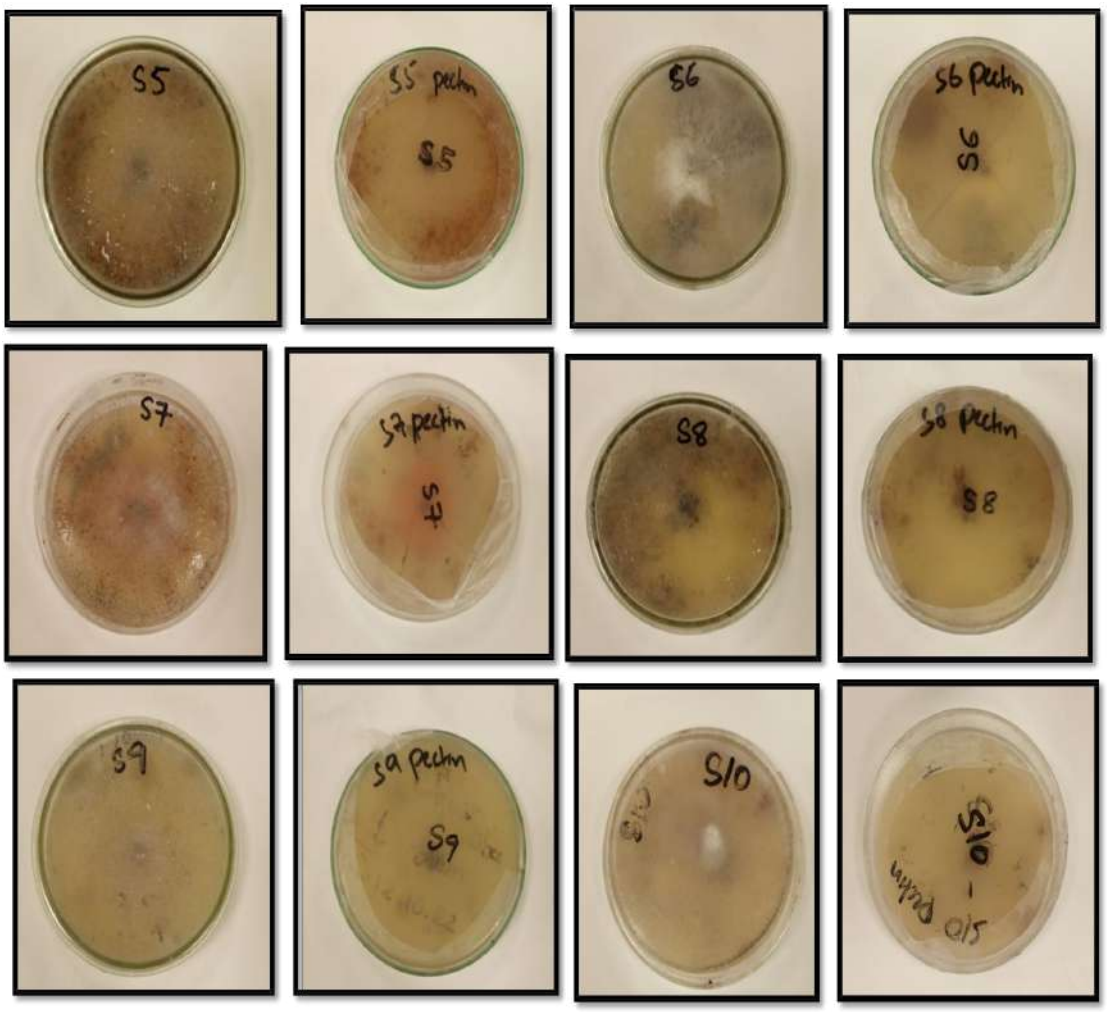

FIGURE 4.6: Images for the growth and color change observed on Pectin Media; from S1 to S10 (S stands for Strain)

4.1.8 Molecular Characterization

4.1.8.1 DNA Extraction Results

The presence of bands confirmed that the DNA extraction procedure effectively isolated and retained the genomic DNA from the fungal strains. These bands served as a visual confirmation that sufficient DNA was obtained, setting the stage for the subsequent PCR amplification step (Figure 4.7).

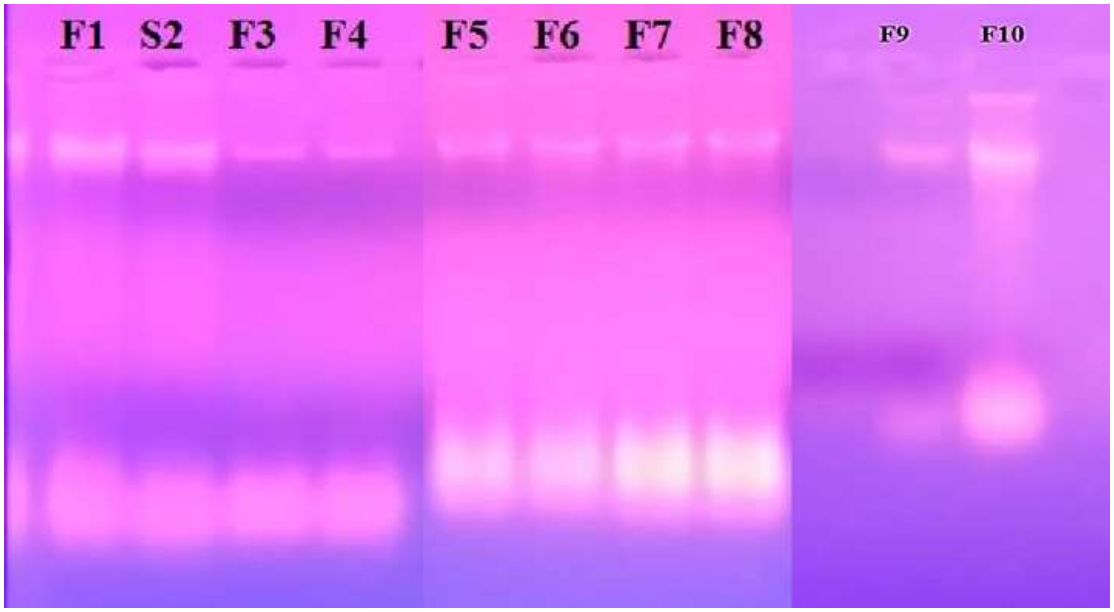

FIGURE 4.7: Gel with clear bands of DNA of isolated fungal strains

4.1.8.2 Gel Electrophoreses Results

The size of the bands corresponded to the length of the amplified DNA fragments, which can vary among different fungal species or strains. The presence of clear and well-defined bands indicated that the PCR amplification was effective, and the target DNA regions were successfully amplified. These bands were then further analyzed and sequenced to gain insights into the genetic diversity and taxonomic identification of the fungal strains based on the ITS region (Figure 4.8).

4.1.8.3 18s RNA Sequencing

The sequencing of ten isolates showed their nucleotide sequence and number of base pairs. Each sequence revealed % identity and highest identity 100% was of samples S1 with Aspergillus niger strain S1-C1, S3 with Aspergillus fumigatus strain S1-31, S5 with Fusarium fujikuroi strain S5-32, S7 with Schizophyllum commune strain S1-1A, S9 with Fusarium proliferatum strain S4-1, S10 with Fusarium oxysporum strain S1-C and lowest % identity was observed in sample S1 of 98.71% with Rhizopus delemar strain S4-2 (Table 4.8).

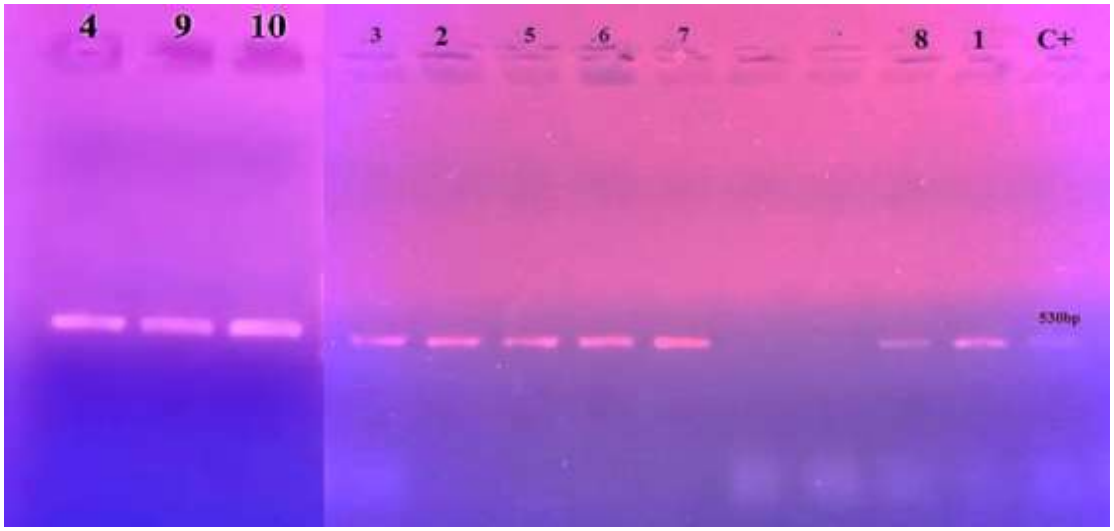

FIGURE 4.8: Gel with PCR amplification bands

TABLE 4.8: Fungal Isolates Sequencing Results & BLAST Analysis

Fungal Isolates	**Fungal Strain Code**	**Sample from which Strain is isolated**	**Species Name**	**Accession Number**	**Percent Identity**	**PE Plastic Degradation capability**
S1	(S4-2)	Sample 4	Rhizopus delemar	MK108424. 1	98.71%	Reported
S2	(S1-C1)	Sample 1	Aspergillus niger	MT628904.1	100%	Reported
S3	(S1-31)	Sample 1	Aspergillus fumigatus	MT316338.1	100%	Reported
S4	(S3-33)	Sample 3	Penicillium chrysogenum	MT300180.1	100%	Reported
S5	(S1-B2)	Sample 1	Rhizopus arrhizus	MH869027. 1	99.1%	Not Reported
S6	(S5-32)	Sample 5	Fusarium fujikuroi	MT436828.1	100%	Reported

4.1.9 Evaluation of PE Plastic Degradation Using Rhizopus arrhizus Strain on PE Strips

Throughout the incubation period, the strip underwent degradation, and the reduction in weight was evident. The passive reduction of strip's weight to 0.02g indicated the effectiveness of the fungal culturein breaking down the polyethylene material. The fungal culture of *Rhizopus arrhizus* demonstratedits capability to actively degrade the polyethylene strip under the given conditions (Figure 4.9, 4.10).

The in vitro analysis provides valuable insights into biodegradation process of polyethylene by *Rhizopus arrhizus*. These findings contribute to our understanding of fungal-mediated degradation mechanism and hold promise for potential applications in the management of plastic waste.

FIGURE 4.9: Weight measurement of polyethylene sample before and after degradation using analytical balance.

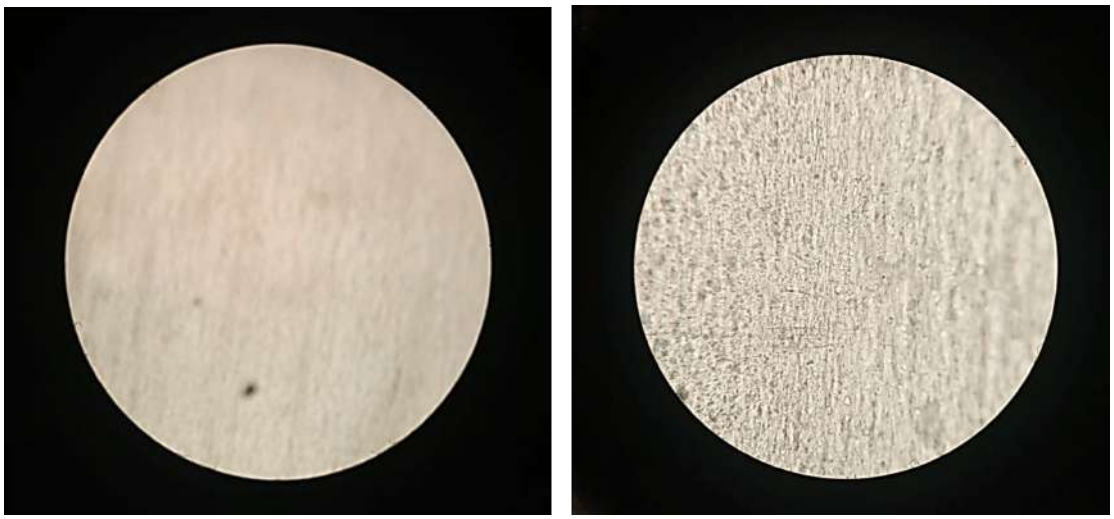

FIGURE 4.10: Surface morphology of polyethylene sample before and after fungal treatment showing visible degradation effects.

4.2 Phase 2: Whole Genome Analysis of Selected Fungi DNA Extraction Results

4.2.1 Quality Assessment of the Genome Assembly

Consensus sequence was provided by the sequencing services. The fastQc was performed by the commercial sequencing provider.

4.2.1.1 Assessment of Genome Assembly using QUAST

The fugal genome (FF1_ consensus_fa) assembly was evaluated with QUAST, which computes contiguity, completeness, and per-base quality values directly from the contig sequences without a reference genome (Table 4.9).

TABLE 4.9: Summary of structural assembly quality parameters generated by QUAST for the fungal (Rhizopus arrhizus) genome assembly

Assembly Metric	**Value**
General Statistics	
Assembly name	FF1_consensus_fa
Total number of contigs	41
Total assembly length	50,257,580 bp (∼50.26 Mb)
GC content (%)	35.58
Ns per 100 kbp	0.00
Contig Size Statistics	
Largest contig	3,235,061 bp (∼3.24 Mb)
Smallest contig	180,397 bp
Mean contig length	1,225,795 bp
Median contig length	1,080,074 bp
Contiguity Metrics (N- and L-Statistics)	
N50	1,791,908 bp
N75	1,080,074 bp
N90	664,539 bp
L50	12 contigs
L75	21 contigs
L90	30 contigs
auN (area under Nx curve)	1,679,825 bp

bp = base pairs; Mb = megabases. N50: contig length at which 50% of the assembly is covered by contigs of equal or greater length. L50: minimum number of contigs needed to cover 50% of the assembly. auN: area under the Nx curve, a composite contiguity index. The assembly length was 50,257,580 bp (∼50.26 Mb) across 41 contigs, all exceeding 100,000 bp, which is consistent with fungal (ascomycete) genome sizes (25-70 Mb). There were no uncalled bases (Ns) (0.00 per 100 kbp), which shows a fully resolved sequence with no gaps, this indicates a high-quality long-read assembly. GC content was 35.58%, within the fungal range (30-60%). The genome-wide GC distribution histogram (Figure 4.1), exhibits a narrow peak centered around 35-40% GC, and over 20,000 pieces of the genome clustering within this range. The absence of other peaks shows homogeneity of the genome and absence of significant contamination from organisms with divergent GC content.

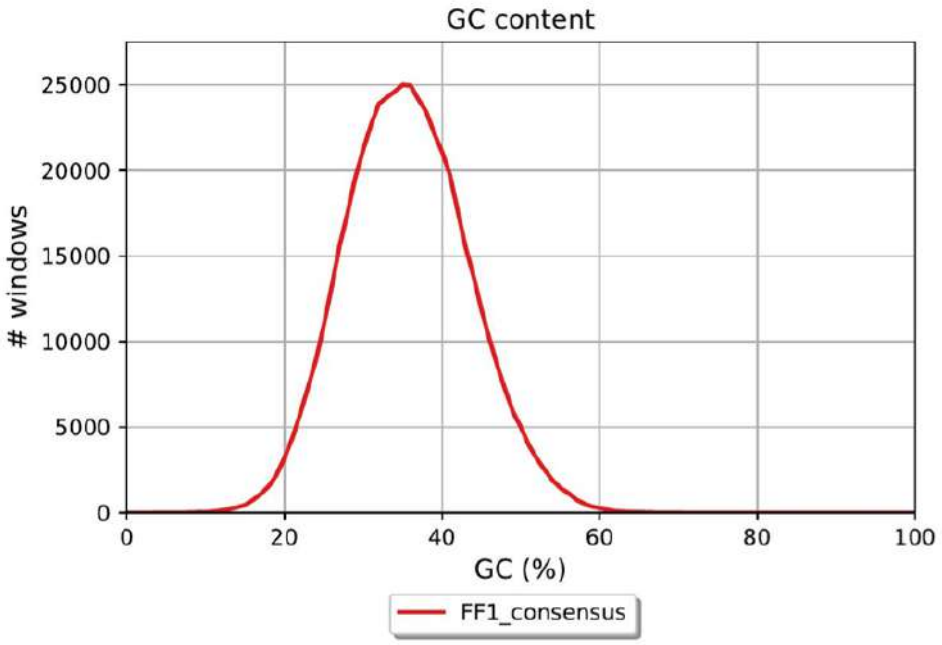

FIGURE 4.11: Genome-wide GC content distribution for fungal genome. The x-axis shows GC percentage (%) and the y-axis shows the number of sliding windows. The narrow unimodal peak centred at ∼35-40% GC indicates compositional uniformity across the assembly.

The per-contig GC content plot (Figure 4.2) confirmed that all 41 contigs share a nearly identical GC content with no random outliers. This regularity proves the DNA sample is clean and free from contamination

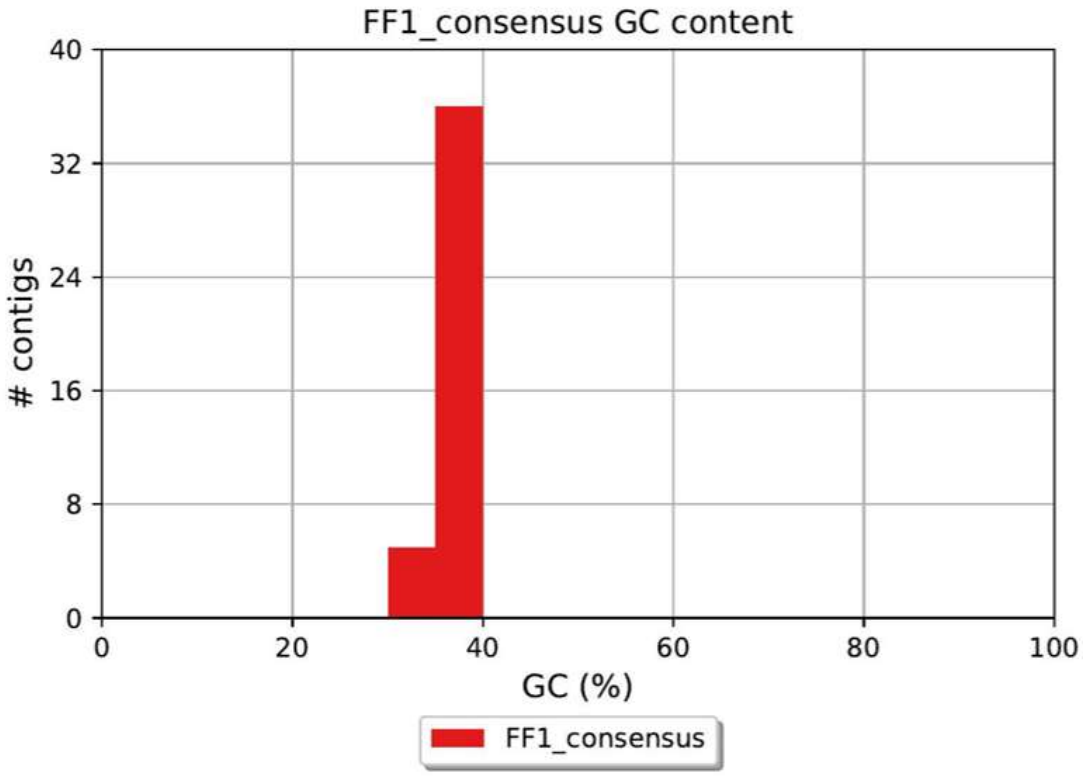

FIGURE 4.12: Per-contig GC content for fungal genome. Each data point represents an individual contig. All 41 contigs fall within a consistent GC range, confirming compositional homogeneity and absence of contaminant sequences.

4.2.1.2 Contig Length Distribution

Contig lengths ranged from 180,397 bp to 3,235,061 bp having a mean 1,225,795 bp and median 1,080,074 bp. This reflecting a uniform distribution with no short-fragments (Table 4.9).

The collective length plot (Figure 4.3) represents the gradual increase in total assembled sequence as contigs were arranged from largest to smallest. A sharp rise was observed by the curve initially. Tfirst 12 contigs (L50) collectively accounting for over half of the total 50.26 Mb assembly. The cumulative length plate was observed near the total assembly size after approximately 30-35 contigs, and the remaining contigs contributing to the final assembly length. This distribution pattern is consistent with a high-quality, complete genome assembly containing the majority of genomic content.

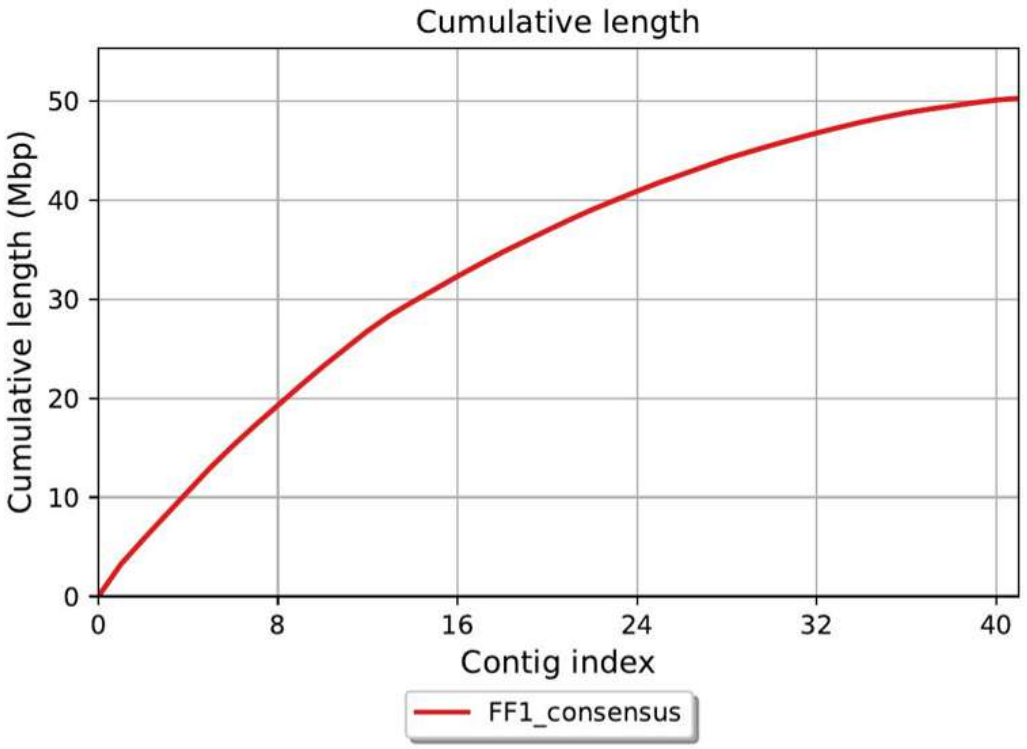

FIGURE 4.13: Cumulative contig length plot for fungal genome. Contigs are ordered from largest to smallest (x-axis: contig index) and the y-axis shows cumulative assembly length (Mbp). The steep initial rise reflects that the first 12 contigs (L50) account for over half the total assembly.

4.2.1.3 N- and L-Statistics

The highly continuous genome assembly is demonstrated by an N50 value 1,791,908 bp, N75 of 1,080,074 bp (L75 = 21) and N90 of 664,539 bp (L90 = 30). This shows that the genome is not broken into small pieces; even the shorter fragments which make up the bulk of the assembly are very large (over 664 kb).

The L50 and L90 values, the minimum number of contigs required to cover 50% and 90% of the assembly were 12 and 30. These low values prove that the assembly dominance by a small number of large, contiguous sequences, consistent with chromosome-level resolution. A gradual decline was shown by Nx curve from high contig lengths at low x-values, which indicates uniform long-read coverage and successful assembly of large genomic regions without fragmentation (Figure 4.4).

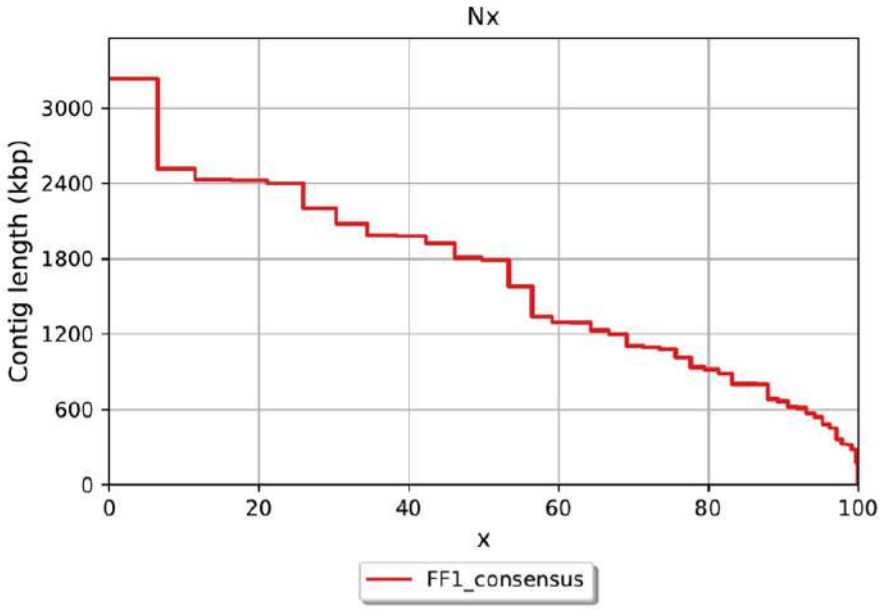

FIGURE 4.14: Nx plot for fungal genome. The x-axis represents the percentage of total assembly (0-100%), and the y-axis represents contig length (kbp). The curve demonstrates a high N50 of ∼1.8 Mb, reflecting excellent assembly contiguity.

4.2.2 Assessment of Genome Assembly using BUSCO

The QUAST metrics established a highly contiguous assembly with N50 value of 1,791,908 bp, physical contiguity does not guarantee biological completeness. Therefore, to evaluate the genic integrity and completeness of the assembled fungal genome, Benchmarking Universal Single-Copy Orthologs (BUSCO) analysis was performed using BUSCO version 5.8.0 against the mucorales_odb10 lineage dataset, which covers 2,449 conserved single-copy orthologs derived from 15 reference genomes. The assembly was evaluated in eukaryotic genome mode (euk_genome_aug) using Augustus (v3.5.0) as the gene prediction tool.

The BUSCO analysis revealed a high degree of genome completeness, with 96.0% (n = 2,350) of the searched BUSCO groups (Table 4.10). From these groups, 89.6% (n = 2,194) were identified as complete and single-copy, this indicates that majority of expected conserved genes are present in a non-redundant manner. A small percentage (6.4%; n = 156) were classified as complete and duplicated, which reflects gene duplication. Fragmented BUSCOs created 1.2% (n = 30)

of the total, indicating that a small portion of genes were partially assembled. Missing BUSCOs accounted for 2.8% (n = 69) of the dataset, indicating that these orthologs were absent from the genome. Collectively, the BUSCO score of C:96.0% [S:89.6%, D:6.4%], F:1.2%, M:2.8% exhibits a highly complete and contiguous fungal genome assembly, suitable for downstream comparative genomic and functional annotation analyses.

TABLE 4.10: BUSCO completeness summary for the fungal genome assembly against the mucorales_odb10 lineage dataset (n = 2,449).

BUSCO Category	**Count**	**Percentage (%)**
Complete BUSCOs (C)	2350	96.0
Complete and Single-copy (S)	2194	89.6
Complete and Duplicated (D)	156	6.4
Fragmented BUSCOs (F)	30	1.2
Missing BUSCOs (M)	69	2.8
Total BUSCO Groups Searched (n)	2449	100.0

4.2.2.1 Assembly Statistics and Visualization

The genome assembly comprised 41 scaffolds and 41 contigs, with a total assembly length of approximately 50.3 megabases (Mb) (Table 4.11). The absence of any detected gaps (0.000% gap content) reveals the high-quality nature of the assembly, consistent with the high BUSCO completeness scores. Both the scaffold N50 and contig N50 values were approximately 1 Mb. This indicated that half of the assembled sequence is present within contigs or scaffolds of 1 Mb or greater. This finding suggests that the assembly is highly contiguous, which is helpful for gene prediction and structural annotation.

TABLE 4.11: Assembly statistics for the fungal genome.

Assembly Metric	**Value**
Number of Scaffolds	41
Number of Contigs	41
Total Assembly Length	50,257,580 bp (∼50.3 Mb)
Percent Gaps	0.000%
Scaffold N50	∼1 Mb

Table 4.11 continued from previous page

Assembly Metric	Value
Contig N50	∼1 Mb

The heatmap displays the genomic positions and copy-number status of each BUSCO ortholog across the assembly scaffolds. The colour gradient represents chromosomal coordinates (in megabases) at which each ortholog was detected (Figure 4.5). The majority of BUSCO groups being displayed on the y-axis, were recovered at high completeness across both primary scaffolds (columns 1 and 2 of the heatmap). The most groups showing uniform, deep blue colouration indicate consistent recognition across expected positional coordinates. A limited number of orthologs display high positional values (orange to red in the colour scale, representing positions ¿2.5 Mb). This matches to BUSCO groups localised toward the distal regions of larger scaffolds. Minimal or absent cells along certain rows are consistent with the small segment of fragmented or missing BUSCOs reported above.

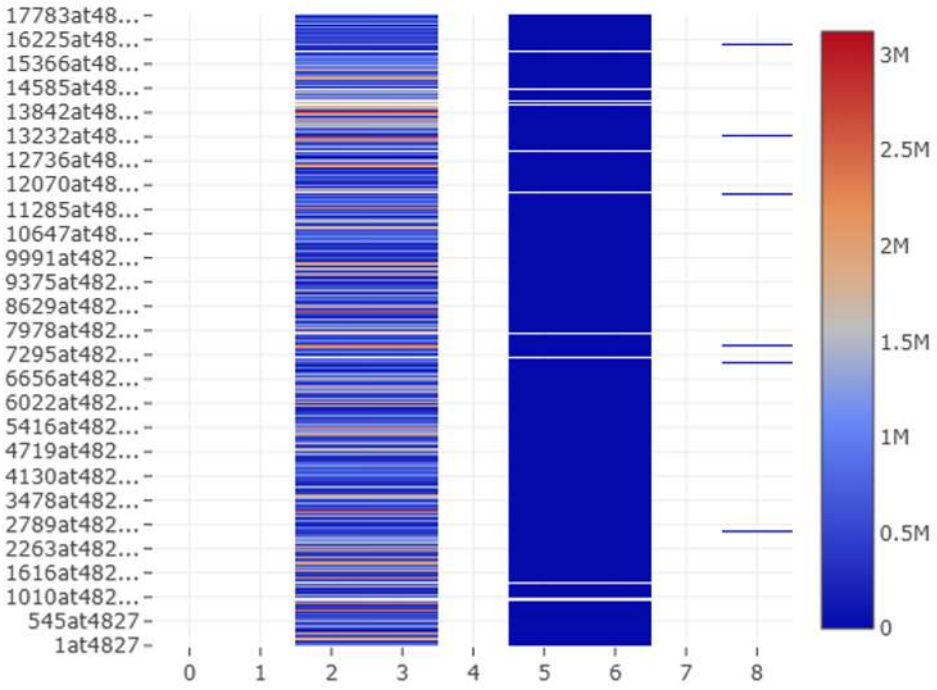

FIGURE 4.15: BUSCO heatmap showing the positional distribution of ortholog groups across the fungal genome assembly scaffolds. Colour intensity (blue to red) represents genomic coordinate values (0-3 Mb). Y-axis labels denote individual BUSCO ortholog identifiers; x-axis represents scaffold indices.

The QUAST and BUSCO analyses provides complete evidence that the fungal genome assembly (Rhizopus arrhizus) is of high quality and fit for downstream analyses. QUAST metrics confirmed unique structural contiguity: the assembly spans ∼50.26 Mb across only 41 contigs, with an N50 of 1,791,908 bp, which indicates complete absence of uncalled bases (0.00 Ns per 100 kbp). It also showed a uniform GC content of 35.58% all consistent with a compact, well-resolved fungal genome. BUSCO assessment against the mucorales_odb10 lineage dataset (n = 2,449) further confirmed biological completeness. It indicated 96.0% of conserved orthologs recovered, out of which 89.6% were complete and single copy. The low proportions of fragmented (1.2%) and missing (2.8%) BUSCOs indicate that sequencing complexity and assembly parameters were enough to resolve even potentially challenging genomic regions. The modest duplication rate (6.4%) duplications or residual heterozygosity rather than assembly artefacts. Collectively, these results found that the genome assembly is both structurally contiguous and genetically complete, providing a strong and reliable resource for gene annotation, comparative genomics, and phylogenomic analyses.

4.2.3 Structural Annotation

4.2.3.1 Gene Prediction

Structural annotation of the genome assembly (FF1_consensus_fa) was done using AUGUSTUS (v3.x). It is an extensively used ab initio gene prediction tool that uses a Generalized Hidden Markov Model (GHMM) to isolate protein coding genes from genomic sequence listed in Appendix III. A complete overview of the structural annotation is given in Table 4.12.

Table 4.12: Structural annotation data generated by AUGUSTUS for the Rhizopus arrhizus genome assembly

Structural Annotations	**Value**
Gene Predictions	
Total predicted genes	16,813
Total predicted transcripts	16,813

Table 4.12 continued from previous page

Structural Annotations	**Value**
Gene density (genes/Mb)	334.6
Contigs with gene predictions	41 / 41 (100%)
Strand distribution (+ / -)	8,296 / 8,517
Gene Structure	
Total CDS segments	55,785
Mean CDS segments per gene	3.32
Single-exon genes	4,878 (29.0%)
Multi-exon genes	11,935 (71.0%)
Maximum CDS segments per gene	28
Gene and CDS Length Statistics	
Gene length — minimum (bp)	201
Gene length — maximum (bp)	21,331
Gene length — mean (bp)	2,080.2
Gene length — median (bp)	1,398.0
CDS length — mean (bp)	1,371.0
CDS length — median (bp)	987.0
Total genomic sequence in genes	34,973,590 bp (69.6% of assembly)
Total CDS nucleotides	23,050,584 bp
Protein Statistics	
Total predicted proteins	16,813
Protein length — minimum (aa)	66
Protein length — maximum (aa)	6,730
Protein length — mean (aa)	456.0
Protein length — median (aa)	328.0
Proteins >= 100 aa	15,634 (93.0%)
Proteins >= 300 aa	9,209 (54.8%)
Total amino acids predicted	7,666,715

Total protein-coding genes predicted by AUGUSTUS were 16,813 and an equal number of transcripts were produced across the 50.26 Mb assembly. Estimated gene density was approximately 334.6 genes per Mb. Gene predictions were distributed across all 41 contigs Contig1 (∼3.24 Mb) was the largest contig and got the highest number of predicted genes (n = 1,081). The smallest annotated contig was Contig36 (∼180 kb) contained 64 predictions. Genes were evenly distributed between the forward and reverse strands as 8,296 on the positive strand; 8,517 on

the negative strand. This indicates prediction model does not favor any strand and is consistent with transcription across the genome in both directions.

The predicted genome had 16,813 genes. This number falls within the normal range between 8,000 and 20,000 genes of fungal genomes. These genes yield upto 34,973,590 bp, or 69.6% of the total genome.

4.2.4 Gene Structure and Organization of Exon-Intron

Total 55,785 CDS segments were identified from the 16,813 predicted genes. A mean of 3.32 CDS segments per gene and a median of 2 segments was identified which indicates that the majority of predicted genes are multi-exonic,these are genes with two or more CDS segments. Multi-exon genes comprised 71.0% of all predictions (n = 11,935). Single-exon genes accounted for 29.0% (n = 4,878). The maximum number of CDS segments calculated per gene was 28. This indicates the presence of complex, highly spliced loci. This proportion is consistent with the exon-intron gene design typical of eukaryotes and exactly fungal genomes.

Predicted gene lengths ranged from 201 bp to 21,331 bp, with a mean of 2,080.2 bp and a median of 1,398.0 bp. CDS lengths ranged from 201 bp to 20,193 bp, with a mean of 1,371.0 bp and a median of 987.0 bp. The difference between mean gene and mean CDS lengths (2,080.2 bp vs. 1,371.0 bp) reflects the presence of introns within the predicted loci, further supporting the multi-exonic gene structure described above.

4.2.5 Predicted Protein Sequences

The 16,813 predicted genes yielded an equal number of protein sequences with a total of 7,666,715 amino acid residues. Predicted protein lengths ranged from 66 to 6,730 amino acids (aa), with a mean of 456.0 aa and a median of 328.0 aa. The majority of predicted proteins (93.0%; n = 15,634) were 100 aa or longer, and 54.8% (n = 9,209) exceeded 300 aa — both thresholds commonly used as quality

filters in genome annotation pipelines. No protein sequences shorter than 50 aa were detected, indicating that the predictions are largely free of spurious short open reading frames.

4.3 Functional Annotation

Functional annotation of the predicted fungal proteome was independently performed using two complementary platforms: InterProScan (ver 5) and eggNOG - Mapper (version 2). The two tools differ fundamentally in their approach. InterProScan integrates multiple protein signature databases including ProSitePatterns, ProSiteProfiles, PRINTS, PANTHER, SMART, MobiDBLite, Gene3D, and Pfam to assign structural domains, motifs, and conserved sites to individual query sequences.

In contrast, eggNOG-Mapper employs DIAMOND-based sequence alignment to assign proteins to orthologous groups within the eggNOG database, yielding COG functional categories, KEGG orthologs, pathway mappings, Pfam domains, and GO terms derived from ortholog inference. This comprehensive pipeline successfully addresses potential characterization biases, ensuring that both specific multidomain active sites and broad evolutionary metabolic networks are accurately identified and cross-validated.

4.3.1 InterProScan-Based Functional Characterization

Functional classification of the predicted protein sequences was led using InterProScan (version 5), a bioinformatics platform that incorporates multiple protein signature databases for the identification of domains, families, and functional sites. Out of 662 non-redundant protein sequences, 741 annotation hits were yielded (Table 4.12). Among these, 628 proteins (94.9%) were assigned at least one InterPro accession, conforming to 29 distinct InterPro entries. All 741 annotation hits were categorized as true positives, which confirmed that each match met the particular database significance thresholds.

The length of the predicted proteins ranged from 201 to 11,892 amino acids, having a mean length of 2,114.0 aa and a median of 1,611 aa. This wide-ranging variation in protein size is constant with the presence of complex multi-domain structures. From the total hits, 626 (84.5%) were associated with pathway annotations derived from the Reactome and MetaCyc databases. 191 proteins (28.9%) were assigned Gene Ontology (GO) terms, which represent 14 unique GO identifiers.

TABLE 4.13: Annotation hits by the InterProScan member database.

Tools/Database	**Hits (n)**	**Percentage (%)**	**Database Type**
ProSitePatterns	522	70.4	Motif patterns
ProSiteProfiles	140	18.9	Profiles
PRINTS	62	8.4	Fingerprints
PANTHER	9	1.2	Phylogenomics
SMART	3	0.4	Domain annotation
MobiDBLite	3	0.4	Disordered regions
Gene3D	1	0.1	3D structural
Pfam	1	0.1	Protein families
Total	741	100.0	—

4.3.2 Contribution of Member Databases

Annotation was achieved using eight integrated databases within the InterProScan outline (Table 4.13). ProSitePatterns added the highest number of annotations, providing 522 hits (70.4%), reflecting the plenty of short conserved motifs mainly cysteine-rich and disulfide-bonded regions within the dataset. ProSiteProfiles provided 140 hits (18.9%), while PRINTS added 62 fingerprint-based matches (8.4%).

Other databases contributed smaller proportions; PANTHER accounted for 9 hits (1.2%), SMART and MobiDBLite each contributed 3 hits (0.4%), and Gene3D and Pfam each identified a single hit (0.1%). The predominance of ProSite-based annotations indicates that the dataset is enriched for proteins characterized by conserved short sequence motifs than full-length structural domains, which is commonly observed in secreted cysteine-rich protein families.

4.3.3 Distribution of InterPro Domain Families

InterPro domains analysis identified 29 distinct functional entries across 628 annotated proteins. The ten most repeatedly occurring domains and their distribution between unique proteins are presented in Table 4.14.

TABLE 4.14: Top 10 InterPro domain families recognized in the predicted proteome

IPR Accession	**Domain Description**	**Unique Proteins (n)**	**% of Total Proteins**
IPR017891	Insulin-like growth factor binding protein, N-terminal, Cys-rich conserved site	154	23.3
IPR015812	Integrin beta subunit	83	12.5
IPR006207	Cystine knot, C-terminal	52	7.9
IPR001938	Thaumatin family	52	7.9
IPR007112	Expansin/pollen allergen, DPBB domain	48	7.3
IPR000020	Anaphylatoxin/fibulin	47	7.1
IPR027300	Agouti domain	34	5.1
IPR006081	Alpha-defensin, C-terminal	33	5.0
IPR006058	2Fe-2S ferredoxin, iron-sulphur binding site	30	4.5
IPR017900	4Fe-4S ferredoxin, iron-sulphur binding, conserved site	22	3.3

Note: Percentage values are relative to the total number of distinctive proteins in the dataset (n = 662). After detecting 154 proteins(23.3%), the most dominant domain was the Insulin-like Growth Factor Binding Protein (IGFBP) N-terminal cysteine-rich conserved site (IPR017891), creating it as the dominant functional group within the dataset. The second most common was the integrin beta subunit domain (IPR015812), which was recognized in 83 proteins (12.5%), and plays roles in cell adhesion and extracellular matrix interactions.

The cystine knot C-terminal domain (IPR006207) and the thaumatin family domain (IPR001938) were both identified in 52 proteins (7.9%). The expansin/pollen

allergen DPBB domain (IPR007112) was observed in 48 proteins (7.3%). A number of domains associated with defense mechanisms and venom-related functions were also recognized. The anaphylatoxin/fibulin domain (IPR000020) was identified in 47 proteins (7.1%), the agouti domain (IPR027300) in 34 proteins (5.1%), and the alpha-defensin C-terminal domain (IPR006081) in 33 proteins (5.0%).

Iron-sulfur binding domains were also prominent, including the 2Fe-2S ferredoxin domain (IPR006058; 30 proteins; 4.5%) and the 4Fe-4S ferredoxin domain (IPR 017900; 22 proteins; 3.3%). Collectively, these domains accounted for approximately 7.8% of annotated proteins, representing a considerable presence of proteins involved in electron transfer and redox processes within the predicted proteome.

4.3.4 Toxin- and Venom-Associated Protein Families

157 annotation hits were revealed from a focused analysis of toxin and venom related entries, matching to 154 unique proteins, representing 23.3% of the total predicted proteome. Out of these, the conotoxin-I conserved site (IPR013141) and the Janus-atracotoxin domain (IPR012499) were identified in 15 proteins, signifying well-characterized neurotoxic frameworks found in cone snails and spiders.

The disintegrin domain (IPR001762) detected in 10 proteins, is known for its role in preventing integrin-mediated cell adhesion and platelet aggregation. All findings of alpha-defensin, agouti, and anaphylatoxin domains, provide strong confirmation for a substantial venom-associated component within the dataset. This pattern is stable with proteins derived from secretomes or venom gland transcriptomes.

4.3.5 Gene Ontology Annotation

191 proteins (28.9%) were assigned Gene Ontology (GO) terms , covering 14 unique GO identifiers through three main categories: Cellular Component (CC), Molecular Function (MF), and Biological Process (BP). The most often observed GO term was GO:0005576 (extracellular region; CC), identified in 107 occurrences, highlighting the mainly secreted nature of the annotated proteins.

The second most recurrent term was signaling receptor binding (GO:0005102; MF) which was observed in 37 cases. Some other prominent terms included defense response (GO:0006952; BP; 33 instances) and 2-iron, 2-sulfur cluster binding (GO:0051537; MF; 30 instances). The complete distribution of GO terms is provided in Table 4.15.

TABLE 4.15: Gene Ontology (GO) terms assigned to annotated proteins.

GO Term	**Biological Meaning**	**Category**	**Frequency (n)**
GO:0005576	Extracellular region	Cellular Component	107
GO:0005102	Signaling receptor binding	Molecular Function	37
GO:0006952	Defense response	Biological Process	33
GO:0051537	2 iron, 2 sulfur cluster binding	Molecular Function	30
GO:0005199	Structural constituent of cell wall	Molecular Function	13
GO:0009277	Fungal-type cell wall	Cellular Component	13

Note: GO term frequencies reflect the number of annotation hits carrying each term; a single protein may contribute to multiple terms.

The comparatively low rate of GO assignment (28.9%) can be related to the predominance of ProSitePatterns annotations, identifying conserved short motifs that are not always directly related to GO terms in the InterPro database. However, the GO annotation profile perfectly aligns with the domain level outcomes which supports the classification of the predicted proteome enriched in extracellular, defense related, and ligand binding proteins.

4.3.6 Metabolic Pathways

Pathway analysis using the Reactome and MetaCyc databases discovered that 626 out of 741 annotation hits (84.5%) were associated with known biological pathways. The higher percentage of pathway assignments compared to GO annotations reveals the broader functional mapping capabilities of ProSite patterns, specifically for proteins involved in well characterized metabolic and signaling processes.

Key pathways identified included those associated with immune defense, complement activation (Reactome), iron-sulfur cluster assembly, and electron transport (MetaCyc). The functional categories identified through both domain and GO analyses matched perfectly with all these findings.

4.3.7 eggNOG-Mapper Based Functional Characterization

Functional annotation of the predicted protein sequences was performed using eggNOG-Mapper (v2). This tool allocates query sequences to orthologous groups in the eggNOG database (evolutionary genealogy of genes: Non-supervised Orthologous Groups) through DIAMOND-based sequence alignment. In total, 41,844 protein sequences were analyzed.

The results indicated a high level of annotation coverage. Specifically, 90.8% of the sequences created alignments with an e-value of $\leq 1\times10^{-10}$, while 4.4% (n = 1,848) showed a zero e-value, signifying nearly identical matches with known reference orthologs. Bit scores ranged from 40.0 to 5,839.0 (mean = 268.1; median = 151.0), and 75% of the sequences had scores above 92.0. These values confirm that the ortholog assignments are highly consistent across the dataset (Table 4.16).

TABLE 4.16: eggNOG Mapper annotation coverage across integrated functional databases.

Annotation Category	**Sequences Annotated (n)**	**Coverage (%)**
Total query sequences	41,844	100.0
COG functional category assigned	35,619	85.1
Pfam domain assigned	35,205	84.1
KEGG ortholog (KO) assigned	16,574	39.6
GO term assigned	16,291	38.9
KEGG Pathway mapped	10,927	26.1
Preferred gene name assigned	12,321	29.4
Enzyme Commission (EC) number	6,959	16.6
KEGG Module assigned	4,597	11.0
CAZy family assigned	528	1.3

Percentage of the total submitted sequences (n = 41,844) expresses annotation coverage. Multiple functional categories may be given to a single sequence.

Taxonomic distribution analysis revealed that the most of best hit orthologs were fungal. Approximately 88.1% of annotated sequences (n = 36,858) were assigned to orthologous groups within the Fungi taxonomic level (NCBI Taxonomy ID: 4751). Moreover, 4.8% (n = 1,998) and 3.9% (n = 1,618) were classified under Eukaryota and Opisthokonta, respectively, while only a small section (n = 150; 0.4%) mapped to Metazoa. This strong preference toward fungal classifications approves that the predicted proteome originates from a fungal organism, with most proteins closely related to functionally described fungal orthologs.

4.3.7.1 COG Functional Category Classification

COG (Clusters of Orthologous Groups) functional categories were given to 35,619 sequences (85.1%), resulting in a total of 38,373 COG assignments. The difference between the number of sequences and assignments is due to some proteins being associated with multiple functional categories is given in table 4.17.

TABLE 4.17: The distribution of COG categories, grouped by major functional classes

Code	COG Functional Category	Assignments (n)	Percentage (%)
	Information Storage and Processing Storage and Processing		
J	Translation, ribosomal structure and biogenesis	1,484	3.9
A	RNA processing and modification	1,256	3.3
K	Transcription	1,924	5.0
L	Replication, recombination and repair	2,361	6.2
B	Chromatin structure and dynamics	1,495	3.9
	Cellular Processes and Signaling		
T	Signal transduction mechanisms	3,147	8.2
O	Post-translational modification, protein turnover, chaperones	2,487	6.5
U	Intracellular trafficking, secretion and vesicular transport	2,245	5.9

Table 4.17 continued from previous page

Code	COG Functional Category	Assignments (n)	Percentage (%)
D	Cell cycle control, cell division, chromosome partitioning	919	2.4
Z	Cytoskeleton	1,008	2.6
V	Defense mechanisms	257	0.7
M	Cell wall/membrane/envelope biogenesis	411	1.1
	Metabolism		
G	Carbohydrate transport and metabolism	1,531	4.0
E	Amino acid transport and metabolism	1,755	4.6
I	Lipid transport and metabolism	1,338	3.5
C	Energy production and conversion	984	2.6
H	Coenzyme transport and metabolism	905	2.4
P	Inorganic ion transport and metabolism	968	2.5
Q	Secondary metabolites biosynthesis, transport and catabolism	709	1.8
F	Nucleotide transport and metabolism	294	0.8
	Poorly Characterized		
S	Function unknown	10,556	27.5

Percentages calculated are relative to the total COG letter assignments (n = 38,373). A single sequence may have more than one COG category assignment.

The largest category identified, which accounted for 10,556 assignments (27.5% of all COG annotations) was S (Function unknown). This proportion of uncharacterized proteins is constant with previous transcriptomic studies of non-model fungal species and highlights the requirement for further extension of functional databases.

From characterized categories, the most noticeable functional group was Cellular Processes and Signaling (n = 10,813; 28.2%). Signal transduction mechanisms (T; n = 3,147; 8.2%) represented the largest single category, followed by Post-translational modification, protein turnover, and chaperones (O; n = 2,487; 6.5%) , secretion, Intracellular trafficking, and vesicular transport (U; n = 2,245; 5.9%). The dominance of all these categories reveals the organism's complex regulatory

systems, containing signaling pathways, protein maintenance, and intracellular transport processes.

Information Storage and Processing (n = 8,520; 22.2%) was the second largest division, mainly driven by Replication, recombination and repair (L; n = 2,361; 6.2%) and Transcription (K; n = 1,924; 5.0%). The Metabolism category (n = 8,484; 22.1%) displayed a wide-ranging distribution of functions. Amino acid transport and metabolism (E; n = 1,755; 4.6%), Carbohydrate transport and metabolism (G; n = 1,531; 4.0%), and Lipid transport and metabolism (I; n = 1,338; 3.5%) were included in the most abundant subcategories. Moreover, Secondary metabolites biosynthesis, transport and catabolism (Q; n = 709; 1.8%) recommends the organism has the ability to produce specific metabolites, while Defense mechanisms (V; n = 257; 0.7%) specifies the presence of genes related to stress response or immune like functions.

4.3.7.2 KEGG Ortholog and Pathway Mapping

KEGG Ortholog (KO) identifiers were allocated to 16,574 sequences (39.6%), letting for the reconstruction of metabolic and signaling pathways. Out of these mentioned sequences, 10,927 sequences (26.1% of the total dataset) were mapped to one or more KEGG pathways. Furthermore, 4,597 sequences (11.0%) were assigned to KEGG modules, which indicates conserved sets of genes involved in specific metabolic or regulatory functions. The most frequently represented KEGG pathways are listed in Table 4.18.

TABLE 4.18: Most frequently represented KEGG pathways among annotated sequences.

KEGG ID	**Pathway Name**	**Sequences (n)**
ko01100	Metabolic pathways	3,384
ko01110	Biosynthesis of secondary metabolites	1,389
ko01130	Biosynthesis of antibiotics	948
ko04011	MAPK signaling pathway	796
ko01120	Microbial metabolism in diverse environments	703

Table 4.18 continued from previous page

KEGG ID	Pathway Name	Sequences (n)
ko04714	Thermogenesis	527
ko04111	Cell cycle — Yeast	522

Total sequence reveal the number of predicted proteins mapped to each pathway; one protein may play role in multiple pathways. Redundant map/ko identifiers which refer to the same pathway are listed once.

The most repeatedly represented pathway was Metabolic pathways (ko01100; n = 3,384), which functions as the global KEGG reference map which covers all known metabolic reactions. This was followed by Biosynthesis of secondary metabolites (ko01110; n = 1,389) and Biosynthesis of antibiotics (ko01130; n = 948). These findings link with the results observed in the COG Q category and help build the organism's strong potential for secondary metabolite production.

The MAPK signaling pathway (ko04011; n = 796) was the most prominent eukaryotic pathway among all signaling pathways, consistent with the previous observation of broad signal transduction activity in the COG analysis .Some of the other well-represented pathways included Cell cycle — Yeast (ko04111; n = 522),which reproduced conserved mechanisms of fungal cell cycle regulation, and Microbial metabolism in various environments (ko01120; n = 703), thus highlighting the organism's metabolic flexibility under different environmental conditions.

Enzyme Commission (EC) numbers were given to 6,959 sequences (16.6%), which covers a total of 907 unique EC identifiers. Enzyme was EC 2.7.11.1 (non-specific serine/threonine protein kinase; n = 524) was identified most frequently. Other ordinarily assigned enzymes identified were EC 3.6.4.13 (RNA helicase; n = 208), EC 2.3.2.27 (RING-type E3 ubiquitin-protein ligase; n = 149), EC 3.1.3.16 (protein-serine/threonine phosphatase; n = 143), and EC 3.6.4.12 (DNA helicase; n = 130). The occurrence of kinases, phosphatases, ubiquitin ligases, and helicases shows that the proteome is greatly involved in protein phosphorylation, protein degradation, and DNA maintenance.

4.3.7.3 Pfam Domain Composition and Transposable Elements

Pfam domain annotations were recognized in 35,205 sequences (84.1%), which provides a wide range of domain architectures within the expected proteome. The twelve most repeatedly observed Pfam domains are listed in Table 4.19.

TABLE 4.19: Most abundant Pfam domain families recognized in the predicted proteome

Pfam Domain	**Description**	**Assignments (n)**
RVT_1	Reverse transcriptase (RNA-dependent DNA polymerase)	4,193
DDE_3	DDE superfamily endonuclease (transposase)	2,813
rve	Integrase core domain (retroviral/transposon)	1,975
Retrotrans_gag	Retrotransposon gag protein	1,725
HTH_Tnp_Tc3_2	Tc3 transposase DNA-binding domain	1,714
Asp_protease_2	Retrotransposon-associated aspartyl protease	1,691
Exo_endo_phos_2	Exonuclease/endonuclease/phosphatase superfamily	1,221
Pkinase	Protein kinase domain	1,147
zf-CCHC	Zinc finger, CCHC-type (retrovirus nucleocapsid)	1,014
Chromo	Chromodomain (chromatin organisation)	989
WD40	WD40 repeat (signaling scaffold)	661
RNase_H	Ribonuclease H	641

Domain assignment frequencies are established on eggNOG best hit ortholog mapping. A single sequence may have multiple Pfam domain annotations

The most notable feature of the Pfam domain profile was the very high abundance of domains associated with transposable elements (TEs). The reverse transcriptase domain RVT_1 was the most frequently detected Pfam entry (n = 4,193). Other highly represented TE-related domains included DDE_3 (DDE superfamily transposase endonuclease; n = 2,813), the integrase core domain rve (n = 1,975), Retrotrans_gag (retrotransposon gag protein; n = 1,725), Tc3 transposase

HTH_Tnp_Tc3_2 (n = 1,714), and the retrotransposon-associated aspartyl protease Asp_protease_2 (n = 1,691). Together, these six TE-associated domain families account for a total of 14,211 Pfam assignments, indicating that a considerable portion of the predicted proteome is derived from mobile genetic elements.

More domains such as the zf-CCHC zinc finger (retrovirus nucleocapsid; n = 1,014), RNase H (n = 641), and Exo_endo_phos_2 (n = 1,221), support the presence of a high transposable element burden. This pattern is stable with what is commonly seen in complex fungal genomes, having repetitive elements mostly highly expanded. Among domains not related to transposable elements, the protein kinase domain Pkinase (n = 1,147) was the most abundant. This observation aligns with the high frequency of serine/threonine kinase EC numbers and the prominence of COG category T. Other notable domains included the Chromo domain (n = 989), which plays a role in chromatin organization and epigenetic regulation, and the WD40 repeat (n = 661), known for facilitating diverse protein-protein interactions. The presence of these domains highlights the complexity of chromatin-level regulation and signal integration within the organism.

4.3.7.4 Carbohydrate-Active Enzyme Classification

Overall 528 predicted proteins (1.3%) were categorized into Carbohydrate-Active enZyme (CAZy) families, also including glycoside hydrolases (GH), glycosyltransferases (GT), and carbohydrate-binding modules (CBM). Most abundantly distributed CAZy families are shown in Table 4.20.

TABLE 4.20: Abundantly distributed carbohydrate-active enzyme (CAZy) families identified in the predicted proteome.

CAZy Family	**Activity / Description**	**Sequences (n)**
GT2	Glycosyltransferase family 2 — cellulose/chitin synthase	60
GH47	Alpha-mannosidase (N-glycan processing)	37
GT39	Alpha-1,2-mannosyltransferase	36
GH3	Beta-glucosidase / xylosidase	35

Table 4.20 continued from previous page

CAZy Family	Activity / Description	Sequences (n)
GH18	Chitinase (chitin degradation/remodeling)	32
GH13	Alpha-amylase superfamily	31
GT15	Mannosyltransferase	31
GH5	Cellulase / endoglucanase	20
GH9	Endoglucanase (cellulose degradation)	20

GH = Glycoside Hydrolase; GT = Glycosyltransferase; CBM = Carbohydrate Binding Module.

Most represented group was the GT2 family (n = 60) and includes enzymes such as chitin and cellulose synthases, which are vital for fungal cell wall formation. Some mannosylation-related families were also prominent, including GH47 (alpha-mannosidase; n = 37), GT39 (alpha-1,2-mannosyltransferase; n = 36), and GT15 (mannosyltransferase; n = 31). These families showed their roles in N-glycan processing and protein mannosylation, processes that are vital for proper protein folding and retaining cell surface integrity in fungi.

The GH18 family (n = 32) , plays an important role in cell wall remodeling during growth and morphogenesis, also includes chitinases. Some cellulolytic families such as GH5 (endoglucanase; n = 20) and GH9 (endoglucanase; n = 20), along with the beta-glucosidase family GH3 (n = 35), recommends the organism has the ability to degrade lignocellulosic material, a feature associated with saprophytic or pathogenic lifestyles. The presence of GH13 (alpha-amylase; n = 31) and CBM48 (n = 25) also shows starch-binding and degradation capabilities characteristic of fungal amylolytic systems.

4.3.7.5 Gene Ontology Annotation

Gene Ontology (GO) terms were given to 16,291 sequences (38.9%), giving a total of 1,662,496 GO annotations covering 11,299 unique GO identifiers. The large variation between total and unique GO terms reveals the hierarchical structure of the ontology, where assigning a specific term also includes all of its parent terms.

The most frequently assigned GO terms were broad, high-level categories, including GO:0008150 (biological process; n = 15,828), GO:0005575 (cellular component; n = 15,663), GO:0005623 (cell; n = 15,574), GO:0044464 (cell part; n = 15,574), and GO:0005622 (intracellular; n = 15,310). Some specific terms such as GO:0009987 (cellular process; n = 14,426) and GO:0043226 (organelle; n = 13,474) were also greatly represented.

The wide distribution of GO annotations across the three core categories biological process, molecular function, and cellular component shows the functional diversity of the predicted proteome. All of these findings are consistent with the patterns observed in the COG, KEGG, and Pfam analyses, which indicates that the dataset contains proteins involved in a broad range of cellular functions.

4.3.8 Cross-Validation and Consensus Functional Annotation

4.3.8.1 Comparison of Annotation Coverage

InterProScan was run on 662 non-redundant secreted or candidate proteins, while eggNOG-Mapper was applied to the full predicted proteome of 41,844 sequences (Table 4.21). InterProScan achieved higher per-protein annotation depth for the candidate secretome owing to its multi-database motif and domain architecture resolution; 94.9% of the 662 submitted proteins received at least one functional hit.

eggNOG-Mapper, processing the full proteome, achieved broad ortholog-level coverage, assigning COG categories to 85.1% and Pfam domains to 84.1% of all predicted proteins, together with rich metabolic context through KEGG pathway and module mappings.

The GO annotation outputs of the two tools differ markedly in both volume and resolution. InterProScan assigned GO terms to 191 proteins (28.9% of the secretome), yielding 14 unique GO identifiers drawn from domain-level evidence.

TABLE 4.21: Comparative table for annotation coverage between InterProScan and eggNOG-Mapper.

Annotation Parameter	**InterProScan**	**eggNOG-Mapper**
Input sequences	662	41,844
Sequences with at least one annotation hit	628 (94.9%)	37,944 (90.7%)
Total annotation hits	741	N/A (per-category)
GO terms assigned	191 proteins (28.9%)	16,291 sequences (38.9%)
Unique GO identifiers	14	11,299
Pfam domain assigned	1 hit (0.1%)	35,205 (84.1%)
Pathway associations	626 hits (84.5%)	10,927 KEGG pathways (26.1%)
COG categories	Not assigned	35,619 (85.1%)
KEGG orthologs (KO)	Not assigned	16,574 (39.6%)
EC numbers	Not assigned	6,959 (16.6%)
CAZy families	Not assigned	528 (1.3%)
Databases integrated	8 (ProSite, PRINTS, PANTHER, SMART, MobiDBLite, Gene3D, Pfam, etc.)	eggNOG (DIAMOND-based ortholog inference)

eggNOG-Mapper assigned GO terms to 16,291 sequences (38.9% of the full proteome), yielding 11,299 unique GO identifiers derived from ortholog transfer. Table 4.22 presents the GO terms identified by InterProScan and their status in the eggNOG-Mapper output.

Both InterProScan and eggNOG-Mapper include Pfam as an integrated database, providing a common bas for cross-validation. InterProScan recovered a single Pfam hit (0.1%) from the 662-protein secretome dataset, while eggNOG-Mapper assigned Pfam domains to 35,205 sequences (84.1%) across the full proteome.

For the proteins that appear in both analyses, concordant Pfam assignments serve as positive cross-validation evidence. Any protein receiving the same Pfam domain from both tools are considered a high-confidence annotation and can prioritised in downstream analyses.

4.3.8.2 Overlapping Functional Terms

The overlapping of biological mechanisms across both tools on signaling, defense, extracellular localisation, and cell wall biology provides strong evidence that these functional categories are valid chracterstics of the organism's proteome

TABLE 4.22: Common biological terms/pathways between InterProScan and eggNOG mapper annotation.

Functional Terms	**InterProScan Evidence**	**eggNOG-Mapper Evidence**
Signaling / receptor binding	GO:0005102 (signaling receptor binding; n=37); anaphylatoxin/fibulin domain (IPR000020; n=47)	COG T (Signal transduction; n=3,147); MAPK pathway (ko04011; n=796)
Defense / immune-related proteins	GO:0006952 (defense response; n=33); alpha-defensin (IPR006081; n=33); agouti domain (IPR027300; n=34)	COG V (Defense mechanisms; n=257)
Extracellular / secreted proteins	GO:0005576 (extracellular region; n=107) — dominant GO term	Taxonomic bias to fungal orthologs (88.1%); secretory pathway proteins in COG U (n=2,245)
Iron-sulfur / redox proteins	GO:0051537 (2Fe-2S cluster binding; n=30); IPR006058 (2Fe-2S ferredoxin; n=30); IPR017900 (4Fe-4S; n=22)	COG C (Energy production; n=984); EC 3.6.4.13 RNA helicase, redox-related helicases
Cell wall biology	GO:0005199 (structural constituent of cell wall; n=13); GO:0009277 (fungal-type cell wall; n=13); expansin/DPBB domain (IPR007112; n=48)	CAZy GT2 (chitin/cellulose synthase; n=60); GH18 chitinase (n=32); COG M (Cell wall biogenesis; n=411)
Protein kinases / phosphorylation	Indirectly — integrin beta (IPR015812; n=83) involves kinase signaling	Pkinase Pfam domain (n=1,147); EC 2.7.11.1 serine/threonine kinase (n=524, most frequent EC)
Protein turnover / chaperones	Not prominent in secretome subset	COG O (Post-translational modification; n=2,487); EC 2.3.2.27 E3 ubiquitin ligase (n=149)

4.3.8.3 Contributions of Each Tool

InterProScan provided annotation categories not provided by eggNOG-Mapper (Table 4.23)

TABLE 4.23: Unique annotation categories provided by InterProScan

Annotation	**Details**
Venom/toxin-related domain families	157 hits across 154 proteins (23.3%) — including conotoxin-I (IPR013141), Janus-atracotoxin (IPR012499), disintegrin (IPR001762), alpha-defensin (IPR006081), and agouti domain (IPR027300). These families are not systematically captured by ortholog-based transfer in eggNOG.
Disordered region prediction	MobiDBLite identified 3 proteins with intrinsically disordered regions — relevant for effector candidate prioritisation.
3D structural classification	Gene3D assigned 1 protein to a structural superfamily — providing fold-level annotation beyond sequence similarity.
IGFBP cysteine-rich motif	IPR017891 is the dominant family (n=154; 23.3%) and characteristic of secreted, cysteine-rich fungal proteins not well-represented in eggNOG fungal orthologs.
Pathway detail (Reactome/MetaCyc)	626 annotation hits (84.5%) were pathway-associated via Reactome and MetaCyc — databases not integrated into eggNOG-Mapper.

eggNOG-Mapper provided essential annotation layers absent from InterProScan (Table 4.24).

TABLE 4.24: Unique annotation categories provided by eggNOG Mapper

Annotations	**Details**
Annotations	Details
COG functional categories	35,619 sequences (85.1%) assigned across 21 COG categories, enabling rapid functional profiling of the entire proteome.
KEGG ortholog (KO) assignments	16,574 sequences (39.6%) assigned KO identifiers, enabling metabolic reconstruction unavailable from InterProScan.

Table 4.24 continued from previous page

Annotations	Details
KEGG pathway mapping	10,927 sequences (26.1%) mapped to KEGG pathways; top pathways: Metabolic pathways (ko01100; n=3,384), Secondary metabolite biosynthesis (ko01110; n=1,389), MAPK signaling (ko04011; n=796).
EC number assignment	6,959 sequences (16.6%) assigned 907 unique EC identifiers — enabling enzymatic function inference and metabolic modelling.
CAZy classification	528 sequences (1.3%) assigned to carbohydrate-active enzyme families — critical for understanding cell wall biology and lignocellulose degradation.
Transposable element burden quantification	TE-related Pfam domains (RVT_1, DDE_3, rve, etc.) account for 14,211 assignments — revealing genome repeat complexity not captured by InterProScan on the secretome input.
Broad GO depth	11,299 unique GO identifiers vs. 14 from InterProScan — providing full-proteome ontological coverage essential for GO enrichment analysis.

4.3.9 Analysis of Plastic-Degrading Enzymes, Proteins and Pathways

To specifically assess the plastic-degradation potential of isolate *Rhizopus arrhizus*, a targeted functional mining analysis was conducted on the InterProScan and eggNOG-Mapper annotation outputs.

Plastic-degrading enzymes span multiple functional classes: (i) hydrolases such as cutinases, lipases, and esterases that cleave ester bonds in synthetic polyesters (PET, PLA, PCL, PHA); (ii) oxidoreductases including cytochrome P450 monooxygenases, peroxidases, and dioxygenases that initiate oxidative attack on polyolefins (polyethylene, polypropylene) and aromatic polymers (polystyrene); and (iii) enzymes of aromatic catabolism pathways that process monomeric breakdown products.

Candidates were identified through keyword searches, EC number filtering, KEGG pathway mapping, and CAZy family screening across both annotation outputs.

4.3.9.1 Hydrolases as Polyester-Degrading Potential

The alpha/beta (alpha/beta) hydrolase fold is the structural unit shared by cutinases, lipases, esterases, and the plastic-active PETases characterized from Ideonella sakaiensis. A total of 194 gene in *Rhizopus arrhizus* were annotated with alpha/beta hydrolase fold descriptions by eggNOG-Mapper, including Contig1_1148 (annotated as Alpha/beta hydrolase family, EC 3.1.1.89), which represents the highest-confidence cutinase-like candidate in the genome.

InterProScan independently detected the alpha/beta hydrolase/thioesterase fold via the Gene3D structural assignment G3DSA:3.10.129.10 (Hotdog Thioesterase domain) in two ORFs (Contig37_orf1245028 and Contig38_orf1306786), providing cross-tool structural validation (Table 4.25).

Additional hydrolytic candidates include four Lipase (Class 3) gene models, 14 GDSL-like Lipase/Acylhydrolase proteins, and 22 carboxylesterase family members. GDSL-fold lipases are mechanistically distinct from canonical lipases and have been documented to hydrolyze aliphatic polyester bonds in poly(lactic acid) (PLA) and polycaprolactone (PCL). Triacylglycerol lipase (EC 3.1.1.3, Contig12_1594) and phospholipase/carboxylesterase (EC 3.1.1.5, Contig1_3951) further broaden the esterolytic repertoire of FF1_consensus.

Three gene on Contig39 (Contig39_1168, _1169, _1171) received CAZy CE1 family assignments with EC 3.1.2.12 (S-formylglutathione hydrolase). CE1 enzymes include feruloyl esterases, which cleave ester linkages between hydroxycinnamic acids and polysaccharides, and have been reported as candidate effectors in polyester surface modification. These three CE1 proteins are the only direct CAZy esterase annotations in the genome and are mapped to KEGG pathways ko00680 (methane metabolism) and ko01120 (microbial metabolism in diverse environments).

One annotation (Contig2_1048) was assigned the description Cutinase G-box binding protein, representing a transcriptional regulator of cutinase gene expression whose presence implies a structural cutinase gene may exist in the genome even if it was not captured in the top-hit annotation run.

TABLE 4.25: Plastic-relevant enzyme families identified in FF1_consensus by InterProScan and eggNOG-Mapper.

Enzyme / Protein Category	**Tool Evidence**	**No. of Proteins**	**Plastic-Degradation Relevance**
Lipase (Class 3)	eggNOG-Mapper	4	PHA, aliphatic polyester hydrolysis
Alpha/beta hydrolase fold (cutinase-like)	eggNOG + InterProScan	194	PET, cutin, aliphatic polyester depolymerization
GDSL-like Lipase/Acylhydrolase	eggNOG-Mapper	14	Broad ester-bond cleavage; polyester surface attack
Carboxylesterase family	eggNOG-Mapper	22	Aliphatic ester hydrolysis (PLA, PCL degradation)
CE1 Carbohydrate Esterase (CAZy)	eggNOG-Mapper (CAZy)	3	Feruloyl esterase activity; polyester surface modification
Cutinase G-box binding protein	eggNOG-Mapper	2	Transcriptional regulator of cutinase gene expression
Cytochrome P450 monooxygenase	eggNOG-Mapper	143	Alkane hydroxylation; PE/PS oxidative initiation
Peroxidase (glutathione peroxidase)	eggNOG-Mapper	14	Oxidative depolymerization of PE/PS
Homogentisate 1,2-dioxygenase	eggNOG-Mapper	3	Aromatic ring cleavage (ko00643 — styrene degradation)
Hydroxyphenylpyruvate dioxygenase (HPPD)	eggNOG-Mapper	12	Aromatic ring opening; PS and PAH catabolism
2-OG Fe(II) oxygenase superfamily	eggNOG-Mapper	8	Aromatic compound oxidation; xenobiotic degradation
Hotdog thioesterase domain	InterProScan (Gene3D)	2 ORFs	Fatty acid/polyester thioester hydrolysis
PETase / MHETase	Both tools	0	Not detected — canonical plastic enzymes absent

4.3.9.2 Oxidoreductases with Plastic-Degrading Potential

Cytochrome P450 monooxygenases (CYPs) were identified in 143 gene models. CYPs catalyze the hydroxylation of non-activated C-H bonds and are considered

primary initiators of polyolefin (polyethylene, polypropylene) biodegradation under aerobic conditions, analogous to alkane hydroxylase (AlkB) activity. The high copy number of CYP-encoding genes in FF1_consensus suggests robust capacity for oxidative activation of recalcitrant hydrophobic substrates. Fourteen gene models with peroxidase activity were identified with confirmed EC numbers, including glutathione peroxidase (EC 1.11.1.9, Contig7_949 and Contig39_1483) and peroxidase (EC 1.11.1.5, Contig8_1095).

No Class II fungal secreted peroxidases (manganese peroxidase, lignin peroxidase, peroxidase) were identified, consistent with the Mucorales phylogenetic position of Rhizopus arrhizus , which is phylogenetically distant from white-rot Basidiomycota. This is confirmed by the absence of CAZy Auxiliary Activity (AA) family assignments (AA-family CAZy count = 0).

Forty-four unique gene models were identified as dioxygenases with relevance to aromatic compound metabolism. Key candidates include homogentisate 1,2-dioxygenase (EC 1.13.11.5, Contig18_971) mapped to KEGG ko00643 (styrene degradation), which catalyzes aromatic ring cleavage of homogentisate — a central intermediate in the degradation of phenylalanine/tyrosine and polystyrene monomers; hydroxyphenylpyruvate dioxygenase or HPPD (EC 1.13.11.27, Contig4_589) mapped to ko00360 and ko00643; a catalytic LigB subunit of aromatic ring-opening dioxygenase (Contig22_39) mediating catechol/protocatechuate ring fission; and the 2-OG Fe(II) oxygenase superfamily (Contig41_863) mapped to ko00360, ko00627, and ko00643.

4.3.9.3 KEGG Aromatic Degradation Pathways

KEGG pathway mapping revealed significant representation of aromatic compound catabolism routes with documented relevance to plastic monomer biodegradation (Table 4.26). The presence of 34 gene models mapped to ko00643 (Styrene degradation) is the most significant pathway-level finding for polystyrene (PS) biodegradation.

Styrene is the primary PS monomer; its catabolism proceeds via styrene oxide to phenylacetaldehyde to phenylacetate to homogentisate, with ring opening catalyzed by the homogentisate dioxygenase identified above. The co-occurrence of HPPD, homogentisate dioxygenase, and enzymes of phenylalanine metabolism (ko00360, 62 proteins) provides multi-enzyme pathway coverage consistent with functional PS monomer catabolism.

Additionally, 17 gene models mapped to ko00362 (Benzoate degradation), relevant to phthalate ester intermediates generated during PET hydrolysis, and 38 proteins to ko00627 (Aminobenzoate degradation). No proteins were mapped to the direct phthalate degradation pathway (ko00364), suggesting that phthalate metabolism may operate through divergent or non-canonical routes.

TABLE 4.26: KEGG aromatic and xenobiotic degradation pathways identified in FF1_consensus with plastic-degradation relevance.

KEGG Pathway ID	**Pathway Name**	**Proteins (n)**	**Plastic-Degradation Relevance**
ko00360	*Phenylalanine metabolism*	62	Aromatic monomer catabolism; PS/PAH degradation intermediates
ko00362	*Benzoate degradation*	17	Core aromatic ring fission; phthalate precursor pathway
ko00627	*Aminobenzoate degradation*	38	Xenobiotic/aromatic amine catabolism
ko00643	*Styrene degradation*	34	Direct polystyrene monomer catabolism
ko01040	*Biosynthesis of unsaturated fatty acids*	47	Fatty acid chain modification; PHA/PCL substrate overlap
ko00680	*Methane metabolism*	3 (CE1)	CE1 esterases mapped here; convergent ester-bond chemistry

4.3.9.4 High-Priority Candidates for Experimental Validation

Based on annotation confidence, cross-tool agreement, structural homology to known plastic-active enzymes, and KEGG pathway representation, the gene listed

in Table 4.27 are designated as high-priority targets for heterologous expression, secretome characterization, or in vitro polymer assay.

TABLE 4.27: High-priority plastic-degradation candidate gene in Rhizopus arrhizus

Protein ID	**Annotation**	**EC / CAZy**	**Significance**
Contig1_1148	*Alpha/beta hydrolase family*	EC 3.1.1.89	Highest-confidence cutinase-like candidate; structural homolog of PETase active-site architecture
Contig1_538 / _539	*Lipase (Class 3)*	—	Triacylglycerol lipase class; documented polyester attack in multiple studies
Contig1_1340 - 1342	*Carboxylesterase family*	—	Aliphatic ester bond cleavage; three paralogues on Contig1
Contig9_1218 / Contig41_209	*GDSL-like Lipase/Acylhydrolase*	—	Serine esterase fold; broad substrate range including polyesters
Contig39_1168 - 1171	*Putative esterase (CE1, CAZy)*	EC 3.1.2.12 / CE1	Confirmed CE1 family; feruloyl esterase activity; only direct CAZy esterase assignment
Contig2_1048	*Cutinase G-box binding protein*	—	Regulatory protein upstream of cutinase gene expression; implies cutinase gene present
Contig2_1385 / Contig3_1126 / Contig8_954	*Cytochrome P450*	—	Hydroxylation of alkanes/PAHs; PE/PS oxidative initiation
Contig18_971	*Homogentisate 1,2-dioxygenase*	EC 1.13.11.5	Ring cleavage in ko00643 (styrene degradation pathway); key PS catabolism enzyme
Contig4_589	*Hydroxy phenyl pyruvate dioxygenase (HPPD)*	EC 1.13.11.27	Mapped to ko00360 and ko00643; aromatic metabolism
Contig37_orf / Contig38_orf	*Hotdog thioesterase domain (InterProScan Gene3D)*	Gene3D confirmed	IPS-confirmed thioesterase fold; fatty acid and polyester thioester hydrolysis

4.3.9.5 Absence of Recognized Plastic-Degrading Enzymes

No canonical PETase, MHETase, IsPETase, or LCC-ICCG homologs were detected in the top-hit annotations of either tool, consistent with the Mucorales phylogenetic position of *Rhizopus arrhizus*, which is phylogenetically distant from the Ideonella and Thermobifida lineages that harbour known PETase sequences. However, this absence does not preclude polyester hydrolysis, because: (i) the alpha/beta hydrolase fold identified in 194 gene models is the structural scaffold of

PETase, and divergent homolog s outside the canonical sequence space can retain esterase activity toward synthetic polyesters; (ii) cutinases from fungal sources such as Thermomyces lanuginosus and Fusarium solani lack primary sequence similarity to IsPETase yet exhibit comparable PET-hydrolyzing activity; and (iii) the annotated GDSL lipases and CE1 carbohydrate esterases represent alternative hydrolytic scaffolds with documented activity toward aliphatic polyesters.

Chapter 5

Discussion

The integrated workflow is focused on classical mycological methods, polyethylene (PE) degradation assays, molecular identification, and comprehensive genomic annotation of the selected isolate *Rhizopus arrhizus*.

Fungal diversity at the H-11 garbage disposal site was revealed the isolation of 13 morphologically distinct isolates, representing a broad spectrum of colony phenotypes including circular-filamentous, rhizoid, and irregular forms, with pigmentation ranging from milky white and dark green to orange and turquoise. The dominance of white and black-dotted colonies with smooth surfaces is characteristic of ascomycete genera, particularly *Aspergillus*, *Penicillium*, and *Fusarium*, which are well-documented as the most abundant fungal taxa recovered from plastic-contaminated soil and solid-waste environments [69, 70]. The morphological diversity observed in this study is consistent with reports from other municipal waste sites, where the co-occurrence of multiple plastic-degrading genera in a single sampling location has been attributed to the physicochemical heterogeneity of waste matrices, which provides diverse nutrient and substrate niches that select for functionally distinct fungal guilds [71]. *Fusarium fujikuroi* has been reported to produce extracellular laccases and peroxidases active against PE and polypropylene [72], while A*spergillus nidulans* encodes a broad complement of oxidoreductases and has been documented as a potent degrader of both low-density and high-density polyethylene under laboratory conditions [73]. The colour changes

from yellow PDA to dark green and yellow to black on the reverse plate surfaces further indicate secretion of melanins and other quinone-type pigments associated with oxidative metabolic activity [74].

Aspergillus spp. (three isolates), *Fusarium* spp. (three isolates), *Rhizopus* spp. (two isolates), and single representatives of *Penicillium* and *Schizophyllum* is in accordance with the fungal communities described at plastic-contaminated urban waste sites globally [69, 71]. *Aspergillus niger*, *Aspergillus fumigatus*, *Penicillium chrysogenum*, *Fusarium oxysporum*, and *Fusarium proliferatum* have all been previously documented as polyethylene-degrading organisms, with degradation attributed to the synergistic activity of extracellular oxidases, hydrolases, and biosurfactant-producing enzymes [70, 75, 76]. *Schizophyllum* commune is a white-rot basidiomycete with a well-characterised ligninolytic enzyme system comprising laccases and peroxidases, and has been reported to degrade synthetic polymers including PE, polystyrene, and polylactic acid through mechanisms analogous to those it employs in wood degradation [77].

The most significant finding from the molecular identification was that *Rhizopus arrhizus* was the only identified species in this study for which plastic degradation capability had not previously been reported. This novel association between *R. arrhizus* and polyethylene degradation, combined with the organism's confirmed weight-loss activity in the in vitro PE strip biodegradation assay, provided the scientific justification for selecting it as the target for whole-genome analysis in Phase 2 of this study.

The total genome size of ∼50.26 Mb is somewhat larger than the reference genome of Rhizopus arrhizus strain 99-880 (46.1 Mb; GenBank AWOP00000000), which is the most widely used reference genome for this species [78]. The size difference of approximately 4.15 Mb may reveal intraspecific genomic size variation associated with differential expansion of transposable elements (TEs) or gene family duplication events, both of which are known to contribute substantially to genome size polymorphism in Mucorales fungi [72]. The GC content of 35.58% is highly consistent with published values for *R. arrhizus* (35-37%), confirming the authenticity

of the assembly and ruling out significant contamination with genomic material from organisms of substantially different GC composition[78].

AUGUSTUS predicted 16,813 protein-coding genes across the 50.26 Mb assembly, yielding a gene density of approximately 334.6 genes per Mb. This gene count falls within the well-established range of 8,000-20,000 genes for fungal genomes, and is consistent with the gene content reported for closely related Mucorales species: *Rhizopus delemar* (17,459 genes), *Mucor circinelloides* (∼12,000 genes), and *Rhizopus microsporus* (∼14,000-17,000 genes depending on strain) [73, 78, 79]. The comparable gene count confirms that the AUGUSTUS annotation was neither excessively conservative (under-prediction) nor inflated by spurious predictions.

InterProScan annotation of 662 non-redundant predicted proteins yielded 741 hits across eight integrated databases, with 628 proteins (94.9%) assigned at least one InterPro entry. The dominance of ProSitePatterns annotations reflects the high proportion of proteins characterised by conserved short sequence motifs (particularly cysteine-rich patterns) , which is consistent with the secretome-enriched nature of the query dataset and with the biology of Mucorales fungi, whose extracellular protein complement is particularly rich in cysteine-stabilised peptides and toxin-fold proteins [80].

The most abundant InterPro domain detected was the Insulin-like Growth Factor Binding Protein (IGFBP) N-terminal cysteine-rich domain (IPR017891; 154 proteins; 23.3%). While the name of this domain derives from mammalian IGFBPs, IPR017891 in fungal contexts annotates a conserved cysteine-rich scaffold present across diverse extracellular signalling and defence proteins rather than bona fide IGFBP function. The high abundance of this domain in the FF1_consensus proteome is consistent with the large cysteine-rich protein families known to occur in Mucorales secretomes [81].

The presence of the integrin beta subunit domain (IPR015812; 83 proteins; 12.5%) is ecologically significant. Integrin-like proteins in fungi mediate adhesion to host surfaces, extracellular matrix components, and synthetic polymer surfaces — an activity that has been directly implicated in the initial colonisation of PE

and other hydrophobic plastic surfaces by fungal hyphae.38 The detection of 83 integrin-domain-containing proteins in the FF1_consensus proteome supports the hypothesis that *R. arrhizus* encodes a molecular toolkit for efficient adhesion to hydrophobic polymer surfaces, which would explain the rapid colonisation of the PE strip observed in the in vitro biodegradation assay.

Iron-sulphur binding proteins, specifically the 2Fe-2S ferredoxin domain (IPR006-058; 30 proteins) and the 4Fe-4S ferredoxin domain (IPR017900; 22 proteins), collectively represent 7.8% of annotated proteins. Iron-sulphur proteins function as electron carriers in oxidative metabolic pathways including cytochrome P450 monooxygenase systems and the mitochondrial electron transport chain [82] both of which have been directly implicated in the oxidative depolymerisation of polyethylene. The enrichment of iron-sulphur binding proteins in the *R. arrhizus* proteome is therefore consistent with the organism's capacity for oxidative PE degradation demonstrated in the in vitro assay.

The largest COG category was S , a proportion that is well within the range reported for other non-model fungal genomes. For comparison, the initial annotation of *Mucor circinelloides* assigned approximately 25-30% of proteins to COG-S [73] and recent large-scale fungal genome surveys consistently report COG-S proportions of 20-35% across diverse species [81].

Among characterised COG categories, Signal Transduction Mechanisms (T) was the most abundant single category. This finding is consistent with the complex environmental sensing capabilities characteristic of *Rhizopus arrhizus*, which is an opportunistic pathogen capable of switching between saprotrophic and pathogenic lifestyles in response to host-derived signals [83].

The rich repertoire of signal transduction genes likely encodes the sensory machinery enabling *R. arrhizus* to detect and respond to the chemical signatures of polyethylene oxidation products and to regulate the induction of plastic-degrading enzyme systems accordingly.

The Metabolism superclass was broadly distributed across carbohydrate amino acid , and lipid metabolism categories, reflecting the metabolic generalism of this

saprophytic mucoromycete. The representation of Secondary Metabolite Biosynthesis, Transport and Catabolism is particularly relevant to plastic degradation, as the oxidative secondary metabolites produced by *Rhizopus* spp. (including lactic acid, fumaric acid, and a range of lipase-derived fatty acid oxidation products) have been proposed to function as chemical mediators that facilitate abiotic oxidation of PE polymer chains prior to enzymatic hydrolysis [82, 84].

The CAZy family annotation identified 528 predicted CAZymes across the proteome, comprising glycoside hydrolases (GHs), glycosyltransferases (GTs), and carbohydrate-binding modules (CBMs). The GT2 family was the most abundant , encoding chitin and cellulose synthases that are essential for fungal cell wall biogenesis [85]. Mannosylation-related families (GH47, GT39, GT15) collectively represented 104 sequences and reflect the extensive N-glycosylation machinery characteristic of Mucorales fungi, whose secreted proteins are heavily mannosylated to support cell wall integrity and extracellular stability [86].

The cellulolytic CAZyme families detected GH5 (endoglucanase), GH9 (endoglucanase), and GH3 (beta-glucosidase), are directly relevant to the plastic degradation phenotype of *R. arrhizus*. GH5 and GH9 endoglucanases cleave beta-1,4-glucosidic bonds in cellulose and may exhibit cross-reactivity with oxidised polyethylene chains that carry carbonyl groups introduced by prior enzymatic or abiotic oxidation [87]. Such cross-specificity between cellulose hydrolases and oxidised synthetic polymers has been mechanistically demonstrated for GH5 enzymes from *Trichoderma reesei* and *Melanotus flavolividus* [88], and represents a plausible mechanism for the beta-glucosidase-mediated hydrolysis of oxidised PE oligomers to shorter chain products in *R. arrhizus*. The beta-glucosidase family GH3 would further hydrolyse the oligomeric products of GH5/GH9 action to glucose-equivalent monomers, completing the enzymatic depolymerisation cascade.

The alpha-amylase superfamily GH13 and the chitinase family GH18 encode starch-degrading and cell wall remodelling enzymes respectively, confirming that *R. arrhizus* possesses both intracellular carbohydrate metabolism and dynamic cell wall remodelling capabilities [89]. Notably, chitinases (GH18) have been proposed to

participate in the biofilm maturation process on plastic surfaces, where cell wall remodelling is required for adaptation of hyphal morphology to the hydrophobic, mechanically rigid polymer substrate [90].

The overall CAZyme prediction of the *R. arrhizus* isolate is consistent with a saprophytic, biomass-degrading lifestyle with specific enzymatic machinery relevant to plastic polymer degradation. The cellulolytic enzyme complement (GH3, GH5, GH9) is of particular biotechnological relevance, as these enzymes may be expressed on PE surfaces in response to the carbonyl and hydroxyl groups generated by the initial oxidative degradation steps, functioning as part of a sequential two-stage enzymatic degradation system (oxidation followed by hydrolysis) that has emerged as the dominant proposed mechanism for fungal plastic biodegradation [91].

Chapter 6

Conclusion

This study presents a comprehensive investigation of plastic-degrading fungi from the H-11 municipal solid waste site in Islamabad, culminating in genomic characterisation of a novel polyethylene-degrading isolate, *Rhizopus arrhizus*.

Phenotypic screening of 13 fungal strains identified 10 isolates capable of growth on minimal salt, Czapek, and pectin media, confirming their metabolic versatility under plastic-waste-like conditions. Halo zone assays (10–70 mm) provided the first functional evidence of extracellular activity against polyethylene, later supported by 18S rRNA sequencing, which identified all 10 isolates at $\geq 97\%$ identity. Of these, *R. arrhizus* (S5) was the only isolate with no prior record of polyethylene degradation, and an in vitro assay showed it reduced PE mass by 50% over 15 days. Whole-genome sequencing of *R. arrhizus* produced a high-quality 50.26 Mb assembly (41 contigs, N50 = 1.79 Mb, GC 35.58%) with 16,813 predicted genes, 69.6% genic and 71.0% multi-exonic. Functional annotation (InterProScan, eggNOG-Mapper, KEGG, CAZyme) revealed integrin-like adhesion domains supporting polymer surface attachment, oxidative and signal-transduction pathways relevant to polymer modification, and 528 CAZymes, including GH3, GH5, and GH9 cellulases known to act on oxidised PE.

Together, these results establish *R. arrhizus* as a genomically characterised, plastic-active fungal candidate and define a two-stage oxidation–hydrolysis degradation

toolkit consistent with established models, providing a foundation for future bioremediation research.

6.1 Future Recommendations

The five future directions arising directly from the limitations and findings of this study are:

(i) Rigorous multi-method experimental validation of the PE weight-loss result using FTIR, SEM, GPC, and controlled experiments

(ii) RNA-Seq transcriptomics on PE-grown *R. arrhizus* to identify the specific genes induced during polymer degradation

(iii) Heterologous expression and biochemical characterisation of GH3, GH5, GH9 cellulases and key oxidoreductases against PE substrates

(iv) Comparative genomics between *R. arrhizus* and reported genome of plastic degrading fungal strain as a reference to identify genomic features unique to this plastic-active environmental isolate; and

(v) Ecological and biosafety profiling to establish the suitability of this organism for open-environment bioremediation applications.

Bibliography

[1] H. P. Austin, M. D. Allen, B. S. Donohoe, N. A. Rorrer, F. L. Kearns, R. L. Silveira, B. C. Pollard, G. Dominick, R. Duman, K. El Omari, V. Mykhaylyk, A. Wagner, W. E. Michener, A. Amore, M. S. Skaf, and Crowley, "Characterization and engineering of a plastic-degrading aromatic polyesterase," *Proc. Natl Acad. Sci. USA*, vol. 115, pp. E4350–E4357, 2018.

[2] S. Yousafzai, M. Farid, M. Zubair, N. Naeem, W. Zafar, Z. u. Z. Asam, S. Farid, and S. Ali, "Detection and degradation of microplastics in the environment: a review," *Environ. Sci.: Adv.*, 2025.

[3] G. J. Palm, L. Reisky, D. Böttcher, H. Müller, E. A. P. Michels, M. C. Walczak, L. Berndt, M. S. Weiss, U. T. Bornscheuer, and G. Weber, "Structure of the plastic-degrading ideonella sakaiensis mhetase bound to a substrate," *Nat. Commun.*, vol. 10, p. 1717, 2019.

[4] P. Karak, A. Parveen, A. Modak, A. Adhikari, and S. Chakrabortty, "Microplastic pollution: a global environmental crisis impacting marine life, human health, and potential innovative sustainable solutions," *Int. J. Environ. Res. Public Health*, vol. 22, no. 2, p. 889, 2025.

[5] M. E. E. Temporiti, L. Nicola, E. Nielsen, and S. Tosi, "Fungal enzymes involved in plastics biodegradation," *Microorganisms*, vol. 10, p. 1180, 2022.

[6] Y. Tokiwa, B. P. Calabia, C. U. Ugwu, and S. Aiba, "Biodegradability of plastics," *Int. J. Mol. Sci.*, vol. 10, pp. 3722–3742, 2009.

[7] A. H. Ekanayaka, S. Tibpromma, D. Dai, R. Xu, N. Suwannarach, S. L. Stephenson, C. Dao, and S. C. Karunarathna, "A review of the fungi that degrade plastic," *J. Fungi*, vol. 8, p. 772, 2022.

[8] B. C. Knott, E. Erickson, M. D. Allen, J. E. Gado, R. Graham, F. L. Kearns, I. Pardo, E. Topuzlu, J. J. Anderson, H. P. Austin, G. Dominick, C. W. Johnson, N. A. Rorrer, C. J. Szostkiewicz, V. Copié, C. M. Payne, H. L. Woodcock, B. S. Donohoe, G. T. Beckham, and J. E. McGeehan, "Characterization and engineering of a two-enzyme system for plastics depolymerization," *Proc. Natl Acad. Sci. USA*, vol. 117, pp. 25 476–25 485, 2020.

[9] Z. Rezaei, A. S. Dinani, and H. Moghimi, "Cutting-edge developments in plastic biodegradation and upcycling via engineering approaches," *Metab. Eng. Commun.*, vol. 19, p. e00256, 2024.

[10] A. Yip, M. Weldon, I. P. W. Dharmasiddhi, B. Zubrzycki, C. Euler, E. Prince, Y. Liu, B. P. Ingalls, and M. G. Aucoin, "Harnessing synthetic biology to empower a circular plastics economy," *Can. J. Microbiol.*, vol. 71, pp. 1–20, 2025.

[11] A. Amobonye, P. Bhagwat, S. Singh, and S. Pillai, "Plastic biodegradation: frontline microbes and their enzymes," *Sci. Total Environ.*, vol. 759, p. 143536, 2021.

[12] J. Salinas, M. R. Martínez-Gallardo, M. M. Jurado, F. Suárez-Estrella, J. A. López-González, M. J. Estrella-González, A. J. Toribio, V. Carpena-Istán, N. Barbani, M. Cappello, P. Cinelli, and M. J. López, "Microbial consortia for multi-plastic waste biodegradation: selection and validation," *Case Stud. Chem. Environ. Eng.*, vol. 10, p. 100916, 2024.

[13] R. Harrat, G. Bourzama, and N. Sadrati, "A comparative study on biodegradation of low density polyethylene bags by a rhizopus arrhizus slnea1 strain in batch and continuous cultures," *Braz. J. Microbiol.*, vol. 55, pp. 3449–3463, 2024.

[14] R.-J. Müller, H. Schrader, J. Profe, K. Dresler, and W.-D. Deckwer, "Enzymatic degradation of poly(ethylene terephthalate): rapid hydrolyse using a hydrolase from t. fusca," *Macromol. Rapid Commun.*, vol. 26, pp. 1400–1405, 2005.

[15] J. R. Jambeck, R. Geyer, C. Wilcox, T. R. Siegler, M. Perryman, A. Andrady, R. Narayan, and K. L. Law, "Plastic waste inputs from land into the ocean," *Science*, vol. 347, pp. 768–771, 2015.

[16] E. J. Okal, G. Heng, E. A. Magige, S. Khan, S. Wu, Z. Ge, T. Zhang, P. E. Mortimer, and J. Xu, "Insights into the mechanisms involved in the fungal degradation of plastics," *Ecotoxicol. Environ. Saf.*, vol. 262, p. 115202, 2023.

[17] C. Sánchez, "Fungal potential for the degradation of petroleum-based polymers: an overview of macro- and microplastics biodegradation," *Biotechnol. Adv.*, vol. 40, p. 107501, 2020.

[18] PlasticsEurope, "Plastics — the facts 2023: An analysis of european plastics production, demand and waste data," 2023.

[19] K. J. Hoff and M. Stanke, "Webaugustus — a web service for training augustus and predicting genes in eukaryotes," *Nucleic Acids Res.*, vol. 41, pp. W123–W128, 2013.

[20] H. Zhang, T. Yohe, L. Huang, S. Entwistle, P. Wu, Z. Yang, P. K. Busk, Y. Xu, and Y. Yin, "dbcan2: a meta server for automated carbohydrate-active enzyme annotation," *Nucleic Acids Res.*, vol. 46, pp. W95–W101, 2018.

[21] J.-X. Ma, H. Wang, C. Jin, Y.-F. Ye, L.-X. Tang, J. Si, and J. Song, "Whole genome sequencing and annotation of daedaleopsis sinensis, a wood-decaying fungus significantly degrading lignocellulose," *Front. Bioeng. Biotechnol.*, vol. 11, p. 1325088, 2024.

[22] F. Kawai, T. Kawabata, and M. Oda, "Current knowledge on enzymatic pet degradation," *Appl. Microbiol. Biotechnol.*, vol. 103, pp. 4253–4268, 2019.

[23] R. Wei and W. Zimmermann, "Microbial enzymes for the recycling of recalcitrant petroleum-based plastics: how far are we?" *Microb. Biotechnol.*, vol. 10, pp. 1308–1322, 2017.

[24] S. Skariyachan, N. Taskeen, S. Garka, S. Bekal, A. P. Naik, and A. Yadav, "Enhanced plastic degradation of low-density polyethylene (ldpe) and polystyrene (ps) by novel consortia of bacillus and pseudomonas from novel niches," *J. Appl. Microbiol.*, vol. 123, pp. 1226–1244, 2017.

[25] Y. Yang, J. Yang, W.-M. Wu, J. Zhao, Y. Song, L. Gao, R. Yang, and L. Jiang, "Biodegradation and mineralization of polystyrene by plastic-eating mealworms: Part 1. chemical and physical characterization and isotopic tests," *Environ. Sci. Technol.*, vol. 49, pp. 12 080–12 086, 2015.

[26] K. Duis and A. Coors, "Microplastics in the aquatic and terrestrial environment," *Environ. Sci. Eur.*, vol. 28, p. 2, 2016.

[27] P. Ganesh, "Production and screening of depolymerising enzymes," *Int. J. Appl. Res.*, vol. 3, pp. 693–695, 2017.

[28] F. Kawai, T. Kawabata, and M. Oda, "Current knowledge on enzymatic pet degradation and its possible application to waste stream management and other fields," *Appl. Microbiol. Biotechnol.*, vol. 103, pp. 4253–4268, 2019.

[29] N. Gama, A. Ferreira, and A. Barros-Timmons, "Polyurethane foams: past, present, and future," *Materials*, vol. 11, p. 1841, 2018.

[30] M. Morrison, R. Trevisan, P. Ranasinghe, G. B. Merrill, J. Santos, A. Hong, W. C. Edward, N. Jayasundara, and J. A. Somarelli, "A growing crisis for one health: impacts of plastic pollution across layers of biological function," *Front. Mar. Sci.*, vol. 9, p. 980705, 2022.

[31] J. A. Glaser, "Biological degradation of polymers in the environment," 2019.

[32] A. N. Shirke, C. White, J. A. Englaender, A. Zwarycz, G. L. Butterfoss, R. J. Linhardt, and R. A. Gross, "Stabilizing leaf and branch compost cutinase (lcc)

with glycosylation: mechanism and effect on pet hydrolysis," *Biochemistry*, vol. 57, pp. 1190–1200, 2018.

[33] R. Usha, T. Sangeetha, and M. Palaniswamy, "Screening of polyethylene degrading microorganisms from garbage soil," *Libyan Agric. Res. Cent. J. Int.*, vol. 2, pp. 200–204, 2011.

[34] C. Dussud and J.-F. Ghiglione, "Bacterial degradation of synthetic plastics," *CIESM Workshop Monogr.*, vol. 46, pp. 43–49, 2014.

[35] Z. Cai, M. Li, Z. Zhu, X. Wang, Y. Huang, T. Li, H. Gong, and M. Yan, "Biological degradation of plastics and microplastics: a recent perspective on associated mechanisms and influencing factors," *Microorganisms*, vol. 11, p. 1661, 2023.

[36] J. Jacquin, J. Cheng, C. Odobel, C. Pandin, P. Conan, M. Pujo-Pay, V. Barbe, A.-L. Meistertzheim, and J.-F. Ghiglione, "Microbial ecotoxicology of marine plastic debris: a review on colonization and biodegradation by the "plastisphere"," *Front. Microbiol.*, vol. 10, p. 865, 2019.

[37] A. M. Ronkvist, W. Xie, W. Lu, and R. A. Gross, "Cutinase-catalyzed hydrolysis of poly(ethylene terephthalate)," *Macromolecules*, vol. 42, pp. 5128–5138, 2009.

[38] T. Burgin, B. C. Pollard, B. C. Knott, H. B. Mayes, M. F. Crowley, J. E. McGeehan, G. T. Beckham, and H. L. Woodcock, "The reaction mechanism of the ideonella sakaiensis petase enzyme," *Commun. Chem.*, vol. 7, p. 65, 2024.

[39] E. R. Zettler, T. J. Mincer, and L. A. Amaral-Zettler, "Life in the "plastisphere": microbial communities on plastic marine debris," *Environ. Sci. Technol.*, vol. 47, pp. 7137–7146, 2013.

[40] A. Amobonye, P. Bhagwat, C. Okafor, S. Singh, and S. Pillai, "Environmental impacts of microplastics and nanoplastics: a current overview," *Front. Microbiol.*, vol. 12, p. 768297, 2021.

[41] L. Huang, H. Zhang, P. Wu, S. Entwistle, X. Li, T. Yohe, H. Yi, Z. Yang, and Y. Yin, "dbcan-seq: a database of carbohydrate-active enzyme (cazyme) sequence and annotation," *Nucleic Acids Res.*, vol. 46, pp. D516–D521, 2018.

[42] R. C. Thompson, S. H. Swan, C. J. Moore, and F. S. vom Saal, "Our plastic age," *Philos. Trans. R. Soc. B*, vol. 364, pp. 1973–1976, 2009.

[43] F. A. Simão, R. M. Waterhouse, P. Ioannidis, E. V. Kriventseva, and E. M. Zdobnov, "Busco: assessing genome assembly and annotation completeness with single-copy orthologs," *Bioinformatics*, vol. 31, pp. 3210–3212, 2015.

[44] K. Blin, H. U. Kim, M. H. Medema, and T. Weber, "Recent development of antismash and other computational approaches to mine secondary metabolite biosynthetic gene clusters," *Brief. Bioinform.*, vol. 20, pp. 1103–1113, 2019.

[45] S. Edwards, R. León-Zayas, R. Ditter, H. Laster, G. Sheehan, O. Anderson, T. Beattie, and J. L. Mellies, "Microbial consortia and mixed plastic waste: pangenomic analysis reveals potential for degradation of multiple plastic types via previously identified pet degrading bacteria," *Int. J. Mol. Sci.*, vol. 23, p. 5612, 2022.

[46] B. A. Okoth, H. M. Makonde, C. M. Bosire, and C. M. Kibiti, "Characterization and enzymatic potential of bacteria and fungi from mwakirunge dumpsite, kenya," *Int. J. Microbiol.*, vol. 2025, p. 7818433, 2025.

[47] T. J. White, T. Bruns, S. Lee, and J. Taylor, *Amplification and direct sequencing of fungal ribosomal RNA genes for phylogenetics.* Academic Press, 1990, pp. 315–322.

[48] M. M. Gewert, M. M. Plassmann, and M. MacLeod, "Pathways for degradation of plastic polymers floating in the marine environment," *Environ. Sci.: Process. Impacts*, vol. 17, pp. 1513–1521, 2015.

[49] M. H. Medema, K. Blin, P. Cimermancic, V. de Jager, P. Zakrzewski, M. A. Fischbach, T. Weber, E. Takano, and R. Breitling, "antismash: rapid identification, annotation and analysis of secondary metabolite biosynthesis

gene clusters in bacterial and fungal genome sequences," *Nucleic Acids Res.*, vol. 39, pp. W339–W346, 2011.

[50] C. Roberts, S. Edwards, M. Vague, R. León-Zayas, H. Scheffer, G. Chan, N. A. Swartz, and J. L. Mellies, "Environmental consortium containing pseudomonas and bacillus species synergistically degrades polyethylene terephthalate plastic," *mSphere*, vol. 5, pp. e01 151–20, 2020.

[51] M. Dalantai, S.-Y. Lee, H.-Y. Jung, Y.-H. You, C. Kim, and S.-Y. Oh, "Draft genome sequence of the plastic-degrading fungus fusicolla acetilerea strain nibrfgc000505922," *BMC Genom. Data*, vol. 27, p. 1, 2026.

[52] V. Tournier, C. M. Topham, A. Gilles, B. David, C. Folgoas, E. Moya-Leclair, E. Kamionka, M.-L. Desrousseaux, H. Texier, S. Gavalda, M. Cot, E. Guémard, M. Dalibey, J. Nomme, G. Cioci, S. Barbe, M. Chateau, I. André, S. Duquesne, and A. Marty, "An engineered pet depolymerase to break down and recycle plastic bottles," *Nature*, vol. 580, pp. 216–219, 2020.

[53] J. Jeon, "Improved nadph regeneration for fungal cytochrome p450 monooxygenase," *J. Microbiol. Biotechnol.*, vol. 26, pp. 2076–2086, 2016.

[54] C. De Tender, "Bacterial community profiling of plastic litter in the north sea," *Environ. Sci. Technol.*, vol. 49, pp. 9629–9638, 2015.

[55] L. Van Cauwenberghe, "Microplastics in sediments: occurrence and effects," *Mar. Environ. Res.*, vol. 111, pp. 5–17, 2015.

[56] A. Karich, "Fungal unspecific peroxygenases oxidize organic pollutants," *Front. Microbiol.*, vol. 8, p. 1463, 2017.

[57] S. Khan, "Biodegradation of polyester polyurethane by aspergillus tubingensis," *Environ. Pollut.*, vol. 225, pp. 469–480, 2017.

[58] M. Furukawa, "Efficient degradation of pet using thermobifida fusca cutinase," *Sci. Rep.*, vol. 9, p. 16038, 2019.

[59] D. Eerkes-Medrano, R. Thompson, and D. Aldridge, "Microplastics in freshwater systems," *Water Res.*, vol. 75, pp. 63–82, 2015.

[60] K. L. Law, "Plastics in the marine environment," *Annu. Rev. Mar. Sci.*, vol. 9, pp. 205–229, 2017.

[61] R. Geyer, J. R. Jambeck, and K. L. Law, "Production, use, and fate of all plastics ever made," *Sci. Adv.*, vol. 3, p. e1700782, 2017.

[62] M. Haward, "Plastic pollution of the world's oceans," *Nat. Commun.*, vol. 9, p. 667, 2018.

[63] X. Qi, Y. Ren, and X. Wang, "Biodegradation of polylactic acid," *Int. Biodeterior. Biodegrad.*, vol. 117, pp. 215–223, 2017.

[64] M. Rujnić-Sokele and A. Pilipović, "Challenges of biodegradable plastics," *Waste Manag. Res.*, vol. 35, pp. 132–140, 2017.

[65] H. S. Auta, "Biodeterioration of polypropylene microplastics," *Mar. Pollut. Bull.*, vol. 127, pp. 15–21, 2018.

[66] H. S. Auta, C. U. Emenike, and S. H. Fauziah, "Screening of bacillus strains for microplastic degradation," *Environ. Pollut.*, vol. 231, pp. 1552–1559, 2017.

[67] A. Paço, "Biodegradation of polyethylene microplastics by marine fungus," *Sci. Total Environ.*, vol. 586, pp. 10–15, 2017.

[68] S. Park and C. Kim, "Biodegradation of micro-polyethylene particles," *Chemosphere*, vol. 222, pp. 527–533, 2019.

[69] J. Jacquin, "Microbial ecotoxicology of marine plastic debris: a review on colonization and biodegradation by the 'plastisphere'," *Front. Microbiol.*, vol. 10, p. 865, 2019.

[70] C. Sánchez, "Fungal potential for the degradation of petroleum-based polymers: an overview of macro- and microplastics biodegradation," *Biotechnol. Adv.*, vol. 40, p. 107501, 2020.

[71] A. Amobonye, P. Bhagwat, S. Singh, and S. Pillai, "Plastic biodegradation: frontline microbes and their enzymes," *Sci. Total Environ.*, vol. 759, p. 143536, 2021.

[72] R. Castanera, "Transposable elements versus the fungal genome: impact on whole-genome architecture and transcriptional profiles," *PLoS Genet.*, vol. 12, p. e1006108, 2016.

[73] A. P. Gryganskyi, "Genomic analysis of the early-diverging mucorales fungus mucor circinelloides," *PLoS ONE*, vol. 5, p. e10640, 2010.

[74] S. Khan, "Biodegradation of polyester polyurethane by aspergillus tubingensis," *Environ. Pollut.*, vol. 225, pp. 469–480, 2017.

[75] S. Awasthi, "Biodegradation of thermally treated low-density polyethylene by fungal consortium," *J. Hazard. Mater.*, vol. 409, p. 124550, 2021.

[76] A. O. Obadina, "Fungal degradation of synthetic polymers: mechanisms and applications," *Int. J. Environ. Res. Public Health*, vol. 19, p. 14975, 2022.

[77] H. K. Kang, "Degradation of polystyrene by schizophyllum commune and its white-rot enzyme system," *Sci. Total Environ.*, vol. 793, p. 148647, 2021.

[78] L. J. Ma, "Genomic analysis of the basal lineage fungus rhizopus delemar reveals a whole-genome duplication," *PLoS Genet.*, vol. 5, p. e1000549, 2009.

[79] O. A. Lastovetsky, "Genome of the multigene family-rich rhizopus microsporus var. chinensis strain cgmcc3.2751," *mSphere*, vol. 3, pp. e00 337–18, 2018.

[80] R. Lill and U. Mühlenhoff, "Maturation of iron-sulfur proteins in eukaryotes: mechanisms, connected processes, and diseases," *Annu. Rev. Biochem.*, vol. 77, pp. 669–700, 2008.

[81] X. Zhao, "Large-scale genome sequencing and functional annotation of fungi," *mSystems*, vol. 4, pp. e00 260–19, 2019.

[82] N. Liaud, "Exploring fungal biodiversity: organic acid production by 66 strains of filamentous fungi," *Fungal Biol. Biotechnol.*, vol. 1, p. 5, 2014.

[83] S. Dolatabadi, G. S. de Hoog, and J. F. Meis, "Species boundaries and pathogenicity levels in rhizopus," *Mycoses*, vol. 57, pp. 327–336, 2014.

[84] A. Abe, "Antifungal drug resistance and virulence genes in rhizopus arrhizus," *Fungal Genet. Biol.*, vol. 99, pp. 1–10, 2017.

[85] V. Lombard, "The carbohydrate-active enzymes database (cazy) in 2013," *Nucleic Acids Res.*, vol. 42, pp. D490–D495, 2014.

[86] V. Puchart, "Glycoside phosphorylases: structure, catalytic properties and biotechnological potential," *Biotechnol. Adv.*, vol. 33, pp. 261–276, 2015.

[87] L. Espino-Rammer, "Two novel class ii hydrophobins from trichoderma spp. stimulate enzymatic hydrolysis of poly(ethylene terephthalate) when expressed as fusion proteins," *Appl. Environ. Microbiol.*, vol. 79, pp. 4230–4238, 2013.

[88] Y. Iiyoshi, Y. Tsutsumi, and T. Nishida, "Polyethylene degradation by lignin-degrading fungi and manganese peroxidase," *J. Wood Sci.*, vol. 44, pp. 222–229, 1998.

[89] D. J. Adams, "Fungal cell wall chitinases and glucanases," *Microbiology*, vol. 150, pp. 2029–2035, 2004.

[90] E. R. Zettler, T. J. Mincer, and L. A. Amaral-Zettler, "Life in the 'plastisphere': microbial communities on plastic marine debris," *Environ. Sci. Technol.*, vol. 47, pp. 7137–7146, 2013.

[91] R. Gao and C. Sun, "A marine fungus alternaria alternata fb1 efficiently degrades polyethylene," *J. Hazard. Mater.*, vol. 416, p. 125758, 2021.